Spring 1-9-2012

MAGNETOELECTRIC INTERACTIONS BETWEEN AN ORGANIC FERROELECTRIC AND A TRANSITION METAL FERROMAGNET

Abhijit Mardana
University of Nebraska-Lincoln, mardana.abhijit@gmail.com

MAGNETOELECTRIC INTERACTIONS BETWEEN AN ORGANIC FERROELECTRIC AND A TRANSITION METAL FERROMAGNET

By

Abhijit Mardana

A DISSERTATION

Presented to the Faculty of

The Graduate College at the University of Nebraska

In Partial Fulfillment of Requirements

For the Degree of Doctor of Philosophy

Major: Physics and Astronomy

Under the Supervision of Professor Shireen Adenwalla

Lincoln, Nebraska

January, 2012

MAGNETOELECTRIC INTERACTIONS BETWEEN AN ORGANIC FERROELECTRIC AND A TRANSITION METAL FERROMAGNET

Abhijit Mardana, Ph.D.

University of Nebraska, 2012

Adviser: Shireen Adenwalla

The interaction between ferromagnetic and ferroelectric films, the magnetoelectric effect, is a fascinating fundamental research area as well as having potential applications in magnetic data storage devices. We have investigated magnetoelectric coupling effects in thin film heterostructures, consists of metallic ferromagnet, cobalt, and the polymer ferroelectric [P(VDF-TrFE) 70:30]. The work described here encompasses changes in ferroelectric polarization with magnetic field as well as changes in the magnetic anisotropy with ferroelectric polarization.

In samples of Co overlayers on P(VDF-TrFE), in which the Co is not constrained by the substrate, the polarization shows a large change on application of a perpendicular magnetic field. This magnetoelectric effect is reversible, repeatable and possesses odd symmetry with respect to positive and negative magnetic field. Magnetic saturation destroys the effect, implying the presence of multiple magnetic domains is essential for the effect. The flexoelectric effect, the change in polarization due to strain gradients in the ferroelectric film, is a possible candidate for the cause of this effect.

In samples consisting of Co layers overlaid with P(VDF-TrFE), large changes in the magnetic coercivity with changes in ferroelectric polarization are observed. The out-of-plane coercivity is significantly larger for up polarization (i.e. polarization pointing away from the Co layer), whereas the opposite is true for the in-plane coercivity. The magnetic anisotropy, calculated using the areas of magnetization hysteresis loops, is shown to change by as much as 50% as the ferroelectric polarization is switched from up to down. For the thinnest films, the easy axis switches from out-of-plane to in-plane as the ferroelectric polarization is switched. The change in coercivity is proportional to the ferroelectric polarization, as confirmed by taking magnetization loops at intermediate polarization values. Rotation of the magnetization through a large angle, using only electric fields is demonstrated. These large changes in the anisotropy arise from the large electric field at the surface of the Co layer.

Acknowledgments

First of all, I would like to express my sincere gratitude to my advisor, Professor Shireen Adenwalla for her guidance, support and constant motivation throughout my doctoral study. She is always helpful and understanding. Her expertise in the field and innovative ideas played an important role in completion of my thesis work and development of my research career.

Next, I would like to thank Prof. Stephen Ducharme for his encouragement, kindness and sincere contribution through out my PhD studies.

I would like to thank Prof. Alexei Gruverman, Prof. Kirill Belashchenko and Prof. Mathias Schubert for serving on my doctoral committee and providing me suggestions and guidance during PhD.

A special thanks to Prof. Evgeny Tsymbal, Prof. Hermann Kohlstedt and Prof. Arunava Gupta. Also, I would like to express my appreciation to Prof. Sitaram Jaswal, Prof. Dan Claes, Prof. Christian Binek, Prof. Julian Velev and Dr. Andrei Sokolov.

As for my research group, I would like to thank past and current members: Dr. Andrew Baruth, Dr. Ellen Day, Mrs. Nina Hong, Mr. Sam Davis, Mr. Dan Williams, Mr. Cody Mart, and Mr. Uday Singh, Mr. Chun Yang, Mr. Keith Foreman, Mr. Darrin Lim. You've all had a positive affect on my PhD life both personally and as a group.

I say thanks to several group members from Prof. Ducharme and Prof Gruverman for a collaborative research: Dr. Timothy Reece, Dr. Mengjun Bai, Dr. Jihee Kim, Mrs. Kristin Kraemer, Dr. Rafal Korlacki, Mr. Shashi Poddar, Mr. Pankaj Sharma and Mr. Benjamin Hage.

I like to thank Dr. Shah Valloppilly for helping me to X-ray measurements and Dr. Lanping Yue for her help to use the Magnetic Force Microscope.

In addition, I would also like to thank the following people for helpful discussions and support: Mr. Zhen Li, Dr. Srinivas Polisetty, Dr. Venkata Voora, Dr. Juan M. Lopez-Encarnacion, Dr. Steven Michalski, Dr. J. D. Burton, Dr. Anand Moorti, Dr. T. V. Jayaraman, Dr. Alok Srivastava, Dr. Damien Le Roy, Dr. Parashu Kharel, Dr. Balamurugan Balasubramanian, Mr. Anil Kumar Rajapitamahuni, Mr. Tom George, Mr. Shawn Langan, Mr. Brian Jones, Mr. Xumin Chen, Mrs. Karolina Janicka, Dr. Aleksander Wysocki and Mr. Geoffrey Rojas.

A special appreciation to all the staff members in the Physics Department: Verona Skomski, Kay Haley, Theresa Sis, Jenny Becic, Beth Farleigh, Patty Christen, Joyce McNeil, Paula Adama, Michael J. Jensen, Les Marquart, Keith A. Placek, Pat Pribil and Robert L. Rhynalds, Dr. John R. Kelty, Brian Farleigh.

I personally thank to my former roommates Mr. Sourabh Chakraborty, Dr. Prasanta Gorai, and Mr. Anamitra Ghosh. You have been wonderful to me and I cannot forget the fun we had at every instance.

I would like to thank all my other friends for your support throughout my doctoral research at UNL. Your support has been invaluable and has made my stay a really enjoyable experience. Mentioning everyone who has in one way or the other helped and supported me during my stay here would make the list really very long, but I want to thank from the bottom of my heart all my friends, on and off-campus, who have made my stay at UNL worthwhile.

Last but not least, I would like to thank my family. Without your love, affection and support I would not have reached to this stage of my life. I owe my achievements to my parents, Mr. Ashok Kumar Mardana and Mrs. Anima Mardana. I acknowledge their unconditional love and encouragement. They have always given me freedom to fulfill my dreams. For my wife Rinku, I would never have achieved this without your love and support. I would like to express my appreciation to Dave & Gay Traster for being my family away from home. I am dedicating this thesis to my family members.

Finally, I would thank my financial supporter for making this thesis successful. My thesis work is mainly supported by National Science Foundation through the MRSEC program under Grant No. DMR-0820521 and ECCS Grant No. 1101256.

Contents

Chapter 1

Introduction

1.1 Introduction

The experiments described in this thesis investigate interactions between the ferroelectric copolymer polyvinylidene fluoride ($C_2H_2F_2$) with trifluoroethylene (C_2HF_3) [P(VDF-TrFE)] and the transition metal ferromagnet, Cobalt. We have demonstrated sizable magnetoelectric coupling in these ferromagnetic-ferroelectric thin film heterostructures.

The magnetoelectric (ME) effect is defined as the control of ferroelectric polarization by applied magnetic fields or the control of magnetization by applied electric fields. The magnetoelectric effects can occur in single-phase multiferroic materials or in composite materials with separate ferro-phases, in which the interaction between the materials is the source of magnetoelectric coupling.

Our choice of materials has the following advantages over conventional perovskite ferroelectric/ferromagnet layers: (i) the ferromagnetic metal is much stiffer (200 GPa) than the soft polymer film (2 GPa), effectively minimizing the strain at the much stiffer metallic Co layer. (ii) Low energy Langmuir Blodgett deposition of a crystalline ordered polymer film leads to little or no disruption of the interface.

This thesis focuses on the following topics:

1. ME coupling in a ferroelectric polymer / transition metal ferromagnetic heterostructure. (For details see chapter 4). Much of this chapter is taken from a

published article in Applied Physics Letters [A. Mardana, Mengjun Bai, A. Baruth, Stephen Ducharme & S. Adenwalla, Magneto-Electric Effects In Ferromagnetic Cobalt / Ferroelectric Copolymer Multilayer Films, *Applied Physics Letters* 97, 112904 (2010)].

2. Ferroelectric control of magnetic anisotropy. (For details see chapter 5 and chapter 6). These chapters are taken from a published article in Nano Letters [A. Mardana, Stephen Ducharme & S. Adenwalla, Ferroelectric control of magnetic anisotropy, *Nano Letters* 11 (9), 3862 (2011)] and an accepted article in Journal of Applied Physics [A. Mardana, Stephen Ducharme & S. Adenwalla, The sweep rate dependence of the electrical control of magnetic coercivity, *Journal of Applied Physics* 111, 7 (2012)] respectively.

1.2 Magnetoelectric effects in general: A review

In recent years ME effects, in both single phase multiferroics and composite samples have been reported[1] in which the polarization (magnetization) is altered by the application of a magnetic (electric) field, either directly or by introducing piezo-strain via magnetostriction. The variety of applications, ranging from memory devices to microwave applications, magnetic field sensors and the ability to sense magnetic or electric fields with electrical or magnetic responses are motivating the search for materials with larger ME coupling.

Magnetic ordering occurs in materials in which the exchange between electrons spins lead to ordering of the magnetic moments. Multiferroic materials[2,3,4,5,6] are special types of materials in which two or three ferro-order parameters (ferroelectric,

ferromagnetic, ferroelastic) occur. The coupling between these ordered phases is often weak, and the mechanisms for the ME coupling in multiferroics are highly dependent on the details of the electronic structure and the underlying lattice. Early investigations of ME coupling by P. Curie[7] in 1894 discussed the correlation of magnetic and electric properties in low-symmetry crystals, followed by P. Debye's[8] discussion in 1926 of the "magneto-elektrischer Richteffekt". Dzyaloshinskii[9] in 1959, predicted ME coupling in Cr_2O_3, which was experimentally observed by Astrov[10,11] in 1960.

The Landau free energy for a multiferroic material may be written as[1]

$$F(\vec{E},\vec{H}) = F_0 - P_i^S E_i - M_i^S H_i - \frac{1}{2}\varepsilon_0\varepsilon_{ij}E_iE_j - \frac{1}{2}\mu_0\mu_{ij}H_iH_j - \alpha_{ij}E_iH_j - \frac{1}{2}\beta_{ijk}E_iH_jH_k - \frac{1}{2}\gamma_{ijk}H_iE_jE_k - \ldots$$

where P and M are the spontaneous polarization and magnetization respectively, and E_i and H_i are the components of external electric and magnetic fields. The 2nd and 3rd terms are the dipolar and Zeeman energy terms, the 4th and 5th terms are the permittivity and permeability effects respectively. The magnetoelectric effects are contained in the last three terms, with linear and quadratic magnetoelectric effects.

The ME coupling can be defined as $P_i(H_j)$ and $M_i(E_j)$ and can be obtained by differentiating the above equation and setting E_j and H_j equal to 0,

$$P_i(H_j) = -\left.\frac{\partial F}{\partial E_i}\right|_{E_j=0} = \alpha_{ij}H_j + \frac{1}{2}\beta_{ijk}H_jH_k$$

$$\mu_0 M_i(E_j) = -\left.\frac{\partial F}{\partial H_i}\right|_{H_j=0} = \alpha_{ij}E_j + \frac{1}{2}\gamma_{ijk}E_jE_k$$

α_{ij} is the linear ME coupling coefficient and the third-rank tensors β_{ijk} and γ_{ijk} are the quadratic ME coefficients. The two equations above quantify the magnetoelectric effect, by defining the polarization change induced by magnetic field, and vice versa.

1.3 Magnetic control of ferroelectricity

1.3.1 Multiferroic materials

Materials which exhibit both magnetic and electrical ordering are scarce, but the growing interest in magnetoelectric phenomena has led to the development of new materials as well as renewed investigations into well known multiferroics with a view to enhancement of the ME coupling. Single crystal $BiFeO_3$ is a well known multiferroic material, exhibiting weak ferromagnetism and ferroelectricity with a Neel temperature of ~ 640 K and Curie temperature of ~ 1100 K.[12] The magnetization and the polarization both increase substantially in thin films of $BiFeO_3$, as seen by the group of Ramesh, who have reported a spontaneous polarization ~ 55 μC/cm^2 much higher than the single crystal value of ~ 3.5 μC/cm^2. The magnetization value was reported to be ~ 150 emu/cc at room temperature much higher than the single crystal value of ~ 2 emu/cc.[13] This enhancement of the polarization and magnetization is attributed to the lattice mismatch with the substrate and the distortion of the thin film from rhombohedral to tetragonal. The ME coupling coefficient dE/dH was measured to be 3 V/cm-Oe.

Compounds of $RMnO_3$ (where R is a rare earth atom Y, Ho, Er, Tm, Yb, Lu or Sc) display ME coupling with ferromagnetic and ferroelectric phase transitions as well as changes in the polarization and dielectric constant with applied magnetic field.[14,15] The

coupling is limited by high magnetic field (3-4 Tesla) and low magnetic ordering temperature (~30 K) requirements. Room temperature polarization switching with moderate magnetic field in the ceramic hexaferrite $Sr_3Co_2Fe_{24}O_{41}$ has been reported.[16]

The linear magnetoelectric coupling in Cr_2O_3 reaches a maximum value of α = 4.1 ps/m close to the Neel temperature of 307 K.[10] A recent experiment[17] revealed an unconventional ferromagnetism at the (0001) surface of the magnetoelectric Cr_2O_3. Using a ferromagnetic multilayer, Pd/Co, deposited on the Cr_2O_3, a reversible room temperature electric control of exchange bias was demonstrated. [Exchange bias is defined as the shift in the magnetization loop of a ferromagnetic film and is most often seen in bilayer structures consisting of a ferromagnetic (FM) and an antiferromagnetic (AFM). When this is cooled below the Neel temperature (T_N) of the AFM, unidirectional exchange anisotropy is induced in the FM layer.]

1.3.2 Composite materials

The paucity of room temperature multiferroics with strong ME coupling has motivated the fabrication of heterostructured materials with separate magnetic (or magnetostrictive) and ferroelectric (or piezoelectric) components.[18,19,20,21] ME coupling in composite materials may occur due to one or both of the following mechanisms. The first one[22] arises from strain coupling between the two components, with piezoelectric strain giving rise to magnetostriction, which alters the magnetization. Conversely, changes in magnetization result in magnetostriction, and with sufficiently strong strain coupling may alter the polarization of a strain coupled ferroelectric. The other effect

arises directly from the electric field at the interface, which alters the magnetization, or due to changes in interfacial bonding upon polarization switching.[23]

In heterostructures that are designed for strain coupling, magnetic materials are chosen to have the largest possible magnetostriction in order to maximize the polarization change with an applied magnetic field. For example, heterostructured laminates of metglas (with high magnetostriction) and polyvinylidene-fluoride (a piezo-polymer) resulted in large ME effects, with dE/dH values of 7.2 V/cm-Oe at low frequencies and up to 310 V/cm-Oe at the mechanical resonance of the heterostructure.[24]

These composite materials may consist of fairly coarse scale laminates[25,26,27,28] or heterostructured columnar nanostructures[20] or epitaxial multilayered films.[29] Examples of laminated composites are PZT/Terfenol-D[30] bonded with silver epoxy or PZT and Terfenol-D powders,[31] mixed with PVDF and hot-pressed into a three-layer stack of PZT/Terfenol-D/PZT. PVDF is required for the insulating matrix binder, which prevents eddy current loss in the Terfenol-D. In epitaxial columnar nanostructures of $BaTiO_3$-$CoFe_2O_4$ the elastic magnetoelectric coupling between ferroelectric and ferromagnetic layers is reported to be $dM/dE = 1x10^{-2}$ G-cm/V.[20,32] The columnar nanostructure effectively reduces the clamping effect of the substrate, while increasing the surface area for interaction. Heterostructured materials of Fe or LSMO on ferroelectric $BaTiO_3$ have shown straininduced changes in the magnetic properties arising from the piezoelectricity.[33,34]

1.4 Electric control of magnetic properties

The physics behind electric control of magnetism is not only exciting but also has the potential for developing a new era of electronic devices.[35] Potential applications include nano-sensors and electrically tunable magnetic data storage in Magnetoresistive Random-Access Memory (MRAM). Overheating is a major problem in nano-electronic devices and electric field control requires much lower power compared to current driven magnetic devices, such as spin transfer torque elements, which require current densities ~10^6 A/cm^2 in magnetic tunnel junctions with MgO and AlO_x tunnel barriers.[36] Applied electric fields have been shown to control a wide range of magnetic properties including the Curie temperature,[37] magnetic anisotropy, surface magnetization, exchange bias and the spin polarization. Electric fields are supplied either via applied voltages, or alternatively by means of an adjacent ferroelectric. The mechanism behind electric control of magnetic properties arises either by induced strain from the piezoelectric materials or by means of polarization charge induced effects. The electric control of magnetism has been largely based on the elastic strain.[33,38,39,40] of the piezoelectric material. The disadvantage of the piezoelectric strain based control of a thin magnetic film is that it is constrained by the substrate.

Research results of the electric control of magnetic anisotropy are presented in this dissertation, focused on mechanisms that are not strain induced but charge induced effects. Such charge induced effects have been observed in composite materials with both volatile and non-volatile electric fields.[41,42,43,44,45]

Isothermal and reversible[46] electric control of ferromagnetism has been reported in magnetic semiconductors. The hole concentration changes with the applied electric

field and changes the ferromagnetic transition temperature by altering the exchange interaction[47] among the Mn ions. Magnetization reversal[48] by electric field in [(In,Mn)As] has also been reported at low temperature. Above room temperature the electric field control ferromagnetism has been reported in quantum dots of $Mn_{0.05}Ge_{0.95}$[49] Non-volatile electric field induced changes in the Curie temperature and magnetic anisotropy of the ferromagnetic semiconductor (Ga,Mn)As have been seen, with the source of the electric field being the remanent polarization of ferroelectric P(VDF-TrFE).[50] The electric field induces change in the carrier densities in the relevant material. The electric field due to the polarization switching of the ferroelectric PVDF layer at the interface of the (Ga, Mn)As produces a change in hole concentration, thereby changing the Mn-Mn exchange interaction, which is mediated by the holes.

Magnetic anisotropy changes have been predicted[51] in thin Fe films on $BaTiO_3$ with ferroelectric polarization switching of $BaTiO_3$ using density functional theory (DFT). The effect arises from the ferroelectric displacements and electronic structure changes at the FE/FM interface. A large change in the magnetic anisotropy energy is predicted for up and down polarization states. Figure 1.1 showed the calculated value of magnetic anisotropy energy (MAE) for two different polarization orientations. However, experimental measurements of MAE in Fe-$BaTiO_3$ heterostructures are dominated by strain effects at the interface.

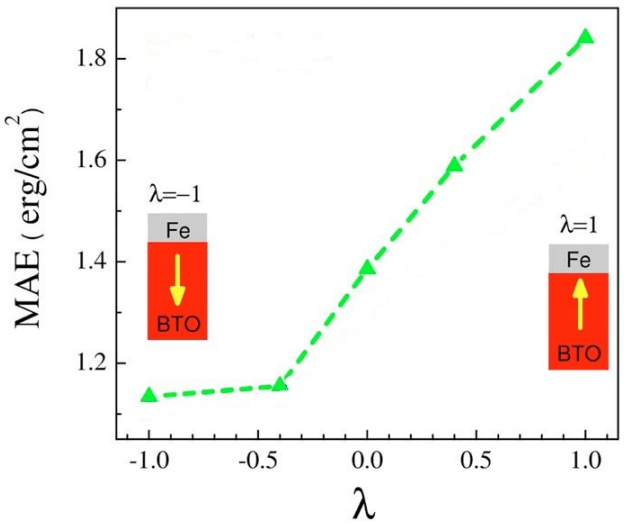

Figure 1.1: Magnetic anisotropy energy as function of a polarization scaling factor λ. Here, λ=1 and λ= -1 correspond to the spontaneous polarization up and down, respectively (After reference 51).

In epitaxial FePt or FePd films that are immersed in a liquid electrolyte, the magnetic coercivity can be reversibly modified by an external applied electric field.[52] Changes in the magnetic anisotropy from in-plane to out-of-plane in Fe/MgO[53] and $Fe_{80}Co_{20}$/MgO[54] thin film heterostructures in the presence of large externally applied fields has been experimentally demonstrated. This change possibly originates due to the change in the number of d-orbitals in Fe atoms[55,56] at the MgO interface. Thickness-dependent magnetic anisotropy changes have been reported with applied electric field in $Co_{40}Fe_{40}B_{20}$/MgO heterostructures.[57] Both the coercivity of the perpendicular magnetization region and the perpendicular magnetic anisotropy of the in-plane magnetization region can be modified by applying electric fields at room temperature.

1.5 References

[1] M. Fiebig *J. Phys. D: Appl. Phys* **38,** R123 (2005).

[2] W. Eerenstein *et al., Nature* **442,** 759 (2006).

[3] R. Ramesh *et al., Nature Materials* **6,** 21 (2007).

[4] N. A. Spaldin *et al., Science* **309,** 391 (2005).

[5] S.W. Cheong *et al., Nature Materials* **6,** 13 (2007).

[6] H. Zhen *et al., Science* **303,** 661-663 (2004).

[7] P. Curie *J. de Physique (3rd Series)* **3,** 393 (1894).

[8] P. Debye *Z. Phys.* **36,** 300 (1926).

[9] I. E. Dzyaloshinskii *J. Exptl. Teor. Fiz.* **37,** 881 (1959); *Sov. Phys.-JETP* **10,** 628 (1959).

[10] D. N. Astrov *J. Exptl. Teor. Fiz.* **38,** 984 (1960); *Sov. Phys.-JETP* **11,** 708 (1960).

[11] V. J. Folen *et al., Phys. Rev. Lett.* **6,** 607 (1961).

[12] J. Wang *et al., Science* **299,** 1719 (2003).

[13] K.Y. Yun *et al., J. Appl. Phys.* **96,** 3399 (2004).

[14] T. Kimura *et al., Nature* **426,** 55 (2003).

[15] T. Kimura *et al., Phys. Rev. B* **71**, 224425 (2005).

[16] Y. Kitagawa *et al., Nature Materials* **9,** 797 (2010).

[17] X. He *et al., Nature Materials* **9,** 579 (2010).

[18] P. Murugavel *et al., App. Phys. Lett.* **85**, 4992 (2004).

[19] C. W. Nan *et al., Phys. Rev. B* **71**, 014102 (2005).

[20] H.Zheng *et al., Science* **303**, 661 (2004).

[21] F. Zavaliche *et al, Nano Letters* **5**, 1793 (2005).

[22] S. X. Dong *et al., App. Phys. Lett.* **85,** (2004).

[23] C. G. Duan *et al., Phys. Rev. Lett.* **95,** (2006).

[24] J. Zhai *et al., App. Phys. Lett.* **89**, 083507 (2006).

[25] C. W. Nan *et al., Appl. Phys. Lett.* **81,** 3831 (2002).

[26] Mori et al., Appl. Phys. Lett. 81, 1 (2002).

[27] N. Cai *et al., Appl. Phys. Lett*. **84,** 3516 (2004).

[28] G. Srinvasan *et al., Phys. Rev. B* **65,** 134402 (2002).

[29] M. K. Lee *et al., Appl. Phys. Lett.* **77,** 3547 (2000).

[30] J. Ryu *et al., Japan. J. Appl. Phys.* **40,** 4948 (2001).

[31] C. W Nan *et al., Physical Review B* **71,** 014102 (2005).

[32] F. Zavaliche *et al., Nano Letters* **5**, 1793(2005).

[33] S. Sahoo *et al., Phys. Rev B* **76**, 0092108 (2007).

[34] E. Eerenstein *et al., Nature Materials,* **6**, 348 (2007).

[35] V. E. Wood & A. E. Austin, *Int. J. Magn.* **5,** 303 (1974).

[36] Z. Diao et al., Appl. Phys. Lett. **87**, 232502 (2005).

[37] Y. Nishitani *et al., Physical Review B* **81,** 045208 (2010).

[38] N. A. Spaldin *et al., Science* **33,** 1047 (2008).

[39] S. H. Baek *et al., Nature Materials* **9,** 309 (2010).

[40] Y. H. Chu *et al., Nature Materials* **7,** 478 (2008).

[41] L. F. David *et al., J. Phys. C: Solid State Phys*. **10,** L329 (1977).

[42] S. Zhang *Physical Review Letters* **83,** 640 (1999).

[43] T. Cai *et al., Physical Review B* **80,** 140415(R) (2009).

[44] J. M. Rondinelli *et al., Nature Nanotechnology* **3,** 46 (2008).

[45] C. G. Duan *et al., Phys. Rev. Lett.* **101,** 137201 (2008).

[46] H. Ohno *et al., Nature* **408,** 944 (2000).

[47] T. Diet *et al., Science* **287,** 1019 (2000).

[48] D. Chiba *et al., Science* **301,** 943 (2003).

[49] F. Xiu *et al., Nature Materials* **9,** 337 (2010).

[50] I. Stolichnov *et al., Nature Materials* **7**, 464 (2008).

[51] C. G. Duan *et al., Appl. Phys. Lett.* **92**, 122905 (2008).

[52]M. Weisheit *et al., Science* **315,** 349 (2007).

[53] T. Maruyama *et al., Nature Nanotechnology* **4,** 158 (2009).

[54]Y. Shiota, *et al., Applied Physics Express* **2,** 063001 (2009).

[55]M. K. Niranjan *et al., Appl. Phys. Lett.* **96,** 222504 (2010).

[56]K. Nakamura *et al., Phys. Rev. B* **80,** 172402 (2009).

[57]M. Endo *et al., Appl. Phys. Lett.* **96,** 212503 (2010).

Chapter 2

Sample Preparation and Characterization Techniques

This chapter describes the sample preparation and characterization techniques that were used in this thesis. Sample deposition techniques include sputtering and thermal evaporation for deposition of metallic and insulator films, which are described in 2.1 and 2.3 respectively. Langmuir-Blodgett techniques are used for the deposition of the thin polymer ferroelectric films and are described in section 2.2. Sample characterization techniques include structural characterization using X-ray diffraction (XRD), X-ray reflectivity (XRR) and Atomic Force Microscopy (AFM) measurements for crystalline structure, thickness, roughness and continuity of the samples. Electrical characterization includes pyroelectric measurements, which characterize the polarization hysteresis loops of the ferroelectric layer. Magnetic characterization includes both the polar and longitudinal magneto-optical Kerr effects (MOKE) for in-plane and out-of-plane components of magnetization respectively. Microscopic magnetic domain images were obtained using magnetic force microscopy (MFM) imaging.

2.1 Magnetron Sputtering

Sputtering is a common thin-film deposition process that relies on the ejection of atoms from solid targets by bombardment with energetic particles. All sputtered samples in this thesis were made in an Ar gas atmosphere. The base pressure of the sputtering chamber is of the order of 10^{-8} Torr. An energy source applies either DC (direct current)

or RF (radio frequency) voltages across the electrodes to create and maintain plasma inside the vacuum chamber.

A voltage of -2kV to -5kV is applied across the grounded sample holder and target (cathode), resulting in the emission of free electrons, which accelerate and collide with the Ar atoms. Free electrons with sufficient kinetic energies (>15 eV) are able to repel the outer most electrons of the Ar atoms and knock them out from the atoms [1] leaving behind ionized Ar^+ ions. In turn these positively charged ions (Ar^+) are accelerated to the negatively charged target (cathode), and kick out target atoms. 95% of the incident energy is deposited in the target and 5% of the incident energy is carried off by the target atoms (~100 eV). Free electrons both maintain the plasma by creating more Ar^+ ions, while some free electrons recombine with the Ar^+ ions, creating neutral Ar atoms. This recombination process produces photons, giving the characteristic plasma glow. Conventional sputtering has two major drawbacks: (i) The sputtering yield is very low and (ii) electrons also strike the substrate and can cause structural and heating damage. These problems are overcome by the use of magnetron sputtering. In magnetron sputtering, a magnetic field perpendicular to the applied electric field is applied so that electrons are trapped just above the target in a helical path. This results in increased electron-Ar^+ collisions close to the target, therby increasing the sputtering rate, while at the same time decreasing electron collisions with the substrate.[2]

RF voltage sources are necessary for the sputtering of insulating materials because DC voltages lead to charge accumulation on the insulator cathode surface. At low RF frequencies, electrons and ions both move in the alternating potential and the cathode and anode switch on each half cycle, resulting in sputtering of both the target and

the substrate. At higher RF frequencies (> 50 kHz), the heavier ions cannot move at the RF frequency and the electrons neutralize the positive charge buildup on the cathode making insulator sputtering possible. The majority of RF sputtering is performed at a frequency of 13.56 MHz.

For a given material in a given sputtering gas environment the sputtering rate depends on two factors: (i) gas pressure and (ii) cathode voltage. In a typical deposition we strike the plasma at 25 mT of Ar pressure with a sputtering power of 40 W and then reduced the pressure to 2 mT during deposition. More details on the sputtering procedures can be found in references 1 and 2.

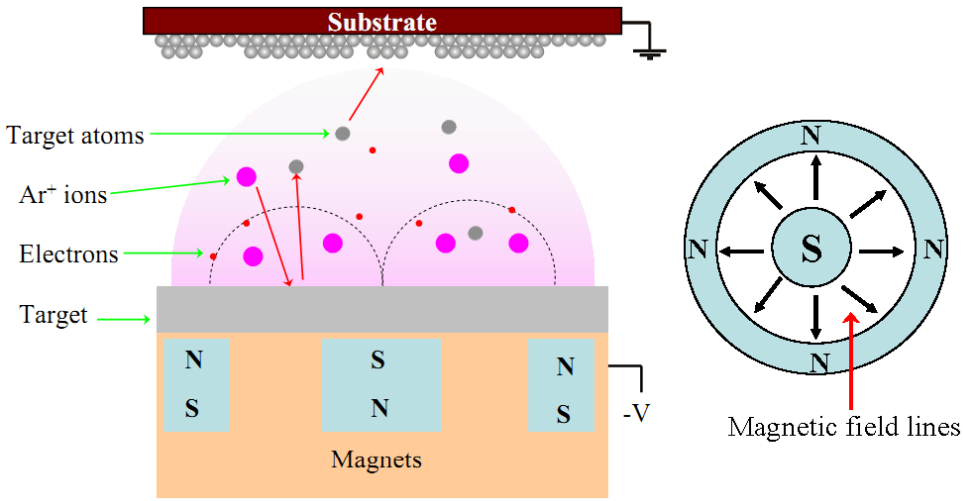

Figure 2.1: Schematic diagram of the sputtering process. The target is installed on the magnetron assembly. Ionized Ar atoms knock out target atoms which are then deposited on the substrate. The inset on the right is a top view of the magnetic field assembly below the target.

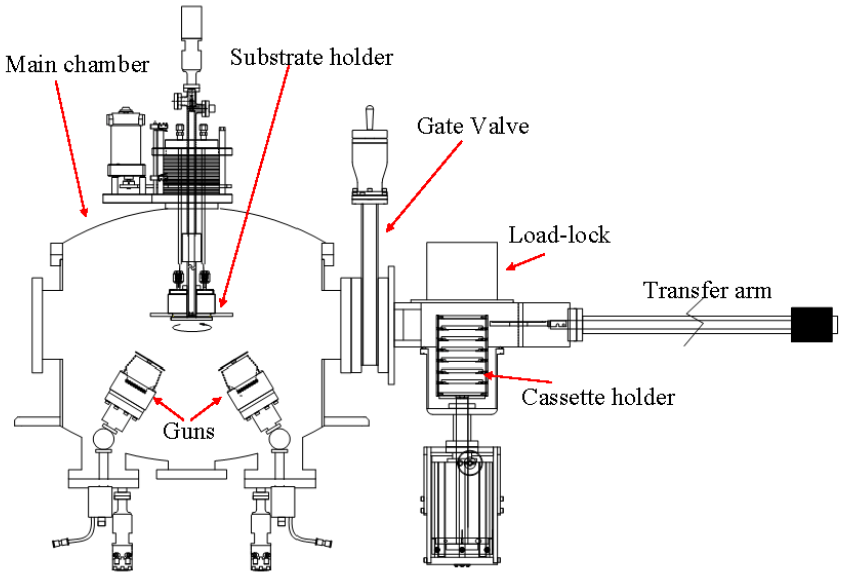

Figure 2.2: This schematic diagram of the AJA ATC-2000V Phase-II sputtering chamber is taken from the AJA website. [3] For details see the text.

The magnetron sputtering chamber used to grow thin films is from AJA International, Inc., model number AJA ATC-2000V Phase-II computer controlled sputtering chamber. [4,5] This has two chambers, a main chamber and a load lock chamber. Each chamber is equipped with its own pumping system and the two chambers are separated by a gate valve. The main chamber is equipped with a Varian TV-551 turbo navigator backed by an Alcatel ACP-28 roots pump and the load lock is equipped with a Varian TV-301 turbo navigator backed by a Varian SH-110 dry scroll pump. There are 4 sputtering guns in a con-focal geometry. Two of them are designed for magnetic targets. Since the magnetic targets produce their own strong magnetic field lines there need to be stronger magnetic fields to trap the electrons near the targets in a helical path. Of the four guns, two are operated as DC guns are using the Advanced Energy MDX 500 power

supply for metallic sputtering and two as RF guns using the Advanced Energy RF-5S for sputtering of insulators as described above. The RF power supply operates at a frequency of 13.56 MHz. Up to 12 substrates may be loaded into the load lock for sequential deposition without breaking the vacuum. In addition, an in situ mask changer in the load lock allows us to change shadow masks without breaking vacuum. The mask changer allows for 90 degree rotation, enabling the in-situ deposition of top and bottom electrodes perpendicular to each other. An advantage of the con-focal deposition system lies in the ability to make either wedges (see chapter 5) or films of uniform thickness by rotation of the guns. The optimal gun angle for uniform film thickness in our system corresponds to a reading of 4.5 mm on a linear scale attached to the bottom of the guns, which corresponds to an angle of approximately 60º to the normal. The substrate is transferred to the main chamber from the load lock using an extended arm and attached to the substrate holder for deposition. For uniform thickness, the substrate is rotated during deposition. During deposition through shadow masks, the rotation is controlled at the minimum speed sufficient to ensure uniform thickness. The substrate holder can be heated up to 500 ºC for high temperature sputtering deposition or in-situ annealing of the deposited films. The argon flow rate is controlled by the mass flow controller at a rate of 13.81 standard cubic centimeters per minute (sccm). The sample thickness is monitored by an Inficon XTM/2 quartz crystal thickness monitor.[6] The sputtering guns and the turbo pumps are cooled using chilled water flow from a water chiller at a typical temperature of 16 ºC with a pressure of 75 psi.

2.2 Langmuir-Blodgett deposition of P(VDF-TrFE) copolymers

A Langmuir-Blodgett (LB) film is defined as monolayer deposition of a film on a solid substrate from a liquid surface that is formed by dipping the substrate into the liquid. [7,8] Ideally, each deposition transfers one monomolecular with uniform thickness. Amphiphilic monolayers, on a water subphase, such as fatty acids, will orient vertically with a hydrophilic head pointing into the subphase and the hydrophobic tail pointing away, so that successive dips result in a single oriented layer.[9] Although P(VDF-TrFE) copolymers are not amphiphilic molecules, a variation of the LB technique, the Langmuir Schaefer technique has been successfully used to grow highly crystalline thin films of P(VDF-TrFE) with monolayer control of the thickness.[10] Because the copolymers are insoluble in water, the P(VDF-TrFE) copolymers form floating metastable monolayers on the water surface.[10]

A NIMA model 622C LB trough was used to fabricate the LB films of P(VDF-TrFE). The trough is first cleaned with ultra-pure distilled water purified by the reverse osmosis process and with a small home made vacuum cleaner, equipped with a pipette. The cleaned trough is then filled with the distilled water (with a water resistance of 18.2 MΩ). The barriers (to control the water surface area and surface pressure) are then closed to the minimum area and the water surface is cleaned thoroughly with the pipette vacuum cleaner. This cleaning procedure is repeated 2-3 times. The water temperature is kept constant at 25 ºC during the deposition. A pressure-area isotherm confirms the cleanliness of the trough- a clean water surface will result in a pressure-area isotherm that is a straight line with pre-set surface pressure of zero. The barriers are open all the way and pre-cleaned glass slides are slid into the water, at an angle ~ 15º to the water surface,

tilted and half-way submerged in the water. Prepared solutions of P(VDF-TrFE) in DMSO with 0.05-0.06% weight concentration are dispersed on the tilted glass slides using a microliter syringe one drop at a time with each drop containing 20 μL of solutions. Droplets of the polymer solution then drain slowly onto the water surface from the inclined glass slide. This process is continued until approximately 1.5 mL of solution is dispersed on the water surface. The glass slides are removed from the water, and a pause of 15-20 minutes allows for evaporation of the DMSO, leaving only the polymer chains on the water surface. The barriers are then slowly closed at a rate of 200 cm^2 / min using pressure control until the solid phase surface pressure of 5 mN / m is achieved and this pressure is maintained throughout the deposition process. The copolymer chains are aligned parallel to the cross-section of the trough and ready to be transferred to the substrate. The monolayers are transferred using the horizontal Schafer method (details can be found in reference 9, 10). This is done by keeping the substrate horizontal to the water surface with a small tilt angle of about 10 degrees to avoid air bubbles. The substrate touches water, the tilt angle is slowly reduced to zero and then tilted back and withdrawn slowly so that the meniscus line moves across the substrate slowly enough to prevent significant strain or damage to the film. The substrate is allowed to dry between layer depositions to remove water droplets.[11] As P(VDF-TrFE) is not amphiphilic, the film on the trough is thicker than one monomolecular layer. The polymer films deposited using this method have a thickness of approximately 1.8 nm per 1 LB layer determined by variable-angle spectroscopic ellipsometry measurements, corresponding to ~ 3ML of P(VDF-TrFE).[12,13]

2.3 Thermal Evaporation

Top electrodes have been deposited on the copolymer using thermal evaporation, because evaporated materials have relatively low energies corresponding to the evaporation temperature (typically 1000 ºC or ~ 0.2 eV), as compared to sputter deposited materials with energies of 10-100 eV. This makes evaporation a much better deposition technique for electrodes on soft polymer films. Thermal evaporation is carried out in a Bal-tec MED 020 evaporation system with a Sycon STM / MF quartz crystal thickness monitor, typically at a base pressure of 4×10^{-5} mbar and at a rate of 1-2 Å/s. Tungsten wire baskets were used to hold the deposition material while a current of 20 A passed though the basket to heat and evaporate the material.

2.4 Annealing of P(VDF-TrFE) films

After deposition, the P(VDF-TrFE) films were annealed at temperatures of 130 – 135 ºC, above the ferroelectric to paraelectric phase transition temperature, but well below the melting temperature resulting in a reorientation of the polymer chains due to increased mobility. Thermal annealing has been shown to substantially increase the crystallinity of the films.[14] The rate of heating is 1.5 ºC/min in an isolated annealing chamber. The sample is kept at 130 – 135 ºC for at least an hour and the temperature is then decreased to room temperature at the same rate. In thinner films of less than 10 ML, the P(VDF-TrFE) films form nanomesas upon annealing.[15]

2.5 Pyroelectric measurements

The polarization of the ferroelectric layers has been measured using the pyroelectric effect, which is defined as the change in electric surface charge developed in certain polar materials on heating or cooling the material. Note that pyroelectricity and thermoelectricity are distinct phenomena. In pyroelectricity the entire sample temperature is changed whereas in thermoelectricity only one end of the sample is heated, resulting in a temperature gradient.[16] Pyroelectric materials have no center of symmetry, resulting in a dipole moment and spontaneous polarization arising from the dipole moment. If an applied electric field can reverse the dipole moment then the material is ferroelectric. In a parallel plate capacitor structure, the polarization cannot be measured directly at constant temperature, because the surface charge is compensated by free charges in the electrode. In a ferroelectric crystal, when the temperature increases (decreases) the polarization decreases (increases) as does the bound charge. The change in the compensating free charge constitutes the pyroelectric current. The pyroelectric coefficient is defined by $p = \left[\frac{\partial P_s}{\partial T}\right]_{(\sigma,E)}$, where (σ, E) specify that the measurements are done at constant stress σ and constant electric field E. Pyroelectric measurements are performed by heating or cooling the sample and measuring the resultant current at the electrodes. The pyroelectric current can be written as $I = Ap_3(eff)\frac{\partial T}{\partial t}$, where $p_3(eff)$ depends on the pyroelectric coefficients p and on the piezoelectric tensors. The pyroelectric measurements are done in a parallel plate capacitor structure with the ferroelectric film in between two metallic electrodes, the film is constrained to the substrate and stress free normal to the surface and strain free in-plane.[17] The measured pyroelectric coefficients $p_3(eff)$ consists of two

terms, the primary effect and the secondary effect: $p_3(eff) = \left(\frac{\partial P_s}{\partial T}\right)_s + \frac{d_{33}^T \alpha_3^s}{s_{33}^s} = \left(\frac{I}{A}\right)\left(\frac{\partial T}{\partial t}\right)^{-1}$, where P_s is the spontaneous polarization, T is temperature, S is the strain, d_{33}^T is the stress-free piezoelectric coefficient, s_{33}^s is the elastic compliance coefficient, α_3^s is the thermal expansion coefficient, I is the pyroelectric current, A is the surface area and $\frac{\partial T}{\partial t}$ is the rate of temperature change.

Careful experiments by Bune *et al.,* [17] have shown that the pyroelectric response is directly proportional to the net sample polarization in P(VDF-TrFE). The piezoelectric coefficient is proportional to the pyroelectric current and both of them are proportional to the spontaneous polarization [see figure 2.4 (a)]. Hence this method can be used to measure the remanent polarization hysteresis loops.

The Chynoweth modulation method is used to measure the pyroelectric current,[18,19] the schematic diagram of which is shown in Figure 2.4 (b). The heat source is a 1-3 mW diode laser and the temperature is modulated using an optical chopper of frequency 2 kHz. The wavelength of the laser light is 658 nm corresponding to a maximum photon flux of 2.5 x 10^{18} photons/m^2s. The laser spot size is comparable to the sample spot size (1 mm^2 or 0.04 mm^2 depending on the sample). The laser light is incident perpendicular to the sample surface. A DC voltage is applied to polarize the sample using the Keithley 2400C source meter. The pyroelectric signal is measured by biasing the sample at each voltage for few minutes and then removing the voltage. Data are taken at zero bias using a Stanford Research System SR830 DSP lock-in amplifier at a frequency of 2 kHz corresponding to the chopper frequency. The sign of the pyroelectric current is arbitrarily chosen so that positive FE saturation polarization

corresponds to positive pyroelectric current. This is done by choosing a suitable phase on the lock-in amplifier, which is subsequently kept constant during the entire pyroelectric hysteresis measurement. This method measures the equilibrium remanent polarization, and for P(VDF-TrFE) films, has been shown to be almost equivalent to the polarization.

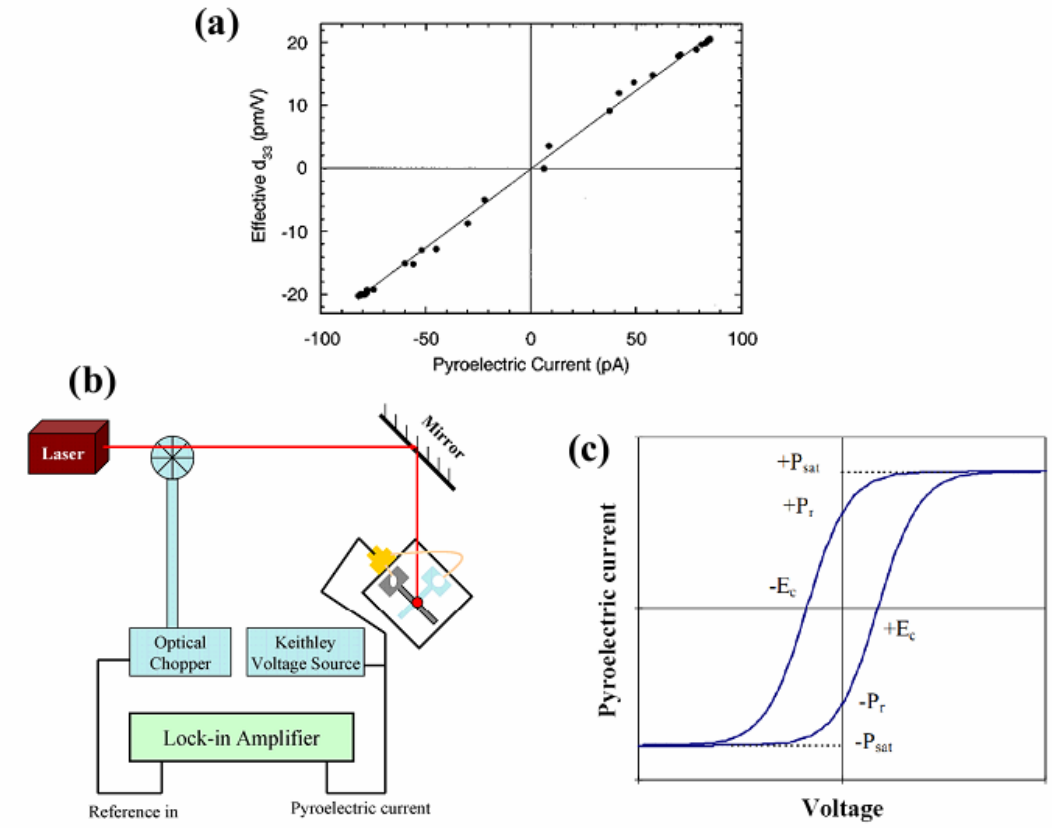

Figure 2.4: (a) Experimentally measured piezoelectric coefficient (d_{33}) is directly proportional to the pyroelectric current after Bune *et al.,* [17]. (B) Schematic diagram of the pyroelectric measurement set up. (c) Schematic of a typical ferroelectric hysteresis loop measured by pyroelectric current with applied voltage.

A schematic diagram of a typical hysteresis loop is shown in figure 2.4 (c). At a high positive saturation electric field all ferroelectric domains are aligned along the applied electric field direction, resulting in saturation polarization P_s. As the field is decreased to zero, the polarization decreases slightly to the remanent polarization P_r, which is defined as the polarization at zero applied voltage. P_r is slightly smaller than P_s because some domains relax back to the original state. The electric field needed to bring the polarization to zero on the opposite side of the saturation electric field is called the coercive field E_c. The hysteresis arises due to the energy loss (area inside the loop) in each cycle during the reversal of the dipoles. In our pyroelectric hysteresis loop measurements the conductivity of the top and bottom electrodes (different metallic electrodes) are different and hence the hysteresis loop is shifted along the vertical axis.

2.6 Magneto-Optical Kerr Effects (MOKE)

When linearly polarized monochromatic light is incident on a magnetized surface, the reflected and transmitted light is in general elliptically polarized, with the polarization axis rotated by an angle with respect to the incident light. The Faraday and Kerr effects refer to the changes in polarization of the transmitted and reflected beams respectively. The off-diagonal elements of the dielectric tensor are responsible for the magneto-optical Kerr and Faraday effects. The diagonal elements describe the optical properties of the film in the absence of magneto-optical effects. Magneto-optical Kerr effects (MOKE) can be defined macroscopically as the interaction of the magnetic sample with the electromagnetic field of the laser light and represented by the dielectric tensor. The off-

diagonal elements of the dielectric tensor are linearly proportional to the magnetization, which occur through different absorption of left and right circular polarized light.

The Kerr effect is directly proportional to the component of magnetization parallel to the plane of incident light and in the first order approximation a hysteresis loop of the magnetization can be measured. The MOKE technique measures the change of the polarization states of the incident light when reflected from the surface of a magnetic material. Linearly polarized light experiences a rotation of the polarization plane (Kerr rotation θ_K) and a phase difference between the electric field components perpendicular and parallel to the plane of the incident light (Kerr ellipticity ε_K).

MOKE is a highly sensitive technique and one of the few techniques that allow for the measurement of in-plane and out-of-plane components of magnetization of the magnetic sample separately. The biggest disadvantage of MOKE is that it measures only relative changes in the magnetization of the magnetic samples. However, it remains a very useful technique to measure surface magnetization and the shape of magnetic hysteresis loops.

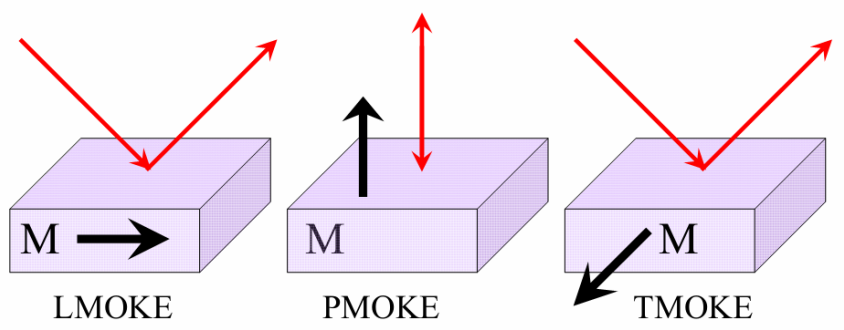

Figure 2.5: Schematic of the three different MOKE configurations, PMOKE, LMOKE, and TMOKE. The black and red arrows depict the magnetization component that is measured and the light propagation direction respectively.

MOKE measurements are usually performed in one of three different configurations, which differ in the polarization direction of the incident light and applied magnetic field direction. These are commonly known as the polar, longitudinal and transverse. Polar MOKE (PMOKE) measures the perpendicular component of the sample magnetization whereas longitudinal MOKE (LMOKE) measures the in-plane component of magnetization. In LMOKE the magnetic field is applied parallel to the sample surface and the plane of incidence is perpendicular to the sample surface. Incident s-polarized or p-polarized light upon reflection from the sample surface will be elliptically polarized due to the component of the magnetization perpendicular to the incident electric field vector. In PMOKE the applied magnetic field direction is parallel to the plane of incidence but perpendicular to the sample surface. PMOKE measurements are maximized at normal incidence whereas for LMOKE no effect will be observed at normal incidence. In TMOKE the magnetization vector is parallel to the sample surface but perpendicular to the plane of incidence. TMOKE only deals with p-polarized light and only measures changes in refractive index.

The experimental set up for MOKE measurements[20,21,22,23] consists of a laser diode, a polarizer, a Hinds photo-elastic modulator (PEM -90), an analyzer, a photo-detector, GMW electromagnets with Kepco power supply and a SRS 830 Lock-in amplifier (Stanford Research Systems, SR830 DSP). The laser diode is set at constant current mode with a current of 45 to 50 mA (~ 0.1 mW) using the controller (ThorLabs model # LDC 205B LD) and the temperature of the laser diode is maintained at ~ 15 ºC with a temperature controller (ThorLabs TED 200). The wavelength of the laser light is 658 nm. For LMOKE measurements the incident light makes an angle ~ 45º to the

sample surface normal where as in case of PMOKE measurements the incident light is normal to the surface. In case of LMOKE measurements the incident angle is smaller than the Brewster angle between the air / Co interfaces (~63º) so the reflection of p-polarized light is minimized while the longitudinal Kerr rotation of s-polarized light increases linearly with increasing angle of incidence up to the Brewster angle.[24,25] The details of the MOKE measurement and optimization which are followed in our measurements can be found in reference 26. [26]

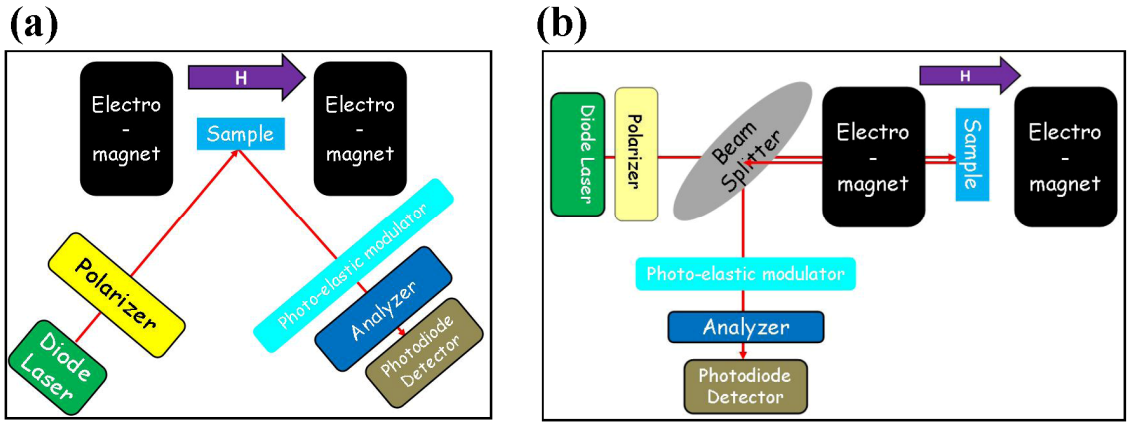

Figure 2.6: Schematic set up of (a) LMOKE and (b) PMOKE.

Linearly s-polarized light is reflected from the desired spot and then transmitted through the photo-elastic modulator (PEM).[27] The PEM consists of a transparent solid material, stressed by compression or stretching, that is birefringent so that different linear polarizations of light have slightly different speeds of light when passing through the material. When the PEM is compressed the polarization component parallel to the modulation axis travels slightly faster than the vertical component. The horizontal component then leads the vertical component. The phase difference between the

components is called the retardation. The output MOKE signal is then modulated by the phase retardation from the PEM. The modulation signal is set up as the reference signal for lock-in measurements. The reflected light is transmitted through an analyzer, which is set almost perpendicular to the polarization direction so that it blocks almost all the incident polarization and transmits the component generated by Kerr interaction to the photo detector. An electromagnet (GMW 3470) with Kepco BOP 50-8M power supply is used to generate the magnetic field. Data collection is done using LabVIEW programs controlled via a GPIB card.

A detailed derivation of the MOKE signal can be found in the PEM application note. [28] As described earlier, the polarization state changes after reflection from magnetic materials and an ellipticity ε_k is introduced with the plane of polarization rotating by an angle θ_k. The intensity of light incident on the detector can be written as, $I(t) \cong I_0[1 + 2\theta_k J_0(A_0) - 4\varepsilon_k J_1(A_0)\sin(\omega t) + 4\theta_k J_2(A_0)\cos(2\omega t)]$, where ω is the angular frequency of the PEM, A_0 is the amplitude of retardation in the PEM which corresponds to the phase angle between the two polarization direction and J_n are the Bessel functions. Setting the PEM amplitude, A_0=2.405 radians, (which is the zero of J_0) eliminates the J_0 term leaving a DC term ($V_{DC} = I_0$), a first harmonic term $4\varepsilon_k J_1(A_0)\sin(\omega t)$ which determines the ellipticity ε_k, and a second harmonic term $4\theta_k J_2(A_0)\cos(2\omega t)$, which determines rotation θ_k. Thus ε_k and θ_k can be measured from the equations $\theta_k = \frac{\sqrt{2}V_{2f}}{4J_2V_{DC}}$ and $\varepsilon_k = \frac{\sqrt{2}V_{1f}}{4J_1V_{DC}}$. The $\sqrt{2}$ factor arises because the lock-in amplifier will measure the

of the rms voltage. Either of the two equations above can be plotted as a function of magnetic field resulting in a magnetic hysteresis loop.[29]

When dealing with MOKE measurements in a heterostructure containing both ferroelectric and ferromagnetic components, the electro-optic effects present in all ferroelectric materials will contribute to the measured MOKE intensity. This will alter the Kerr intensity but will have no effect on the observed coercivity change. This is an important point of consideration when dealing with the polarization induced changes in magnetic coercivity (See chapter # 5).

2.7 Atomic Force Microscopy (AFM) & Magnetic Force Microscopy (MFM)

Atomic force microscopy (AFM) is a useful technique for obtaining topographical images of samples. Our measurements use the model Dimension 3100 from Digital Instrument for AFM measurements with a Si tip of radius of curvature of approximately 6 nm. AFM scanning was done using non-contact tapping mode. The flexible cantilever of the AFM tip oscillates at resonance frequency of ~ 100 kHz with fixed amplitude. This amplitude determines the separation between the tip and the sample surface and is kept constant for the entire sample scan. The force between the tip and sample surface depends on the oscillation amplitude. A piezoelectric transducer is used to mount the AFM tip. This transducer controls the height and oscillation amplitude of the AFM tip depending on the sample surface topography. The position of the AFM tip is detected by a laser beam which is reflected back to the cantilever.

Magnetic force microscopy (MFM)[30,31,32,33] is a powerful tool for imaging magnetic surfaces of a thin film. This is based on the interaction between a sharp magnetized tip and a magnetic surface.[34] The interaction between the magnetic tip and the magnetic surface can be written as, $\vec{F} = \mu_0(\vec{m}.\nabla)\vec{H}$ where $\vec{m}$ is the magnetic moment of the tip and $\vec{H}$ is the magnetic stray field from the magnetic sample. The stray fields of the sample from the nonuniform distribution of the magnetization exert a force on the magnetic tip. The stray fields are different for in-plane films compared to a perpendicular film. For in-plane magnetization the contrast only appears in the vicinity of the domain walls but for perpendicular magnetization a sharp transition between up and down domains is observed. This force deflects the cantilever and using laser reflection from the cantilever, the deflection of the laser spot is measured to measure the cantilever motion, which measures the force gradient.

MFM tips are coated with high coercivity magnetic materials (such as Co) to keep the magnetization direction of the tip unaltered during image scanning. The coated thickness is around 50 nm. MFM scanning is done using the lift method. In this method, normal tapping mode scans are performed first to obtain the topography of the surface followed by scans in which the cantilever is lifted up and the tip follows the topography so that it does not touch the surface (the interleave mode). The distance from the sample to tip is kept constant at approximately 50 nm during the scan depending on the sample roughness. This distance is necessary to avoid other forces such as electrostatic repulsion or atomic forces. A piezoelectric transducer is used at a resonant frequency of 100 kHz to 400 kHz to drive the cantilever.

The disadvantages of using the MFM include lift height dependence and the static charge on the sample. The image depends on the tip magnetic material and magnetic moments from the tip and sample can alter the magnetization of the sample or tip. However this is a very useful technique to measure magnetic profiles. The sample does not need to be electrically conductive and it can be measured at any temperature, in UHV. Long-range magnetic interactions are not affected by surface contamination.[34]

2.8 X-ray Diffraction (XRD)

Both X-ray diffraction (XRD) and X-ray reflectivity (XRR) were used to characterize the structure of thin film samples, in order to obtain the crystal structure as well as details of multilayer thickness and roughness. [35]

Because atomic spacings within a crystal and x-ray wavelengths are of the same order of magnitude, x-ray diffraction is a powerful tool in the investigation of crystal structure. XRD measurements were done using the Rigaku D / Max-B Diffractometer. XRR and XRD measurements were also done in the Bruker-AXS D8 Discover High-Resolution Diffractometer with the HI-STAR area detector or point detector. X-rays for these table top sources are produced by a process of energetic electron bombardment on a metallic target. X-rays are produced in an X-Ray tube with two electrodes, an anode (target metal) and cathode (electron source). The anode is maintained at ground potential and a very high negative voltage (-40 kV in our case) applied on the cathode. The anode is a water cooled block of the desired target material (in our case Cu). The electrons are emitted and accelerated away from the cathode and hit the anode with high momentum, producing X-rays, by ejecting electrons from the K-shell of the target anode. An outer

shell electron jumps into the K shell to fill the vacancy and emits a photon to conserve momentum. These photons are at the characteristic wavelengths of K_α, K_β etc depending on the shells (L, M,…)from which the electrons originate.[36,37] In our case Cu K_α X-rays are used which originate from the electron transitions from the L to K shell with a wavelength of 1.54Å.

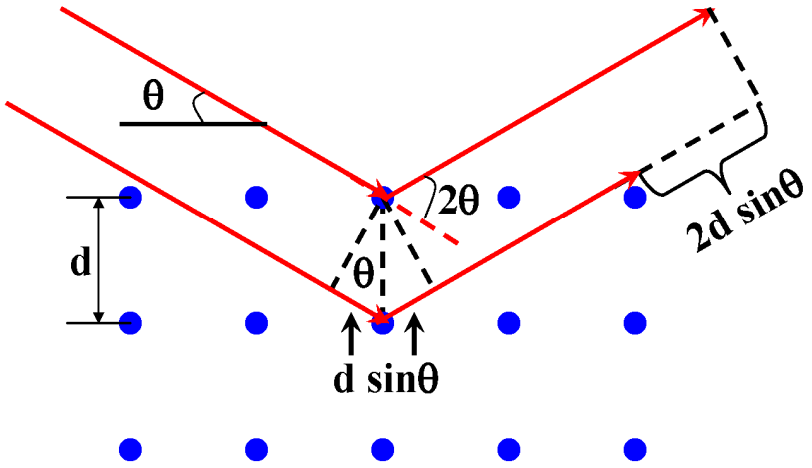

Figure 2.8: Sketch of X-ray diffraction and Bragg's law. X-rays are diffracted from a set of parallel planes separated by a distance d. The path difference between the two diffracted beams from the adjacent planes is 2dsinθ and if this equals an integral multiple of the X-ray wavelength nλ, constructive interference will result in a high intensity.

X-ray diffraction peaks can be explained in terms of Bragg's Law (Figure 2.9).[35] Let us consider a crystal with its atoms periodically arranged in set of parallel planes at a distance d apart as shown in figure 2.9. When a monochromatic X-ray beam is incident on this crystal the X-ray will be scattered in all directions from all the atoms of the

crystal. As the scattered X-ray beam is reflected from successive adjacent planes, certain conditions will lead to constructive interference. If the X-ray is incident at an angle θ to the crystal plane then the reflected X-ray from the next plane will have a difference in path length of $2d\sin\theta$. If the path difference is equal to an integral multiple of the X-ray wavelength, constructive interference will occur. The Bragg equation can be written as, $2d\sin\theta = n\lambda$. In the Bragg geometry, the angle between the diffracted and transmitted beam, the diffraction angle, is always 2θ. The sets of parallel planes are described by the Miller indices <hkl>. The distance between two adjacent hkl planes can be calculated from Bragg's Law. For example in a simple cubic lattice with lattice parameter a the distance between adjacent planes is $d_{hkl} = \frac{n\lambda}{2\sin\theta} = \frac{a}{\sqrt{h^2+k^2+l^2}}$ and hence the position of the peak in 2θ will give the distance between adjacent planes d_{hkl} and allow for a determination of the crystal structure.[36]

2.9 X-ray Reflectivity (XRR)

Besides looking at XRD peaks to obtain information on the crystal structures, X-rays can be used to check the surface roughness, film thickness electron density and density (ρ) of thin films. The Fresnel reflectivity, which is the modulus of the square of the coefficient R(θ), can be written as $R(\theta) = rr^* = \left|\frac{\theta - \sqrt{\theta^2 - \theta_c^2 - 2i\beta}}{\theta + \sqrt{\theta^2 - \theta_c^2 - 2i\beta}}\right|$, where β is the absorption coefficient and θ_c is the critical angle.[5,38] The refractive index of X-rays in any medium is less than unity and defined as $n = 1 - \delta - i\beta$, where δ is the dispersion factor

and β is the absorption factor. The absorption factor is approximately 3 orders of magnitude less than the dispersion factor[39] and we can safely assume no X-ray absorption. The Fresnel reflectivity with angle of incidence θ decreases rapidly at angles greater than the critical angle θ_c, which can be written in terms of the dispersion factor[40] as $\theta_c = \sqrt{2\delta}$.

At the interface of two materials there is a change in density giving rise to a change in refractive index. This change in refractive index will result in reflections and transmission of X-rays at the interface between two materials. X-rays reflected from the top and bottom surfaces of a thin film will result in constructive interference if the path difference is an integral multiple of wavelength $2d\sin\theta = n\lambda$, where d is the thickness of the film and θ in the incident X-ray angle. To obtain the thickness of the films, the interference peak positions are determined. Because it may be difficult to see the small oscillations in the reflectivity data, the Fresnel reflectivity background, which goes as K^4 (where K is the scattering vector defined as $K = \frac{4\pi}{\lambda}\sin\theta$), is subtracted. The modified intensity is now $I_{\text{mod}} = IK^4$. A plot of I_{mod} with 2θ makes it easier to identify the maxima and minima positions in the reflectivity data. The modified Bragg equation can be written as, $(n+\Delta n)\lambda = 2d\sqrt{\sin^2\theta_m - \theta_c^2}$ and is used to calculate the thickness of the film if the first order reflectivity peak is known. Assuming the small angle approximations $\sin^2\theta_m = \theta_m^2 = \frac{\lambda^2}{4d^2}(n+\Delta n)^2 + \theta_c^2$, where n is the reflection order and Δn has values $\frac{1}{2}$ for maxima and 0 for minima if $\rho_{\text{film}} > \rho_{\text{substrate}}$ and 0 for maxima and $\frac{1}{2}$ for minima if

$\rho_{substrate} > \rho_{film}$. A plot of θ_m^2 with $(n+\Delta n)^2$ will result in a straight line with the slope related to the thickness d using the formula $d = \frac{\lambda}{2\sqrt{Slope}}$ and the y-intercept giving the critical angle squared. This method of determining the thickness of the films is called the Kiessig fringe method and is a very precise method for obtaining film thicknesses down to a few monolayers.

For multilayered heterostructures, more complex fitting routines allow us to obtain information on layer thicknesses, roughness and density. The LEPTOS software package from Bruker AXS[41] has been used to fit the XRR data described in this thesis.

2.10 References

[1] Milton Ohring, Materials Science of Thin Films, Academic press, California (2002).

[2] J. Vossen and W. Kern, Thin Film Processes, Academic Press, New York (1978).

[3] http://www.ajaint.com/systems_atc.htm.

[4] http://www.ajaint.com/systems.htm

[5] A. Baruth, Ph. D. thesis, University of Nebraska-Lincoln, (2009).

[6] http://www.inficonthinfilmdeposition.com/en/xtm2thinfilmmonitor.html

[7] http://en.wikipedia.org/wiki/Langmuir%E2%80%93Blodgett_film.

[8] http://www.ksvnima.com/langmuir-and-langmuir-blodgett-troughs.

[9] Hubert Motschmann and Helmuth M¨ohwald, Handbook of Applied Surface and Colloid Chemistry. Edited by Krister Holmberg (John Wiley & Sons, Ltd 2001).

[10] S. Ducharme *et al.,* Ferroelectric and dielectric thin films, edited by H. S. Nalwa (Academic press, 2002).

[11] Timothy Reece, Ph. D. Thesis, University of Nebraska-Lincoln (2007).

[12] Jihee Kim, Ph.D. Thesis, University of Nebraska-Lincoln (2008).

[13] M. Bai et al. J. Appl. Phys. 95, 3372 (2004).

[14] M. Bai, Ph.D. Thesis, University of Nebraska-Lincoln (2002).

[15] M. Bai and S. Ducharme Appl. Phys. Lett. 85, 3628 (2004).

[16] http://en.wikipedia.org/wiki/Pyroelectricity.

[17] A. V. Bune *et al., J. Appl. Phys.* **85,** 11 (1999).

[18] A. G. Chenowyth *J. Appl. Phys.* **27,** 78 (1956).

[19] A. V. Bune *et al., Appl. Phys. Lett.* **67,** 3975 (1995).

[20] K. Sato Japanese Journal of Applied Physics **20,** 2403 (1981).

[21] Hinds instruments Application note "Magneto-Optic Kerr effect".

[22] P. Weinberger Magnetic Anisotropies in Nanostructured Matter, CRC Press LLC, (2008).

[23] J. Kerr, Phil. Mag. **3,** 321 (1877).

[24] M. N. Deeter and D. Sarid *IEEE Trans. Magn. MAG* **24,** 2470 (1988).

[25] S. Tanaka *Jap. J. Appl. Phys.* **2,** 548 (1963).

[26] S. Polisetty *et al.,* Rev. Sci. Instrum. **79,** 055107 (2008).

[27] http://www.hindsinstruments.com/knowlege-center/technology-primer/pem-100photoelastic-modulation/principles-of-operation/.

[28] Hinds instruments Application note "Magneto-Optic Kerr effect".

[29] Z. Q. Qiu and S. D. Bader, Rev. Sci. Instrum. 71, 1243 (2000).

[30] D. Jiles Introduction to Magnetism and Magnetic Materials. (2nd edition) Springer (1998).

[31] U. Hartmann Magnetic Force Microscopy. *Annu. Rev. Mater. Sci.* **29**, 53 (1999).

[32] Y. Martin & K. Wickramasinghe Magnetic Imaging by Force Microscopy with 1000A Resolution. *Appl. Phys. Lett.* **50**, 1455 (1987).

[33] P. Grutter, H.J. Mamin, and D. Rugar, Magnetic Force Microscopy in Scanning Tunneling Microscopy II edited by R. Wiesendanger and H.-J. Gunterodt, Spring-Verlag, Berlin **28,** 151 (1992).

[34] http://en.wikipedia.org/wiki/Magnetic_force_microscope.

[35] B.D. Cullity and S.R. Stock, *Elements of X-Ray Diffraction: Third Edition*, Prentice Hall, America (2001).

[36] N.W. Ashcroft, N.D. Mermin, Solid State Physics, Holt Rinehart & Winston (1976).

[37] Azároff, L. V.; R. Kaplow, N. Kato, R. J. Weiss, A. J. C. Wilson, R. A. Young, X-ray diffraction. McGraw-Hill (1974).

[38] A. Gibaud and S. Hazra, Current Science **78**, 1467 (2000).

[39] F. Huang, 'X-ray Reflectivity Studies of Thin Film' Internal Report (Center for Materials for Information Technology, an NSF Science and Engineering Center).

[40] J. Daillant, and A. Gibaud 'X-ray and Neutron Reflectivity: Principles and Applications (Springer-Verlag Berlin Heidelberg New York, 1999).

[41] http://www.bruker-axs.com/stress.html.

Chapter 3

Structural Characterization

This chapter describes the structural characterization of the thin film heterostructures that have been investigated in this thesis. Because the magnetoelectric effects that are described in chapters 4 and 5 are dependent on the structural characteristics of the interface between the ferroelectric polymer, P(VDF-TrFE) and metallic electrodes, our characterization tools include X-ray reflectivity and atomic force microscopy to enable thickness and roughness measurements. In addition, the ferroelectric polymer has been extensively characterized using variable angle spectroscopic ellipsometry (VASE), scanning tunneling microscope (STM) and X-ray diffraction and we describe those results that pertain to the relevant structure as well. The chapter is divided into the following sections. Section 1 describes the characterization of the ferroelectric polymer layer, section 2 that of the metallic layers and sections 3 describe the characterization of the heterostructured samples. Using a variety of methods, we investigate the crystal structure, the thickness and the surface and interlayer roughness.

3.1 Ferroelectric polymer layer characterization

Previous measurements of the P(VDF-TrFE) layer have confirmed that each dip into the LB trough results in a thickness of approximately 1.8 nm per 1 LB layer as determined by variable-angle spectroscopic ellipsometry measurements, corresponding to

~ 3ML of P(VDF-TrFE).[1,2] Scanning tunneling microscope (STM)[3] and X-ray diffraction (XRD)[4] measurements have confirmed the high crystallinity of the polymer films. Our X-ray reflectivity (XRR) measurements of a 25 monolayer film of P(VDF-TrFE) 70:30 on glass substrate are shown in figure 3.1, showing thickness oscillations that are more clearly visible when the Fresnel background reflectivity has been subtracted out (See inset of figure 3.1). The positions of the maxima and minima give us the total thickness of the film (this Kiessig Fringe method calculation is described in detail in chapter 2) which is 49 nm. This compares well with the ellipsometry calculations of the thickness of the polymer films of 45 nm. A simulation fit curve to the XRR data using the LEPTOS software, supplied with the Bruker-AXS gives a roughness of 2 nm at the air interface.

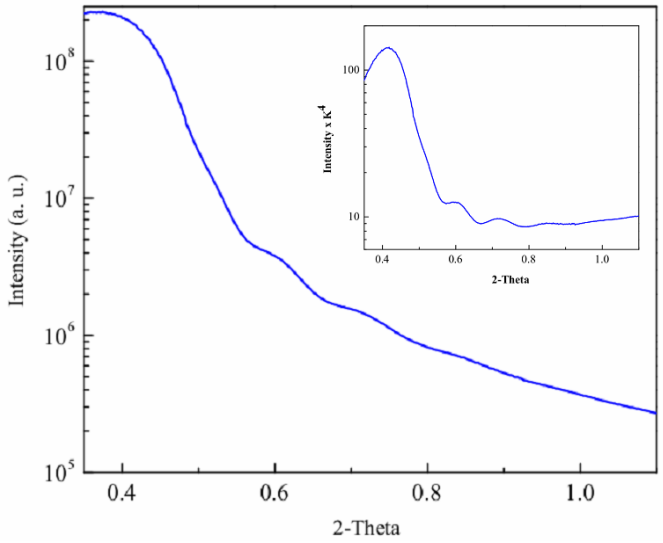

Figure 3.1: XRR data on Glass/ P(VDF-TrFE) 70:30 (25 ML) sample. Inset: Intensity times K^4 is plotted with 2-theta.

Previous measurements[1] of X-ray diffraction (XRD) on PVDF samples show that the crystallinity of the polymer films increases after annealing. Figure 3.2 is the XRD data before (black) and after (red) annealing at 135 ºC for 2 hours for a 20 ML (36 nm)

LB films of P(VDF-TrFE) 50:50 on Si substrates. All the samples described in this thesis have been annealed in a similar fashion.

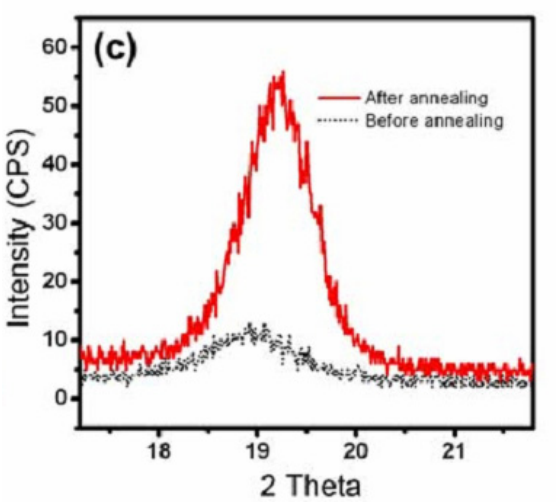

Figure 3.2: XRD measurement data before and after annealing on 20 LB layers of 50:50 copolymers on Si. Annealing condition was 135 ºC for 2 hours. [After reference # 1]

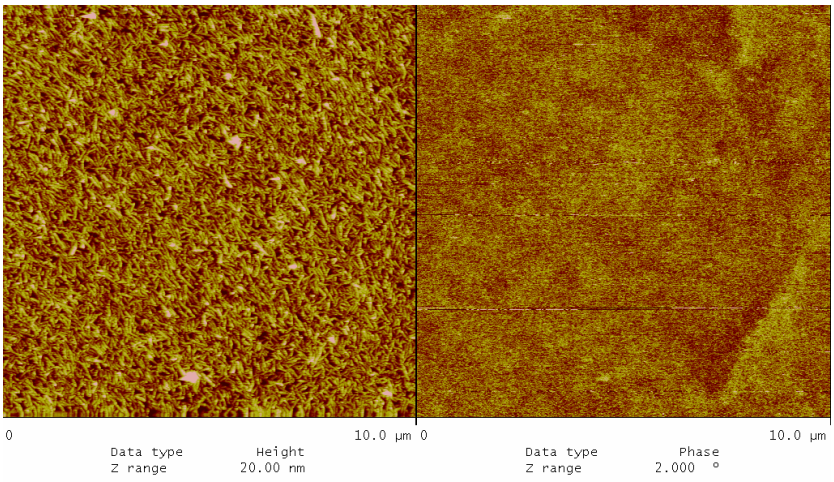

Figure 3.3: AFM and MFM measurements on Pt(50nm)/Co(10nm)/P(VDF-TrFE) 80:20 (15 ML) sample.

Atomic force microscopy (AFM) and magnetic force microscopy (MFM) measurements on a Pt(50nm)/Co(10nm)/P(VDF-TrFE) 80:20 (15 ML) sample is shown in figure 3.3, showing the familiar rice grain structure of the polymer. The MFM images that are taken through the PVDF layer show the presence of magnetic domains in the underlying Co.

3.2 Metallic layers characterization

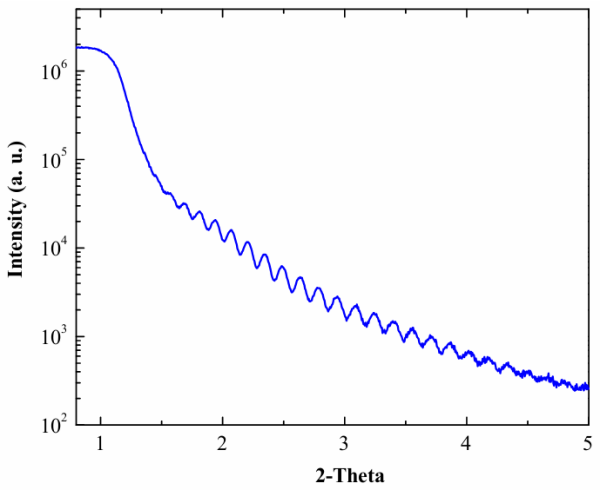

Figure 3.4: XRR measurement data on a Pt(50 nm)/Co(1.8 nm) sample.

The thickness of the metallic layers has been characterized using both the in-situ quartz crystal thickness monitor and X-ray reflectivity (XRR) measurements. The roughnesses of the metallic layers have been characterized using AFM measurements as well as XRR measurements. Figure 3.4 is the XRR data on a Pt(50 nm)/Co(1.8 nm) sample. A simulation fit curve to the XRR data was done with the simulation software LEPTOS, supplied with the Bruker-AXS. In the simulation we assumed a naturally

occurring CoO layer on top of the Co. This simulation curve gives the thickness of the Pt, Co and CoO layers to be 54 nm, 1.2 nm and 1.9 nm respectively, which matches quite well wit the quartz crystal monitor data. The Co thickness measured by the XRR is smaller than the thickness monitor because the few top monolayers top Co form CoO. The Pt seed layer thickness deviates by 8% from the thickness monitor thickness. The roughness of the sample at Co air interface is ~ 0.8 nm.

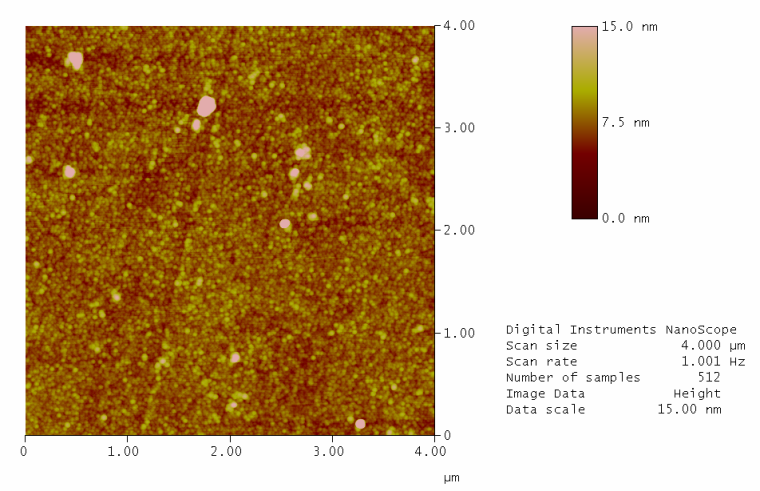

Figure 3.5: AFM images on a bare Pt (70 nm) / Co (10 nm) sample.

An AFM image on a bare Pt(70 nm)/Co(10 nm) sample is shown in figure 3.5. The roughness of the sample is 0.8 nm. This roughness matches well with the XRR data in figure 3.4, indicating that the LB polymer films are deposited on a smooth substrate.

AFM and MFM images on bare Pt(50 nm)/Co(10 nm) sample are shown in figure 3.6. The MFM images after in-plane demagnetization exhibit multiple magnetic domains. Images for the same sample after magnetic saturation, when the Co layer is in single

domain state, are shown in figure 3.7. The MFM image after magnetic saturation shows no multiple magnetic domains.

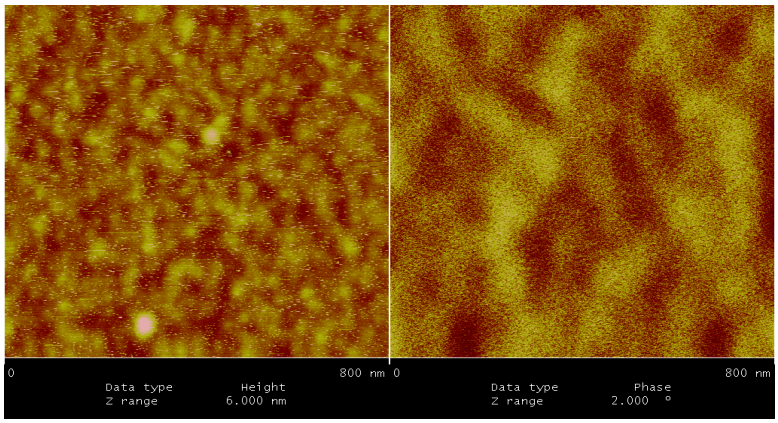

Figure 3.6: AFM and MFM images on a Pt(50nm)/Co(10nm) sample after in-plane demagnetization.

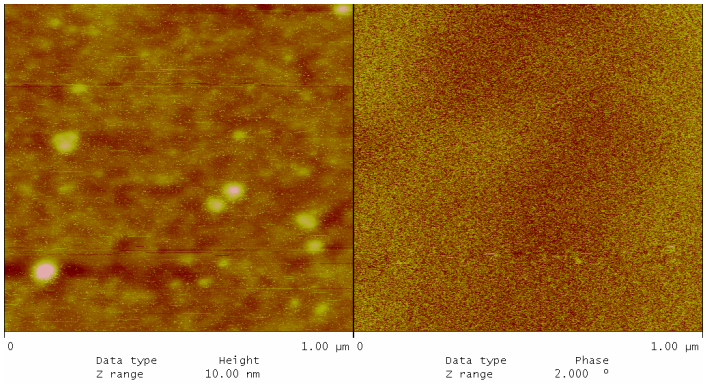

Figure 3.7: AFM and MFM images after magnetic saturation on the Pt(50nm)/Co(10nm) sample.

The thickness calibration for the Co wedge is done using both the in-situ thickness monitor and XRR measurements. A Co wedge sample on a glass substrate with a Pd(100 nm) seed layer is deposited. The palladium layer is of uniform thickness. During Co layer deposition the sample is aligned along the Co sputtering gun and not

rotated resulting in a non-uniform thickness with the thicker end of the wedge closer to the Co gun. The middle of the wedge thickness is our pre-calibrated thickness using the thickness monitor. After deposition, by using the Kiessig Fringe method the thickness of the Co layer was calibrated and plotted as a function of position along the Co wedge. A linear fit to that data set (red line) gives a relationship between position and thickness, as thickness (nm) = 0.474 x position (mm) + 31(nm). The slope of this fit is used for calibrating the thickness of the Co wedge samples for our measurements. The lower inset of figure 3.8 is the XRR data at a distance of 2 mm from thin Co edge, corresponding to a thickness of 30 nm.

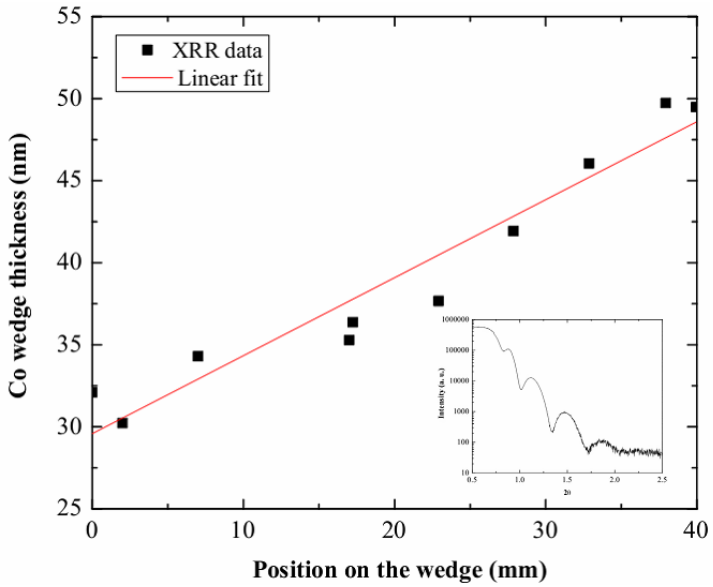

Figure 3.8: Co wedge thickness calibration data. Using the Kiessig Fringe method the thickness of the Co layer was calibrated and plotted with the position along the Co wedge. A linear fit to that data set (red line) gives the slope, used for calibrating the thickness of the Co wedge samples. (Lower inset): XRR data at 2 mm from thin Co edge, at a particular position of the wedge corresponding to a thickness of 30 nm.

3.3 Heterostructure sample characterization

Atomic force microscopy (AFM) images on a sample (similar to our experimental sample described in chapter # 4) of Al (96 nm) / P(VDF-TrFE) (25 ML)/ Al (3.3 nm) / Co (10nm) / Al (31 nm) is shown in Figure 3.9. This sample has a roughness of 2 nm on the multilayer stack, comparable to the bare P(VDF-TrFE) sample we described in section 1.

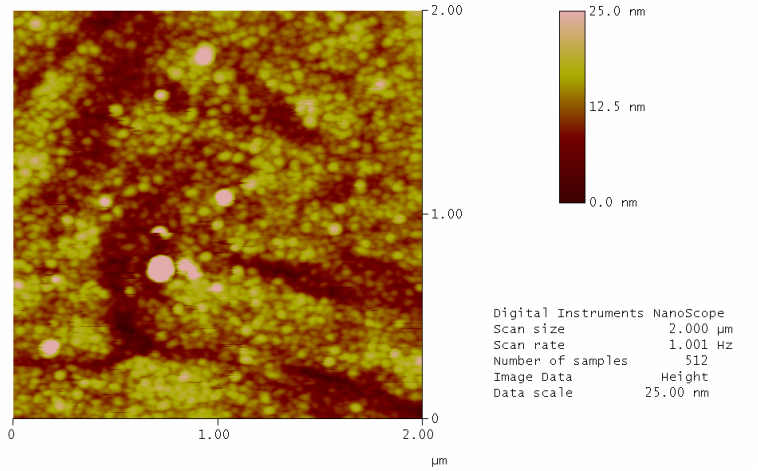

Figure 3.9: AFM images on Al (96 nm) / P(VDF-TrFE) (25 ML)/ Al (3.3 nm) / Co (10nm) / Al (31 nm) sample.

XRR data on a sample of Pt(50nm)/Co(1.5nm)/PVDF(31ML)/Al(15nm) similar to the samples described in chapter # 5 is shown in figure Figure 3.10. The metallic layer thickness values are determined with the in-situ quartz crystal monitor and a simulation fit curve using the LETPTOS software gives values of 57 nm, 1.7 nm, 1.2 nm, 57 nm and 12 nm for Pt, Co, CoO, PVDF and Al layers respectively. The roughness of the sample is ~ 1 nm at the air interface. The sample is smooth and continuous.

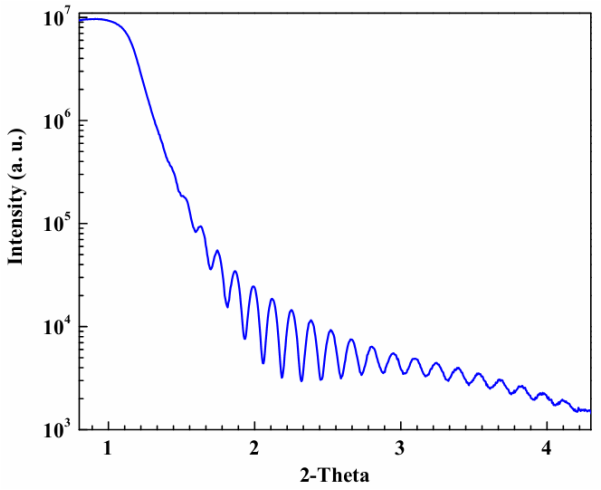

Figure 3.10: XRR data on Pt(50nm)/Co(1.5nm)/PVDF(31ML)/Al(15nm).

3.4 Conclusions

In conclusions, we have characterized our sample structure using AFM and XRR in conjunction with the in-situ quartz crystal monitor to obtain thickness and roughness measurements. The quartz monitor deposition thickness is at worst within 8% of the X-ray reflectivity data. Previous STM and XRD measurements have confirmed the high crystallinity of the polymer films. Our measurements of the PVDF thickness compared with previous measurements of VASE are off by 9%. The heterostructure sample similar to our measurements in chapter 4 has a roughness of ~ 1 nm, confirming that the sample is fairly flat as well as continuous. The magneto-optical-Kerr effect measurements (see chapter 5 for details of the M_r/M_s measurements with Co thickness in figure 5.6) along the Co wedge thickness, which shows clear magnetization loops for Co thickness as low as ~ 6 Å confirm the continuity of the magnetic Co wedge and XRR data indicate that the wedge is smooth.

3.5 References

[1] Jihee Kim, Ph.D. Thesis, University of Nebraska-Lincoln (2008).

[2] M. Bai *et al., J. Appl. Phys.* **95,** 3372 (2004).

[3] Bune *et al., Nature* **391,** 874 (1998).

[4] Choi *et al., Phys. Rev. B* **61,** 5760 (2000).

Chapter 4

Magneto-Electric Effects In Ferromagnetic Cobalt / Ferroelectric Copolymer Multilayer Films

A. Mardana, Mengjun Bai, A. Baruth, Stephen Ducharme & S. Adenwalla

Applied Physics Letters 97, 112904 (2010)

Changes from the original Journal article have been made for this dissertation.

4.1 Introduction

The magnetoelectric (ME) effect and its converse refer to the control of electric polarization and magnetization by magnetic or electric fields, respectively. The wide range of potential applications[1] ranging from memory devices to microwave applications and magnetic field sensors are driving the exploration of multiferroic materials with larger ME coefficients than have previously been seen.[2] Hetero-structured materials with separate magnetic (or magnetostrictive) and ferroelectric components relax the competing demands and constraints on a single material.[3,4,5] Efforts have focused on magnetic materials with the largest possible magnetostriction in order to maximize the piezoelectric/magneto-strictive coupling and has resulted in large magnetoelectric effects[6]. Magnetic flux concentration effects have increased the magnetoelectric coupling to 21.46 V/cm-Oe.[6] Thermally mediated effects[7] in a relaxor ferroelectric polymer result in ME coefficients of 0.9 V/cm-Oe.

This chapter reports results that suggest a different mechanism for ME coupling in a ferromagnetic/ferroelectric heterostructure, viz. the strain gradient created near

magnetic domain boundaries in a multidomain magnetic film and its effect on the ferroelectric polarization through the flexoelectric effect. An organic ferroelectric, the copolymers of 70% vinylidiene fluoride (VDF) with 30% trifluroethylene (TrFE) i.e., [P(VDF-TrFE) 70:30] is overlaid with a transition metal ferromagnet, Cobalt (Co) in a heterostructure with thicknesses that are controllable at the atomic level with films in intimate contact.

4.2 Sample Preparation and Experimental Techniques

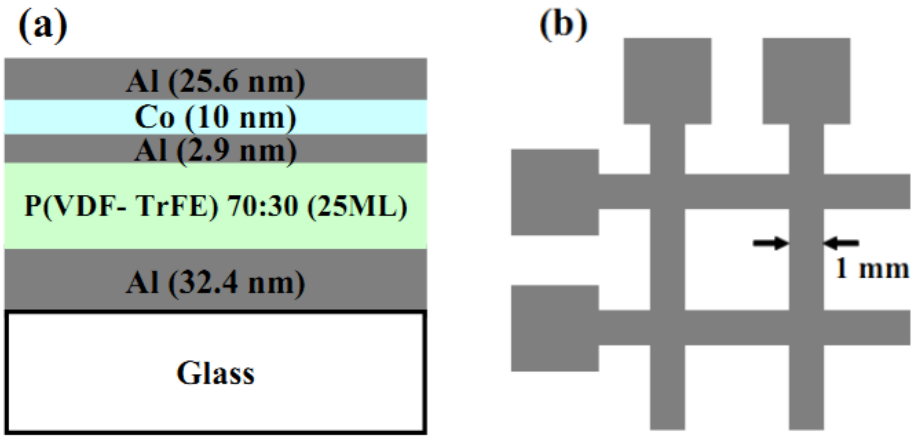

Figure 4.1: Schematic view of the heterostructure (a) Cross-sectional view (b) top view.

The sample, as shown in Figure 4.1, consists of {[glass/ Al (32.4 nm)/ P(VDF-TrFE) (45nm)/Al (2.9 nm)/Co (10 nm)/ Al (25.6 nm)}. The thicknesses of the metallic layers were calibrated using the in-situ quartz crystal thickness monitor. The polymer layer thickness was estimated based on our previous measurements of approximately 1.8 nm per 1 LB layer, determined by variable-angle spectroscopic ellipsometry measurements.[8,9] The metallic layers were made from either evaporated Al or sputtered

Co deposited through shadow masks of 1 mm wide and 15 mm long, with the upper and lower electrodes, perpendicular to each other defining four spots with an overlapping electrode area of 1 mm^2, as shown in figure 4.1 Sample Schematic of the cross-sectional view is shown in figure 4.1 (a) and the top view is shown in figure 4.1 (b). Both Al electrodes were deposited at a rate of 1.2 Å/s as measured by the in-situ thickness monitor. The top Al electrode served to prevent the diffusion of Co atoms into the soft polymer film. The upper Co layer was sputtered at low power, at a deposition rate of 0.056 Å/s, with frequent pauses of 20 minutes after 20 Å of deposition, to prevent shorting through the soft polymer layer.

The [P(VDF-TrFE 70:30] layer was deposited by the Langmuir-Blodgett (LB) method, which results in films with superior crystallinity, excellent ferroelectric properties, [10] and a saturation polarization of up to 0.1 C/m^2.[11] Prior to deposition of the top electrode, the ferroelectric polymer film is annealed at 130 °C for an hour in air to increase its crystallinity. Copper wires were attached to both electrodes with silver paint, allowing for pyroelectric measurements and enabling polarization switching. X-ray diffraction measurements indicate that the polymer grows in the (110) direction with the chains in the films plane and resulting in a polarization vector at 30° to the surface normal (see in chapter # 3 for XRD measurements).[12] The in-plane structure consists of small crystallites, 30 nm to 50 nm in size[13] with the polarization vectors for the various crystallites forming a cone at 30º around the normal, resulting in a net macroscopic polarization along the normal.

Ferroelectric polarization is measured using the Chynoweth modulation method,[14] for pyroelectric current (details of the measurement procedure can be found in chapter 2

of this thesis), which is proportional to the normal component of the film polarization, irrespective of polarization state. Moreover it is perturbative and does not alter the polarization state.[15] In this method, the sample temperature was modulated by a 3-mW helium-neon laser operating at a wavelength of 633 nm, and an optical chopper frequency of 2 kHz. The resulting pyroelectric current was measured by a lock-in amplifier locked to the chopper frequency with a time constant of 1 s.

Magnetization measurements were carried out using the polar magneto-optical Kerr effect (PMOKE), which measures the out-of-plane magnetization. To demagnetize the sample, it was mounted on a rapidly rotating drill in a slowly decreasing magnetic field with the sample surface parallel to the magnetic field.

4.3 Experimental Results and Discussions

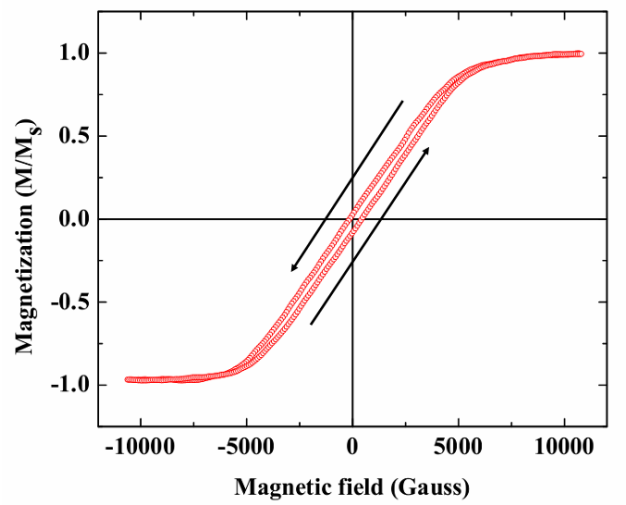

Figure 4.2: The out-of-plane hard axis magnetic hysteresis loop measured by PMOKE of the glass/Al(32.4 nm)/P(VDF-TrFE) (45nm)/Al(2.9 nm)/Co(10 nm)/Al(25.6 nm) sample.

Out-of-plane PMOKE measurements (figure 4.2) reveal a typical narrow s-shaped hard axis magnetization hysteresis loop, as expected for a 10 nm Co thin film with an in-plane easy axis. The variously oriented in-plane magnetic domains rotate into the magnetic field direction, forming a cone of half-angle ($\pi/2-\phi$) with the sample normal. The slope of the loop gives the angle for the magnetization as a function of applied field, $\sin(\phi) = (1.86 \times 10^{-4})\ H$, with H in units of Gauss. Pyroelectric current measurements resulted in the ferroelectric polarization hysteresis loop[12] shown in figure 4.3.

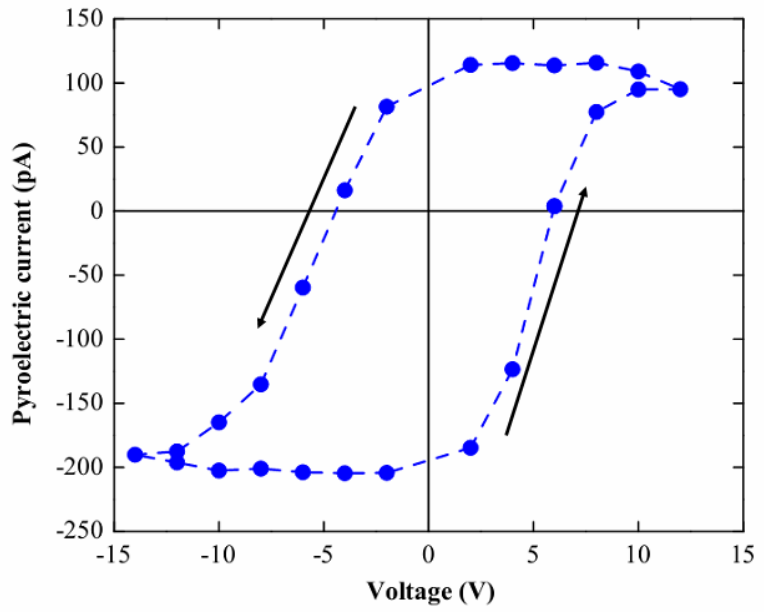

Figure 4.3: Measurements of the pyroelectric current vs. applied voltage showing the ferroelectric polarization hysteresis loop in the glass / Al(32.4 nm) / P(VDF-TrFE) (45nm) / Al(2.9 nm) / Co(10 nm) / Al(25.6 nm) sample.

After electrical saturation but prior to magnetic saturation, the pyroelectric response was measured as a function of both increasing and decreasing perpendicular magnetic field (figure 4.4) sweeps, showing an unexpectedly large (over 5%) change in

the pyroelectric response on application of a 6 kG magnetic field. The sign of the change in pyroelectric current (proportional to polarization) depended on the relative orientation between the polarization direction and the magnetic field. Parallel orientation resulted in a decrease in the absolute value of the polarization with increasing magnetic field, whereas an anti-parallel alignment resulted in an increase. This effect was fully reversible, repeatable and possessed odd symmetry with respect to direction of the out-of-plane magnetic field. We emphasize that this was not an irreversible magnetic poling effect.[16] There was no evident hysteresis in the pyroelectric response as the magnetic field was cycled. Rather, it was a fully reversible and continuous change of the polarization as can be seen in the increasing and decreasing field sweeps.

The thermoelectric and associated thermomagnetic effects, which occur in the presence of a temperature gradient across the sample, may be conclusively ruled out due to the extremely small temperature gradient across the thickness of the sample. A one dimensional calculation using Fourier's law with the appropriate thermal conductivity for P(VDF-TrFE)[17] results in a temperature gradient 0.75 mK, across the 53 nm thick P(VDF-TrFE) film. Note that the pyroelectric current, in contrast, is a displacement current that arises from the lack of structural symmetry in response to a uniform temperature change of the sample. The various thermomagnetic effects (the Ettinghausen, Righi-Leduc and Nernst effects)[18] all depend on the temperature gradient $\frac{dT}{dz}$ whereas the pyroelectric current depends on $\frac{dP}{dT}$, where T is the temperature, P is polarization and z is the thickness across which the current measured. Secondly, thermomagnetic effects occur in a Hall measurement geometry in which the measured current, temperature

gradient and the applied magnetic field are perpendicular to each other. Our measured pyroelectric effect geometry rules out the presence of thermomagnetic effects as in our case the measured current, electric field and applied magnetic field are all parallel or antiparallel to each other. Finally, thermomagnetic effects are inconsistent with the observation that the change in pyroelectric current with magnetic field is seen only in demagnetized samples. In a magnetically saturated sample, there is no change in the pyroelectric current with magnetic field. Thermomagnetic effects, in contrast, depend only upon the applied magnetic field, irrespective of the magnetic state of the sample.

The measured changes in polarization ΔP with applied magnetic field H were fitted to a nonlinear magnetoelectric coupling of the form, $\Delta P = \alpha(H - H_s) + \beta(H - H_s)^3$. Assuming a saturation polarization of P(VDF-TrFE) of 0.1 C/m^2, we obtain a linear ME coefficient of α = 4.78 x 10^{-8} C/m^{2}Oe (equivalent to α = 5.45 V/cm-Oe) and a third-order coefficient of β = 7.82 x 10^{-15} C/m^{2}Oe^3. The linear ME coefficient is comparable to those measured previously in composite materials such as nanopillars[3] of $BaTiO_3$-$CoFe_2O_4$ or laminates[4] of PZT/Terfenol-D, an unexpected result given the much smaller magnetostriction of Co. This is comparable to the results taking into account the magnetic flux concentration effects[6] and thermally mediated effects[7] in relaxor ferroelectric polymer.

The data shown in figure 4.4 are for a virgin magnetic sample, with multiple in-plane magnetic domains. After magnetic saturation, either in-plane of or out-of-plane, the polarization shows negligible changes with applied magnetic field, as shown in figure 4.5 for out-of-plane saturation (red circles). The measurements were done as a function of out-of-plane magnetic field so as we increase the field there is rotation of the many in-

plane magnetic domains into the magnetic field direction. Saturation presumably forms much larger domains and destroys the effect. The necessity of multiple magnetic domains in the cobalt film is further underscored by the blue symbols in figure 4.5, which show the *P* vs. *H* curve after demagnetization of the Co film, which restores the effect, albeit at a lower level, approximately 2.5 % instead of 5% as in figure 4.4.

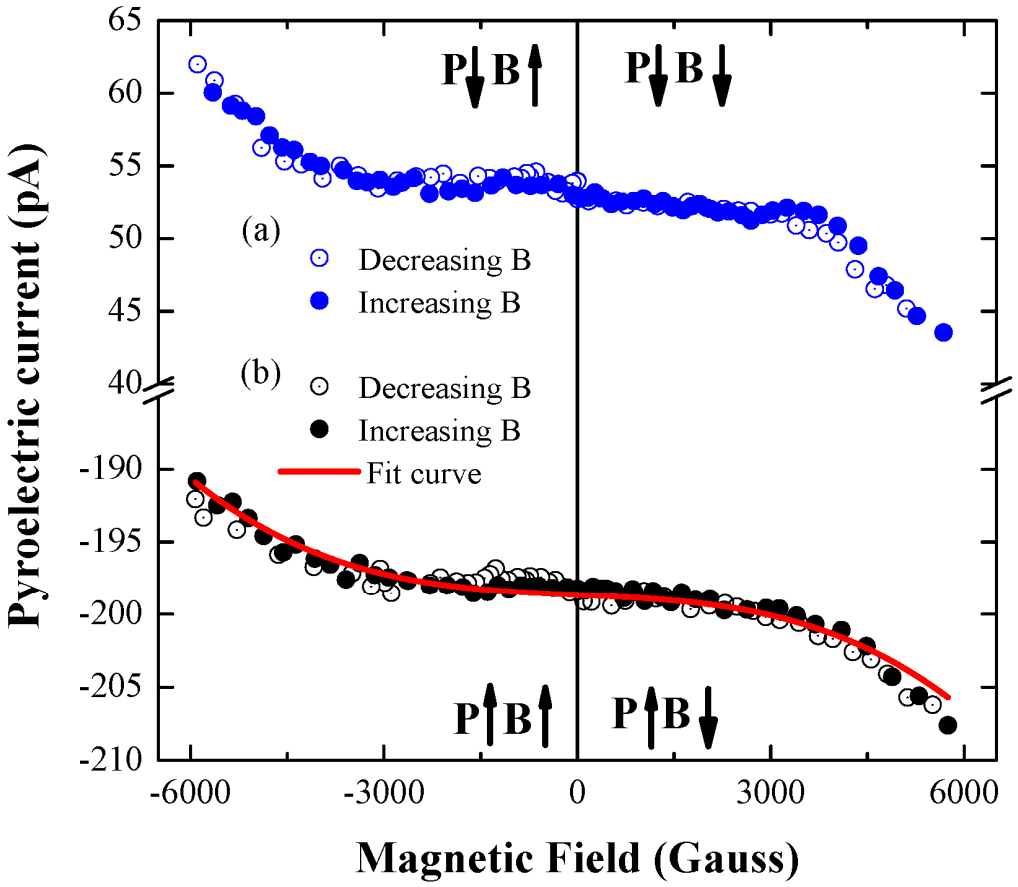

Figure 4.4: Pyroelectric current (proportional to ferroelectric polarization) as a function of applied magnetic field perpendicular to the sample plane. The curves labeled (a) and (b) correspond to the two different ferroelectric polarization directions of the sample. Arrows indicate the relative orientation of the polarization (*P*) and applied magnetic field (*B*). The red line is a fit to one set of data.

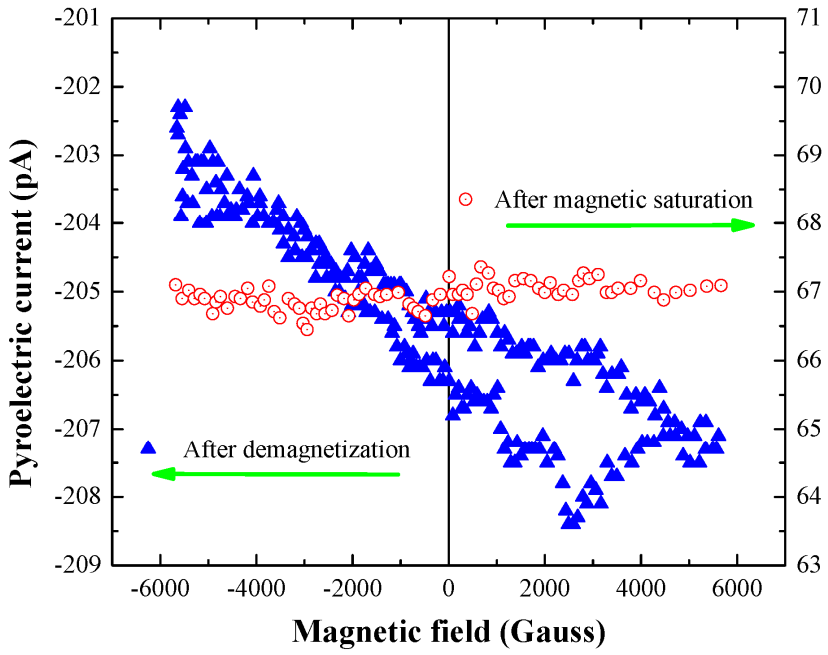

Figure 4.5: Ferroelectric polarization as a function of applied magnetic field perpendicular to the sample plane, after out-of-plane magnetic saturation (circles) and after demagnetization (triangles).

Demagnetization results in smaller domains and hence a higher density of domain walls, confirmed by Magnetic Force Microscopy (MFM) imaging on an identically grown Co sample. Demagnetization reduced the average domain size to 200 nm, approximately 1/3 the size of the domains measured after magnetic saturation. Clearly, the presence of multiple domains plays an essential role in this effect. Any discussion of the origin of this large magneto-electric effect must account for the dependence on the presence of multiple magnetic domains and the odd symmetry with respect to the directions of the applied magnetic field and the sample polarization.

Purely magnetostrictive effects fail on both counts, as well as severely underestimating the magnitude of the change, as we show below. Conventional

magnetostrictive effects refer to changes in the dimensions of the magnetic layer which result in strain in the polymer ferroelectric and a subsequent change in the polarization.

Because the ferroelectric layer is essentially unclamped (i.e. in constant stress), in the out-of-plane direction, out-of-plane magnetostriction should have no effect on the electrical properties via the piezoelectric coefficient and the only effects come from in-plane magnetostriction (Here unclamped means that volume expansion is freely allowed). We define a coordinate system such that the 3 (or z) direction is perpendicular to plane, 1 (x) refers to the direction along the length of the Co electrode, and 2 (y) is perpendicular to it. The ferroelectric is polycrystalline in-plane with numerous small randomly oriented crystals in plane. Hence the symmetry of the ferroelectric is given by class ∞m (in the notation of Nye[19]) or $C_{\infty v}$.

The thin Co magnetic film has an in-plane easy axis. The magnetostrictive strain relative to the direction of magnetization is given by[20] $\varepsilon = \frac{3}{2}\lambda_s(\cos^2\theta - 1/3)$, where θ is the angle between the measured strain and the direction of magnetization, ε is the strain and λ_s is the saturation magnetostriction. The change in magnetization that occurs as the out-of plane field is increased occurs purely through rotation, as evidenced by the shape of the out-of-plane hysteresis loop (see figure 4.2). With λ_s = –62 x 10^{-6} for polycrystalline Co,[16] we calculate the change in strain to be ε_1 = +90 x 10^{-6}, ε_2 = 0 and ε_3 = –90 x 10^{-6} as the magnetization rotates from in-plane to out-of-plane. Assuming the best case scenario of perfect coupling to the copolymer, and using the equations $\sigma_i = c_{ij}\varepsilon_j$ and $P_3 = d_{3j}\sigma_j$, where σ is the strain, c_{ij} are the appropriate stiffness constants, P_3 is the component of polarization in the out-of-plane direction and d_{3j} are the piezoelectric

moduli, we obtain the relation between magnetostrictive stress in the Co and the corresponding change in the polarization in the direction perpendicular to the plane. The stiffness and piezoelectric constants for the P(VDF-TrFE) copolymer[21,22] are c_{11} = 3.7 x 10^9 N/m^2 = c_{22}, $c_{12} = c_{21} = c_{13} = c_{23}$ = 1.5 x 10^9 N/m^2, and d_{31}=21.4 pC/N, d_{32} = 4.3 pC/N and result in in-plane strains of σ_1=2.2 x 10^5 N/m^2 and σ_2=5 x 10^4 N/m^2 in the polymer, (σ_3=0, because the polymer is unclamped). Using these values we obtain a change in polarization of approximately $\Delta P = 0.5 \times 10^{-5}$ C/m^2. Assuming a polarization of 0.1 C/m^2 in the copolymer film (a reasonable value for these LB deposited films) this amounts to a relative change in the polarization $\Delta P/P$ of less than 10^{-4}, many orders of magnitude smaller than the 5 % polarization change that is experimentally measured. Although the magnetostrictive coefficients in thin films may be 3-5 times larger than the bulk value,[23,24] this still fails to account for the large changes in polarization.

An alternative explanation arises from the asymmetric geometry of our sample. Magnetostrictive effects occur only at the Co electrode, inducing a strain gradient in the thickness of the film, $\partial\varepsilon/\partial z$. The flexoelectric effect,[25,26] defined as the polarization change induced by a strain gradient is given by (neglecting the tensor character of the flexoelectric effect[19]) $\Delta P = -f(\partial\varepsilon/\partial z)$, where f is the effective flexoelectric coefficient, and $\partial\varepsilon/\partial z$ is the strain gradient in the ferroelectric film [see the figure 4.6 (a)]. Although the odd symmetry of the polarization changes with magnetic field and the necessity of multiple magnetic domains rule out the effect depicted in figure 4.6 (a), it is instructive to consider the magnitude of the expected changes in polarization resulting from strain gradients. A recently reported value for the flexoelectric coefficient f in PVDF films is 82 μC/m.[27] Theoretical predictions of the flexoelectric coefficients in

dielectrics are very small, limited by e/a, estimated to be ~10^{-10} C/m, where e is the electronic charge and a is the dimension of unit cell.[28,29] However most (if not all) experimentally measured values of the flexoelectric coefficients are many orders of magnitude higher, ranging from 10^{-6} to 10^{-4} C/m.[30,31] This puzzling discrepancy has not been resolved. In at least one ferroelectric, $BaTiO_3$, two different experimental techniques[32] (nanoindentation and the more common bending approach) resulted in identical values of the flexoelectric coefficient. Experimentally measured values of polarization changes due to the flexoelectric effect in epitaxial PZT films are very large, comparable to the spontaneous polarization of the film.[33] There has been some discussion[34] of the effect of strain on ferroelectric domain rotation, an effect that may erroneously contribute to a much larger measured flexoelectric coefficient in a ferroelectric sample. However, similar measurements in the paraelectric phase of ferroelectrics (as was done for the PVDF) and even in dielectrics without either piezoelectric or ferroelectric ordering indicate large values for the flexoelectric coefficient. We will use the reported value of the flexoelectric coefficient in P(VDF-TrFE) in the following analysis.

In the model depicted in figure 4.6(a), the strain gradient arises from the difference in strain between the top and bottom of the ferroelectric. Magnetostrictive strain from the top ferromagnetic Co layer will strain the top ferroelectric layer, resulting in a strain gradient that is given by, $\frac{\partial \varepsilon}{\partial z} = \frac{\varepsilon_{top}}{d} = \frac{62 \times 10^{-6}}{50\ nm} = 1.2 \times 10^{3}\ m^{-1}$ resulting in a very large polarization change $\Delta P = f\frac{\partial \varepsilon}{\partial z} = 0.1$ (or $\frac{\Delta P}{P} = 100\%$), much larger than the observed 5% change. Since the strain gradient $\partial\varepsilon/\partial z$ would be largest for a

uniformly magnetized cobalt film, and smallest for a demagnetized film, this is inconsistent with of the results shown in figure 4.5. Moreover, because the magnetostriction in the Co layer will be identical for magnetic fields pointing either up or down, this is inconsistent with the odd dependence on the magnetic field.

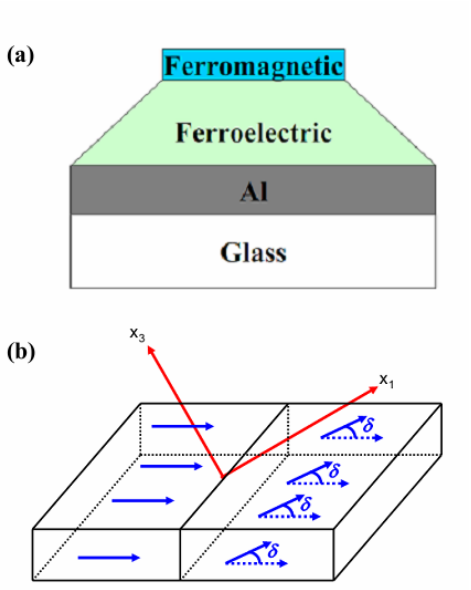

Figure 4.6: Schematic diagram of the (a) strain gradient in the ferroelectric layer due to magnetostriction in the upper ferromagnetic electrode [The actual change will be very small compared to the figure.] (b) Strain gradient across a single domain wall.

However, the presence of multiple in-plane magnetic domains means numerous *in-plane strain gradients* exist in the magnetic film and consequently in the ferroelectric film. The magnetostrictive strain is given by $\varepsilon = \frac{3}{2}\lambda_s(Cos^2\theta - 1/3)$, where λ_s is the magnetostriction of polycrystalline Co,[16] $\lambda_s = -62 \times 10^{-6}$ and θ is the angle between the measured strain direction and the magnetization. The strain gradient across the domain wall between two in-plane magnetic domains oriented at an angle δ with respect to each

other is given by $\partial\varepsilon/\partial x = [(3\lambda_s/2W)(\cos^2\delta - 1)]$, [see figure 4.6 (b)] where W is the domain wall width. Two perpendicularly oriented magnetic domains will result in the largest possible in-plane strain gradient across them. In an out-of-plane magnetic field, each in-plane domain cants in the direction of field, leading to changes in the strain gradient, which would be proportional to the magnetic field. The changes in the magnitude of the polarization resulting from these strain gradients, is given by the various components of the flexoelectric coefficient tensor f_{ijkl}; hence a natural coordinate system is one in which the x_3 axis is parallel to the polarization of the sample, rotated by 30° with respect to the normal (z direction) and the x_1-x_2 plane is canted at 30° to the sample plane. The flexoelectric coefficient is a fourth rank tensor; the components possess the same symmetry as the stiffness tensor of the ferroelectric (crystal class 4mm). Excluding shear strain and taking into account the zeros of f_{ijkl}, the change in polarization can be written as (in the condensed matrix notation of Nye, where pairs '11' becomes '1' and '13' becomes '5', etc.[15]) $\Delta P_3 = f_{33}\frac{\partial\varepsilon_3}{\partial x_3} + f_{44}\frac{\partial\varepsilon_2}{\partial x_3} + f_{55}\frac{\partial\varepsilon_1}{\partial x_3}$. From symmetry consideration $\frac{\partial\varepsilon_1}{\partial x_3} = -\frac{\partial\varepsilon_2}{\partial x_3}$ for all applied magnetic fields and since $f_{44} = f_{55}$ for the crystal class 4mm, the only relevant strain gradient component is $\frac{\partial\varepsilon_3}{\partial x_3}$. Geometrically ε_3 is the strain along the x_3-axis, along the polarization direction at an angle of 120° to the in-plane direction. Calculations show that the strain gradient at zero magnetic fields for two in-plane domains oriented at an angle δ is given by $\frac{\partial\varepsilon_3}{\partial x_3} = \frac{3\lambda_s}{16W}[Cos^2\delta - 1]$. As the out-of-plane magnetic field is increased, the magnetization within each domain rotates towards the magnetic field direction, making an angle with the sample plane given by $\phi(H)$ [obtained

from the magnetic hysteresis loop as explained earlier]. This changes the angle between the two adjacent domains and hence changes the strain gradient across the domain wall which is now given by,

$$\frac{\partial \varepsilon_3}{\partial x_3} = \frac{3\lambda_s}{4W} Cos^2[120^0 - \phi(H)][Cos^2\delta - 1] \quad (1)$$

In this scenario, the change in polarization due to the flexoelectric effect occurs only in the region of a magnetic domain wall. Hence, the net change in polarization averaged over all the domain walls can be written as,

$$\Delta P_3 = f \frac{\partial \varepsilon_3}{\partial x_3} \frac{A_{dw}}{A_d} \quad (2)$$

Where A_{dw} is the area of the domain wall and A_d is the area of the domain. For simplicity we assume a circular domain, leading to $\frac{A_{dw}}{A_d} = \frac{2W}{d}$, where d is the domain size and W is the domain wall size. The average domain width in a demagnetized Co sample is around 200 nm as measured by MFM. We assume that over the width of a ferromagnetic domain wall, the ferroelectric layer consists of a single crystal, with a unique direction of polarization. The measured domain wall widths in Co are approximately 10-30 nm (our calculations use W=10 nm),[35] comparable to the size of the ferroelectric crystallites, 30 nm to 50 nm.[13] The presence of multiple ferroelectric crystallites within a magnetic domain wall will reduce the effect. We also assume that adjacent in-plane domains are oriented at an angle $\delta = 90^o$ corresponding to the maximum strain gradient across the domain wall. From the magnetic hysteresis loop, we obtain a canting angle of $\phi(H) = 48^o$ at an applied field of 6 kG. From the above values and from

equation (1) and (2) we get $\frac{\Delta P_3}{P} = 3.6\%$ close to our experimental measured polarization changes of 5%.

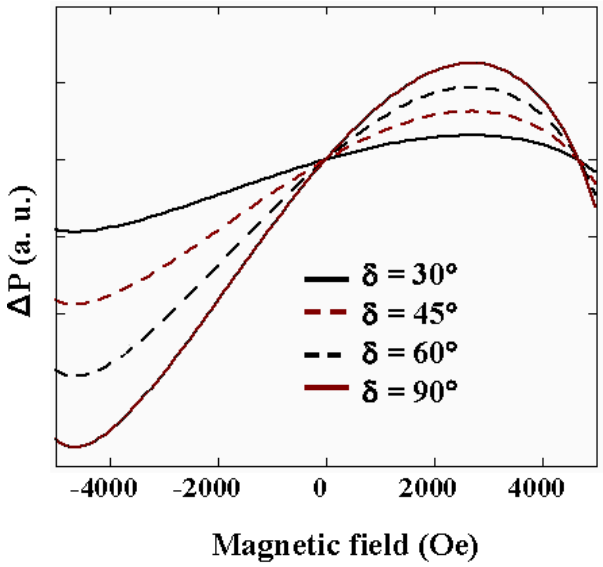

Figure 4.7: Calculation (from equation. 1) of the changes in polarization with applied field across a single domain wall for various values of δ, the angle between magnetization directions for two adjacent domains.

The configuration of domains, including their density and the in-plane angle δ between adjacent domains results in a net strain gradient, and together with the magnitude of the flexoelectric coefficient will determine the magnitude of the change in the polarization. Since the configuration of domains is highly sensitive to roughness, structure, and magnetization history the change in the magnitude of the effect after demagnetization is not surprising. A plot of equation 1 as a function of applied field and for various values of δ, the angle between two adjacent domains, is shown in figure 4.7.

In a perfectly demagnetized isotropic sample, all values of δ are equally probable; in reality there will be a preference for certain angles, depending on the microstructure of the Co layer. A more sophisticated calculation would take into account a distribution function for the angle δ, the density of domains and the net strain gradient that exists across the macroscopic area of the sample.

4.4 Conclusions

In conclusion, we have demonstrated a large converse magnetoelectric effect in a heterostructure composed of a ferromagnetic cobalt film and a ferroelectric polymer film. Application of a magnetic field to the heterostructure results in changes in the electric polarization of up to 5%. The result is highly dependent on the presence of multiple magnetic domains in the cobalt film. We propose a model in which the interaction arises from strain gradients at the magnetic domain walls coupling to flexoelectric response in the polymer layer. These results provide a qualitative look into the phenomenon; quantitative study will require independent measurement probing key features of the underlying mechanisms including the flexoelectric response of the ferroelectric polymer, the effect of the magnetic state in the ferroelectric hysteresis loops, the domain-wall strain of the ferromagnetic film, and the evolution of the magnetic domains with magnetic field. The sensitivity of this effect to the exact domain configuration of the ferromagnet may provide a path for tuning both the magnitude and symmetry of the effect.

4.5 Acknowledgements

This research is supported by the National Science Foundation through the Materials Research Science and Engineering Center program Grant No. DMR-0820521.

4.6 References

[1] V. E. Wood & A. E. Austin, *Int. J. Magn.* **5,** 303 (1974).

[2]T. Kimura, T. Goto, H. Shintani, K. Ishizaka, T. Arima and Y. Tokura, *Nature* **426,** 55 (2003).

[3]H. Zheng, J.Wang, S.E. Lofland, Z. Ma, L. Mohaddes-Ardabili, T. Zhao, L. Salamanca-Riba, S.R. Shinde, S.B. Ogale, F. Bai, D. Viehland, Y. Jia, D.G. Schlom, M. Wuttig, A. Roytburd and R. Ramesh, *Science* **303,** 661 (2004).

[4]Ce-Wen Nan, N. Cai, Z. Shi, J. Zhai, G. Liu, and Y. Lin, *Phys. Rev. B* **71,** 014102 (2005).

[5]Kiyotake Mori, Manfred Wuttig, *Appl. Phys. Lett.* **81,** 100 (2002).

[6] Z. Fang, S. G. Lu, F. Li, S. Datta, Q. M. Zhang, & M. El Tahchi, *Appl. Phys. Lett.* **95,** 112903 (2009).

[7] S. G. Lu, Z. Fang, E. Furman, Y. Wang, Q. M. Zhang, Y. Mudryk, K. A. Gschneidner, V. K. Pecharsky, & C. W. Nan *Appl. Phys. Lett.* **96,** 102902 (2010).

[8] Jihee Kim, Ph.D. Thesis, University of Nebraska-Lincoln (2008).

[9] M. Bai *et al.,* J. Appl. Phys. **95,** 3372 (2004).

[10]A. V. Bune, V. M. Fridkin, S. Ducharme, L. M. Blinov, S. P. Palto, A. V. Sorokin, S. G. Yudin, & A. Zlatkin, *Nature* **391,** 874 (1998).

[11]S. Palto, L. Blinov, A. Bune, E. Dubovik, V. Fridkin, N. Petukhova, K. Verkhovskaya & S. Yudin, *Ferroelectrics Lett.* **19,** 65 (1995).

[12]J. Choi, C. N. Borca, P. A. Dowben, A. Bune, M. Poulsen, S. Pebley, S. Adenwalla, S. Ducharme, L. Robertson, V. M. Fridkin, S. P. Palto, N. N. Petukhova and S. G. Yudin, *Phys. Rev. B* **61 (8),** 5760 (2000).

[13]B. J. Rodriguez, S. Jesse, S. V. Kalinin, J. Kim and S. Ducharme, *Appl. Phys. Lett.* **90**, 122904 (2007).

[14]A. G. Chynoweth, *J. Appl. Phys.* **27,** 78 (1956).

[15]A. V. Bune, Chuanxing Zhu, Stephen Ducharme, L. M. Blinov, V. M. Fridkin, S. P. Palto, N. G. Petukhova, and S. G. Yudin, *J. App. Phys.* **85,** 7869 (1999).

[16]V. R. Palkar, K. Ganesh Kumara, and S. K. Malik, *App. Phys. Lett.* **84,** 2856 (2004).

[17] Y. W. Wong *et al., Journal of Applied Polymer Science* **89,** 3160 (2003).

[18] C. M. Wolfe *et al.,* Physical Properties of Semiconductors (Prentice Hall Series in Solid State Physical Electronics) (1989).

[19] J.F. Nye, *Physical Properties of crystals,* Oxford Science Publications (1985).

[20] B. D. Cullity, C. D. Graham, *Introduction to Magnetic Materials*, 2nd Edition, Wiley (2009).

[21] Kepler *et al., J. Appl. Phys.* **49,** 4490 (1978).

[22] Kepler *et al., J. Appl. Phys.* **49,** 4918 (1978).

[23]Y. K. Kim, T. J. Silva, *Appl. Phys. Lett.* **68**, 2885 (1996).

[24]O. Song, C. A. Ballentine, R. C. O' Handley, *Appl. Phys. Lett.* **64**, 2593 (1994).

[25]Wenhui Ma, *Phys. Scr.* **T129,** 180–183 (2007).

[26]A. K. Tagantsev, *Phys. Rev. B* **34 (8),** 5883 (1986).

[27] Baskaran *et al., Appl. Phys. Lett.* **98 ,** 242901 (2011).

[28] Sh. M. Kogan, *Sov. Phys. Solid State* **5,** 2069 (1964).

[29] A. K. Tagantsev, *Sov. Phys. JETP* **61,** 1246 (1985).

[30] W. Ma and L. E. Cross, *Appl. Phys. Lett.* **79,** 4420 (2001).

[31] W. Ma and L. E. Cross, *Appl. Phys. Lett.* **81,** 3440 (2002).

[32] M. Gharbi *et al*., International Journal of Solids and Structures **48,** 249 (2011).

[33] G. Catalan *et al., Nature Materials* **10,** 963 (2011).

[34] D. Lee *et al., Phys. Rev. Lett.* **107**, 057602 (2011).

[35] Magnetic domains in Co thin films obliquely sputtered on a polymer substrate, A. Lisfi and J.C. Lodder, *Phys. Rev. B* **63,** 174441(2001).

Chapter 5

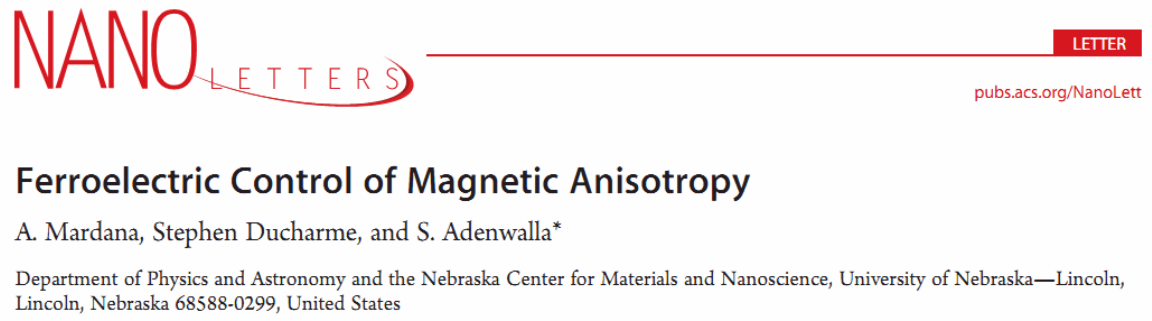

This chapter has been published in Nano Letters 11, 3862 (2011). Minor changes from the original journal article have been made for this dissertation.

5.1 Introduction

The ability to control magnetic properties with an electric field raises exciting possibilities, both for the understanding of the fundamental physics underlying these effects and for potential technological applications. Electric field control of magnetization has a wide range of applicability in spintronics and magnetic data storage devices, ranging from electrically controllable magnetic memories to magnetoelectric transducers and threshold magnetic sensors. Electric fields inside ferromagnets induce spin-dependent screening charges,[1,2] leading to changes in the surface magnetization and surface magnetocrystalline anisotropy.[3,4,5,6] In magnetic semiconductors, the long electric field penetration depths significantly alter the carrier concentration, the Curie temperature and the saturation magnetization.[7,8] Electric field induced changes have also been observed in metallic magnetic thin films, including substantial changes in the coercivity of FePt thin films immersed in a liquid electrolyte,[9] and changes in the

magnetic anisotropy in Fe/MgO,[10] $Fe_{80}Co_{20}$/MgO[11] and $Co_{40}Fe_{40}B_{20}$/MgO heterostructures.[12]

Ferroelectrics offer a convenient source of large, switchable electric fields, as well as satisfying the need for low power consumption, non-volatile devices in the realization of electrically controlled magnetic memories. Typically, however, the strain coupling of the magnetic and electrical order parameters[13,14] in ferroelectric/ferromagnetic heterostructures overwhelms the experimental investigation of more subtle magnetoelectric effects.[15] To explore the effects of electric field penetration into a metallic ferromagnet, we fabricated a heterostructure of a stiff metallic ferromagnet, Co, with a soft copolymer ferroelectric, P(VDF-TrFE) consisting of 70% vinylidene fluoride with 30% trifluoroethylene, with bulk stiffness coefficients of 10^{11} N/m^2 and 10^9 N/m^2 respectively. In general the stiffness coefficients of thin films are expected to differ from those in the bulk by 10-20%, still preserving the large mismatch in stiffness coefficients that will minimize magnetostrictive effects. The soft ferroelectric polymer is unlikely to cause significant strain in the much stiffer metallic Co film. Our experiments provide detailed evidence of the changes in the magnetic anisotropy and free energy of the magnetic film with electric field.

In summary this chapter includes the sample preparations, measurements and results of the electric field control of magnetic anisotropy in a wedge shaped Co film of varying thickness. A copolymer ferroelectric of 70% vinylidene fluoride with 30% trifluoroethylene, P(VDF-TrFE) overlays the Co wedge, providing a large switchable electric field. As the ferroelectric polarization is switched from up to down, the magnetic anisotropy of the Co films changes by as much as 50%. At the lowest Co thickness the

magnetic anisotropy switches from out-of-plane to in-plane as the ferroelectric polarization changes from up to down, enabling us to rotate the magnetization through a large angle at constant magnetic field merely by switching the ferroelectric polarization.

5.2 Sample Preparation and Experimental Techniques

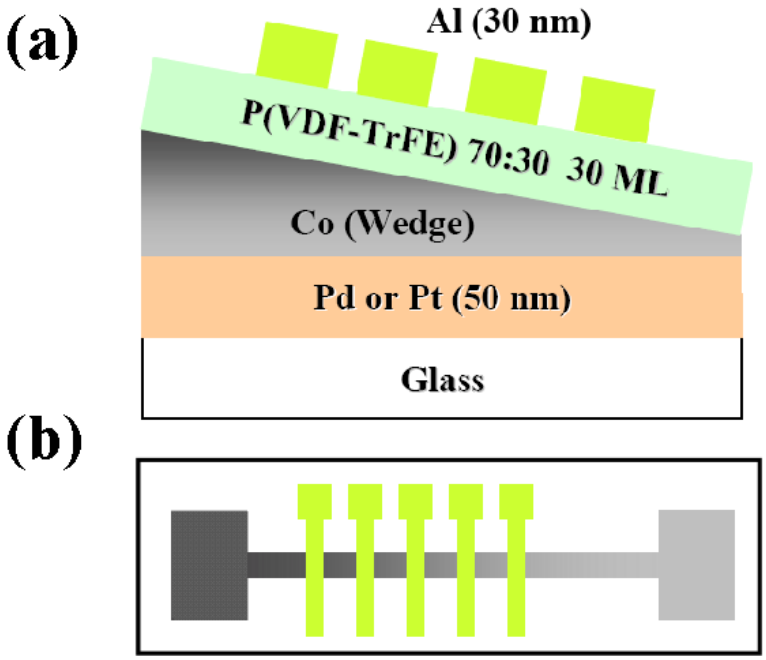

Figure 5.1: (a) Schematic side view of the sample: Glass / Pd or Pt (50nm) / Co (8.5 Å – 27.8 Å) / 30 monolayers P(VDF-TrFE) 70:30 / Al(30nm). The Co strip is 40 mm long resulting in a very shallow wedge angle of 2.7 x 10^{-6} degree (b) Schematic diagram of the top view of the sample with bottom (gray) Co electrode and top Al (green) electrode.

The sample (Figure 5.1(a)) consisted of a shallow-angled Co wedge grown on a Pd or Pt seed layer with a 30 monolayer film of the ferroelectric copolymer, P(VDF-TrFE) 70:30, deposited by Langmuir-Blodgett deposition [16] and covered by Al stripe

electrodes at intervals of 3 mm (Figure 5.1(b)). The metallic bottom electrodes were sputtered through shadow masks 0.2 mm wide and 40 mm long on glass substrates at a base pressure of 3.7 x 10^{-8} Torr. The Co layer with a wedge angle of 2.7 x 10^{-6} degree was deposited on a seed layer of either Pd or Pt (50nm). The deposition rates of Pt, Pd and Co were 0.46 Å/s, 0.65 Å/s and 0.216 Å/s respectively. The polymer ferroelectric films were deposited ex-situ directly on the cobalt films by the Langmuir-Blodgett (LB) technique. The Langmuir layer was formed on an ultrapure water subphase using a 0.05% concentration of P(VDF-TrFE) (70:30) in dimethyl sulfoxide. The layer was then compressed to a surface pressure of 5 mN/m at a temperature of 25 °C and deposited onto the substrate using horizontal Langmuir-Blodgett deposition, with the film thickness determined by the number of transferred monolayers (ML). The LB deposited copolymers of 70% VDF with 30% of TrFE, [P(VDF-TrFE) 70:30] are highly crystalline, excellent ferroelectrics with a saturation polarization of up to 0.1 C/m^2. The sample was then annealed at 130 °C for an hour in air at a ramp rate of 1.6 °C/min for both heating and cooling to increase the crystallinity of the polymer film. The 0.2 mm wide top Al electrode was deposited on top of the polymer film by evaporation at a deposition rate of 1.2 Å/s. The top and bottom electrodes formed a crossed pattern and defined an overlapping electrode area of 0.04 mm^2. Copper wires were attached to the top and bottom electrodes with silver epoxy, allowing for pyroelectric measurements and enabling polarization switching. The ferroelectric properties of the polymer film were characterized by pyroelectric measurements using the Chynoweth method (see chapter # 2 section 2.5 for details). The sample temperature is modulated using a 3 mW laser beam at a chopper frequency of 2 kHz and the pyroelectric current is measured by a lock-in

amplifier with a time constant of 1 s. The magnetic layers of the samples were characterized using the Magneto Optical Kerr Effect (MOKE) method, using longitudinal MOKE for in-plane measurements and polar MOKE for out of plane measurements (see chapter #2 section 2.6 for details). The magnetic anisotropy was calculated using the area method (see figure 5.2), where we assume the bulk magnetization value for Co. The black and red magnetization curve gives the area in the first quadrant of the magnetic hysteresis loop for the easy and hard axis directions respectively. If we assume that domain losses are identical for both in-plane and out-of-plane orientations, the difference between these two areas (shown in green) gives the effective anisotropy energy, which contains both the surface and volume anisotropy energies.

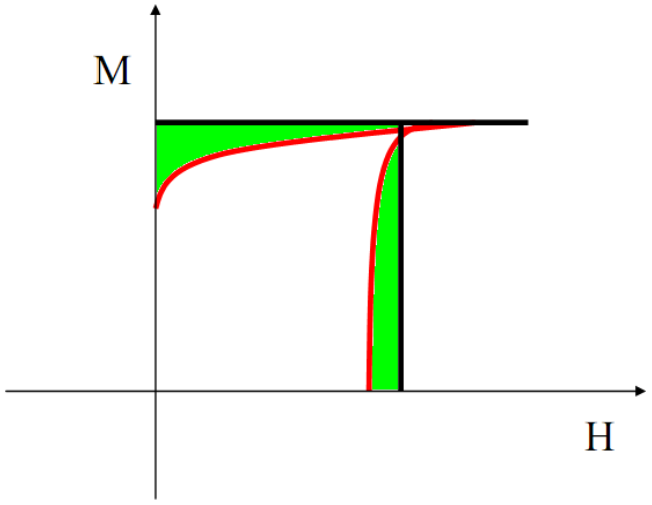

Figure 5.2: Schematics of the magnetic anisotropy calculation using the area method.

5.3 Experimental Results and Discussions

The large surface charge density associated with the ferroelectric polarization in P(VDF-TrFE), of the order of 0.1 C/m^2,[17] is equivalent to an applied field of

approximately 1 GV/m, well above the breakdown field of most dielectrics. The anisotropy of the wedge-shaped magnetic film goes from out-of-plane[18] at the thinnest end to in-plane at the thickest end, undergoing the well-known spin reorientation transition (SRT) at an intermediate thickness.[19] The quantity that determines the orientation of the ferromagnetic film is the anisotropy energy, $K_{eff} = (K_s/t - K_v)$, where t is the film thickness. The surface anisotropy, K_s, favors out-of-plane magnetization and K_v, the volume term, is dominated by the shape anisotropy, favoring in-plane magnetization. At the SRT, the two energies are comparable, resulting in a very small net anisotropy.

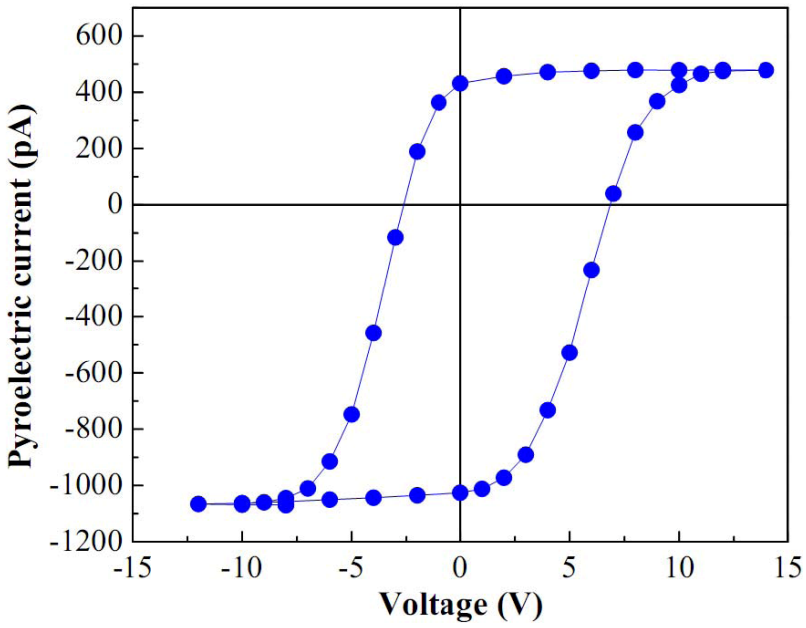

Figure 5.3: Ferroelectric hysteresis loop measured by pyroelectric current with applied voltage on one particular spot.

The ferroelectric polarization hysteresis loop (Figure 5.3) demonstrates that voltages of ±12 V are sufficient to switch and saturate the polarization of the ferroelectric

film between its two opposing states.[20] The essence of the magnetoelectric effect is shown in figures 5.4 (a) and (b), which indicate increased out-of-plane coercivity and decreased in-plane coercivity for up polarization (in which the ferroelectric bound surface charge at the Co surface is negative and the electric field in the Co film points out of the film) vs. down polarization. Similar hysteresis loops were measured at various positions along the Co wedges, corresponding thicknesses of 9Å, indicating that the Co film is both continuous and ferromagnetic at this thickness.

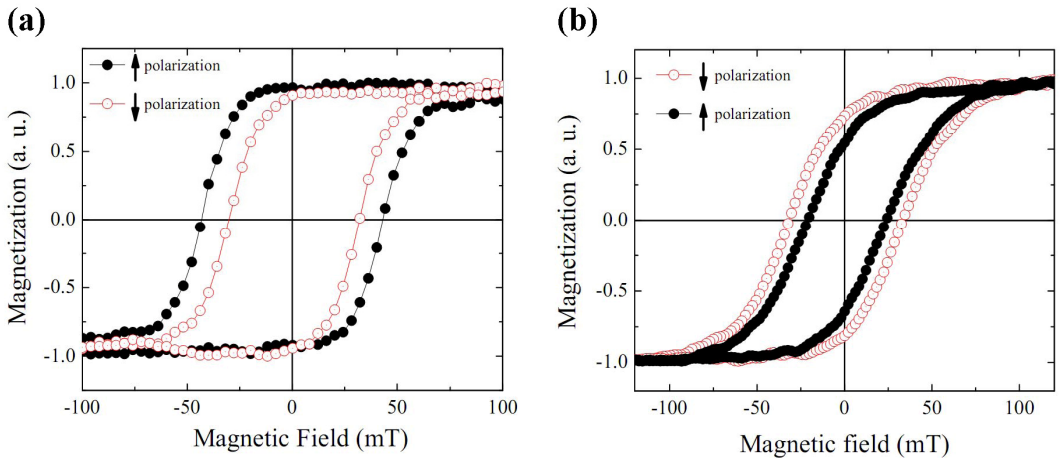

Figure 5.4: (a) Out-of-plane magnetization hysteresis loops using PMOKE (polar magneto-optical Kerr effect) depicting the change in coercivity for two different polarization states. Up polarization results in a *larger* out-of-plane coercivity than down polarization. (b) In-plane magnetization hysteresis loops using longitudinal MOKE (LMOKE) depicting the changes in coercivity indicate that up polarization (solid circle) results in *smaller* in-plane coercivity than down polarization (open circle).

We propose that the influence of the polarization state on the magnetization arises primarily from electric field penetration into the magnetic film. The electric field induces unequal screening for spin-up and spin-down electrons in the ferromagnet changing both

the anisotropy energy and the magnetization for the top few atomic layers. [2,5] We expect the other likely mechanisms of magnetoelectric coupling to be much weaker. Mechanical coupling is weak because of the relative softness of the polymer, as noted above. The polymer should have negligible influence on bonding at the metal surface, an expectation supported by first-principles calculations of the interlayer bonding at the Co/P(VDF-TrFE) interface.[21]

The results of both in-plane and out-of-plane magnetization measurements along the Co wedge for both polarization states are summarized in Figure 5.4, for cobalt films grown on Pd and Pt seed layers, respectively. As measured by the M_r/M_s ratio shown in figures 5.4 (a) and 5.4 (d), the Co wedge thickness spanned the spin reorientation transition from out-of-plane to in-plane anisotropy. The position and width of the reorientation transition depends on the underlying seed layer material. The measurements of the SRT (Figure 5.4) were made with a virgin ferroelectric film, before the application of an external voltage to polarize the film. However, previous measurements indicate that LB deposition results in films with a small preferential up polarization so we expect that the polarization was non-zero even before poling.[22] We performed additional experiments which shows that the presence of the unpoled P(VDF-TrFE) film results in a significant shift of the SRT towards the thicker end of the wedge, an effect that may result from subtle chemical changes at the interface.

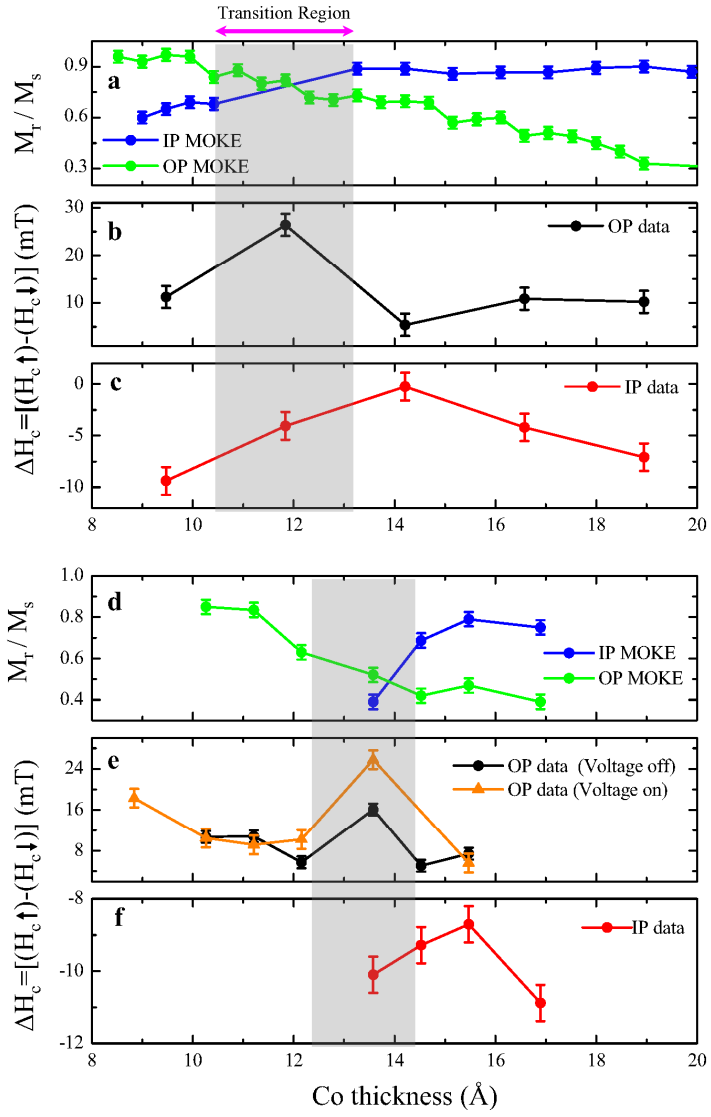

Figure 5.5: (a), (b) and (c) correspond to the Pd/Co sample, and (d), (e) and (f) to the Pt/Co sample). (a) & (d) M_r / M_s data for out-of-plane and in-plane MOKE measurements. M_r / M_s is a measure of the squareness of the magnetization hysteresis loops. Out-of plane and in-plane M_r/M_s measurements indicate the spin reorientation region. Co films grown on both Pd and Pt seed layers show a clear spin-reorientation transition region (gray shadow) from out-of plane to in-plane as the Co thickness increases. (b), (c), (e), & (f) Depicting the difference in coercivity $\Delta H_c = H_c (P\uparrow) - H_c(P\downarrow)$, between up and down polarization. (b) & (e) For out-of plane measurements the up polarization state has a larger coercivity than the down polarization state over the entire thickness of Co, with a maximum difference of 26 mT for the Pd/Co sample and 16mT for the Pt/Co sample in the SRT region. ΔH_c data with voltage-on are shown for the Pt/Co sample (orange). The remaining data are taken at remanence. (c) & (f) In-plane measurements indicate the opposite behavior for the change in coercivity with ferroelectric polarization.

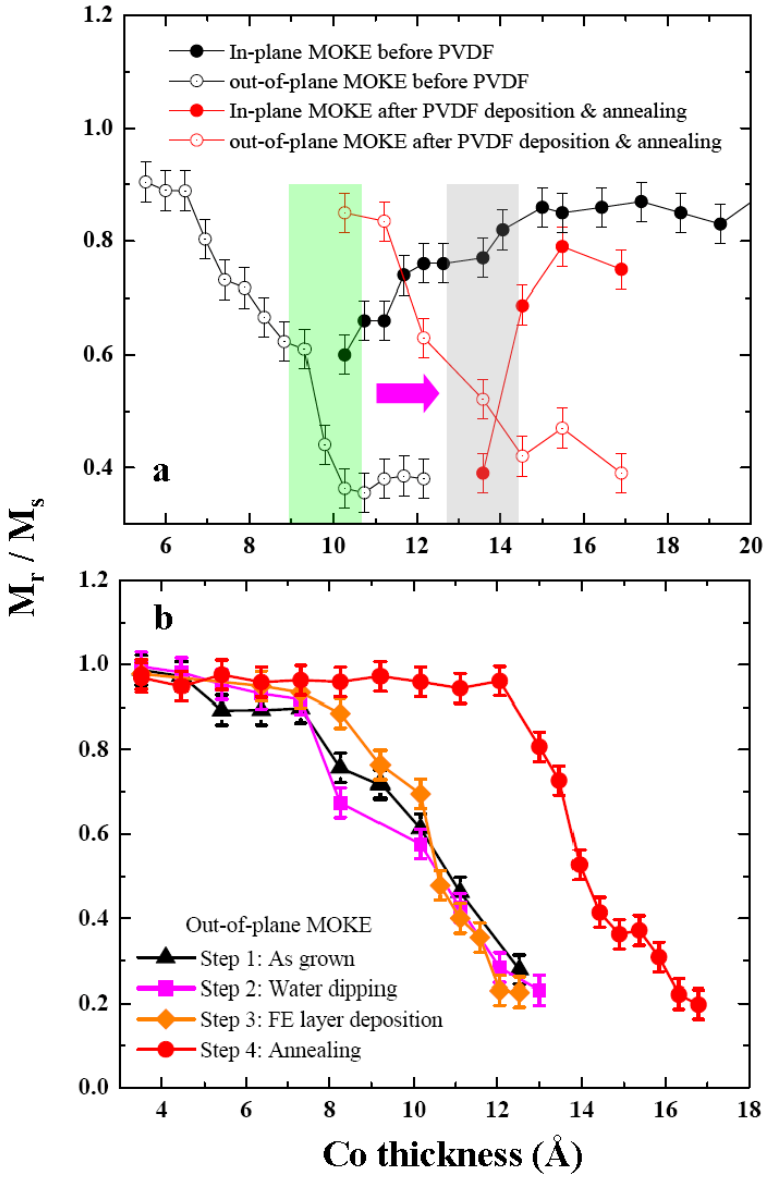

Figure 5.6: (a) M_r / M_s data for both in-plane and out-of plane magnetization loops before and after the growth of the ferroelectric P(VDF-TrFE) 70:30 layer. i) in-plane data without FE layer (solid black) ii) out- of plane data without FE layer (open black) iii) in-plane data with FE layer (solid red) iv) out-of plane data with FE layer (open red) for the magnetization loop measurement. Clearly there is a shift in the transition region to the thicker side of the Co film as shown by the arrow from the green shaded region to the gray shaded region. (b) A set of four sequential MOKE measurements were made on an identical Pt/Co wedge sample with thickness ranging from 4 Å to 17 Å: (i) on the bare Co surface (ii) after immersion into water (iii) after deposition of the PVDF and (iv) after annealing of the PVDF film. The SRT transition remained unaffected by the first three steps, shifting dramatically from 8 Å to 12 Å only after annealing of the PVDF film.

Measurements of both in-plane and out-of-plane MOKE and the corresponding M_r/M_s values indicate that the SRT shifts from a thickness of approximately 10Å without the FE polymer to 13 Å after the polymer film has been deposited and annealed as shown in figure 5.6. This shift is attributed to interfacial chemistry at the metal polymer interface. Cobalt has been shown to be particularly reactive with polymers,[23] with the formation of carboxylates, $Co(OH)_2$ as well as clusters of metallic Co. Cobalt films exposed to ambient conditions, as was this sample, form oxides and hydroxides,[24] with rates of formation dependent on temperature and time, further complicating the issue. A series of experiments to explore the origin of the shift in the position of the SRT were carried out on a Co wedge (identical to the Pt/Co wedge) with thickness ranging from 4 Å to 17 Å using the magneto-optical Kerr effect (MOKE) to pinpoint changes in the SRT (see Figure 5.5 (b)). A set of four MOKE measurements were made in sequence: (i) on the bare Co surface after removal from the deposition chamber (ii) after immersion in ultrapure water, as would occur for the LB deposition process, effected by dipping the sample into a clean LB trough (iii) after deposition of the PVDF and (iv) after annealing of the PVDF film. The SRT remained unaffected by the first three steps, shifting from 8 Å to 12 Å only after annealing of the PVDF film. We attribute this change to interfacial chemical changes that are accelerated by the 130 °C annealing temperature, rather than to electric field effects from the polarized ferroelectric. This is because, although annealing does increase the net polarization of PVDF,[25] magnetic hysteresis loops for the out of-plane easy axis direction recorded above the Curie temperature of the ferroelectric polymer showed no change from the room-temperature measurements (see figure 5.8).

When the ferroelectric polarization is pointing away from the metallic Co layer, there is an increase in the out-of-plane coercivity and a decrease in the in-plane coercivity across the entire range of Co thicknesses explored (see figure 5.5). Clearly, this polarization direction (up) favors out-of-plane anisotropy. Note that for the Co/Pt sample, we present results both at ferroelectric remanence, with zero applied voltage, and with an applied voltage of 12 V. The slightly larger changes seen with the voltage on are attributed to the relaxation of the ferroelectric polarization when the voltage is turned off. [26] The changes in the *out-of-plane* coercivity are most pronounced in the region of the spin reorientation transition. In contrast, the changes in the *in-plane* coercivity are minimized at or close to the SRT.

In contrast to spin-reorientation experiments with Fe/MgO[10] thin films, which require the application of large voltages to perturb the magnetization, the changes seen here are present at zero applied voltage because the *remanent* ferroelectric polarization produces a large interface charge. This has important ramifications for data storage technology, providing a route to non-volatile memory storage, because this large remanent polarization is controlled with a relatively small voltage.

To minimize magnetic domain effects in the interpretation of the magnetization data, the effective uniaxial anisotropy constant K_{eff} for both samples was calculated using the area method (see Figure 5.2).[27] This method assumes that irreversible domain mechanisms are similar for both in-plane and out-of-plane directions and hence the difference in area between the out-of-plane and in-plane magnetization curves yields the effective anisotropy energy K_{eff}. As expected from the data in figure 5.5(a) the anisotropy energy for the *up* polarization state (negative interface charge) changes sign at the SRT

(see figure 5.7 (a)), going from positive to negative, where a positive value of K_{eff} corresponds to out-of-plane anisotropy. For the smallest Co thickness measured, switching the ferroelectric polarization to the *down* state (positive interface charge) alters the uniaxial anisotropy from positive to negative, allowing for electric field controlled switching of the magnetization easy axis from out-of-plane to in-plane.

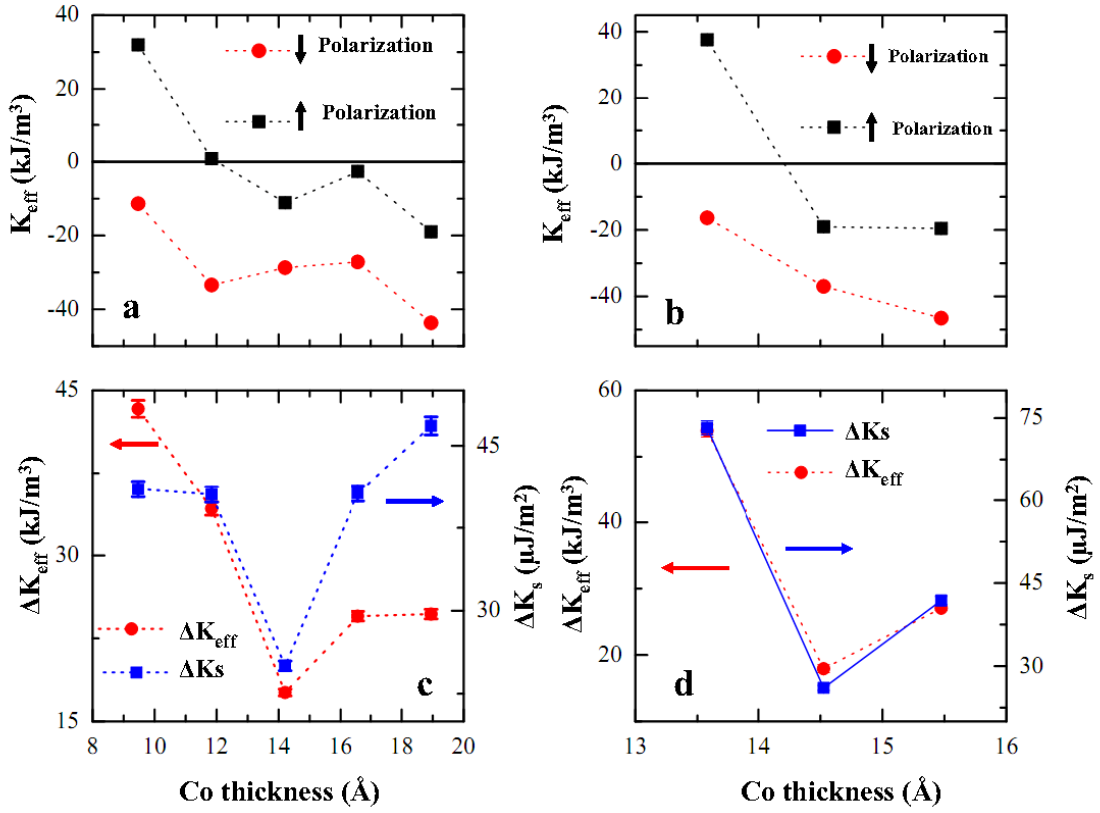

Figure 5.7: (a) & (b) show the effective uniaxial anisotropy constant as obtained from the area method as a function of Co thickness for samples on a (a) Pd seed layer and (b) Pt seed layer. For the lowest thickness (9.4 Å) K_{eff} is positive for up polarization and negative for down polarization indicating a switching of the easy axis from out-of plane to in-plane. At larger thickness, negative values of K_{eff} result in in-plane magnetization. At the spin reorientation region for up polarization the effective anisotropy is close to zero, in agreement with the M_r/M_s data in Figure 2. (c) & (d) The changes in effective anisotropy $\Delta K_{eff} = K_{eff}(P\uparrow) - K_{eff}(P\downarrow)$ (red circle) and surface anisotropy $\Delta K_s = t\,\Delta K_{eff}$ (blue square) resulting from switching of the ferroelectric polarization plotted as a function of Co thickness for samples on (c) a Pd seed layer and (d) a Pt seed layer.

The reversal of the electrical polarization results in changes in the anisotropy energy, $\Delta K_{eff} = K_{eff}(P\uparrow) - K_{eff}(P\downarrow)$. If we assume that these changes arise solely from the changes in the surface anisotropy energy, we can write $\Delta K_s = t\ \Delta K_{eff}$ (where t is the thickness of the Co film). These quantities are shown in figures 5.7 (c) and 5.7 (d) as a function of Co thickness and indicate that polarization reversal results in surface anisotropy changes that are in the range of 30-70 $\mu J/m^2$ for both the Co/Pd and Co/Pt samples. Given the short electric field penetration depth of ~ 1.5 Å in Co, we would expect ΔK_s to be constant across the whole thickness range. The differences may be due to non-uniform surfaces resulting in variations of the local electric field.

In order to confirm the central role of the ferroelectric polarization in the magnetic effects observed, the Pt/Co sample was heated to 119.4 °C, well above the ferroelectric-paraelectric phase transition temperature of 107 °C.[28] At temperatures above the ferroelectric transition temperature of the P(VDF-TrFE), where the spontaneous polarization vanishes, the magnetization hysteresis loops showed no change in coercivity (see Figure 5.8) because in the paraelectric phase, there was no remanent polarization and no net charge at the interface to influence the magnetic film. The out-of plane MOKE measurement at a Co thickness of 11.2 Å corresponding to two different applied voltage of +12 V and -12 V, the same voltage used previously to polarize the FE layer is shown in figure 5.8 (a). There was no significant effect of the sign of the applied voltage in the magnetic coercivity, which was measured at zero voltage in both cases. At this temperature, the ferroelectric film does not remain polarized without a voltage. On cooling back down to room temperature, the polymer film was confirmed to be ferroelectric through polarization hysteresis measurement (see figure 5.8 (b)) and again

the out-of plane MOKE measurements in the two different polarization states, up (-12 V) and down (+12 V), showed the change in coercivity of 8.9 mT as shown in figure 5.8 (c). The much lower coercivity of the magnetic film at high temperature (compare figure 5.8 (a) and (c)) is a feature common to ferromagnets, and not necessarily due to the loss of ferroelectric polarization in the polymer film. To test this hypothesis with our Co films, a new sample of Pd (50 nm)/Co (1.4 nm) was made without the FE layer. The MOKE measurement from this sample (Figure 5.8 (d)) also exhibits a decrease in coercivity by 5.1 mT from room temperature to at 119.4 °C, the same amount observed with the cobalt-polymer heterostructure (figure 5.8 (a)).

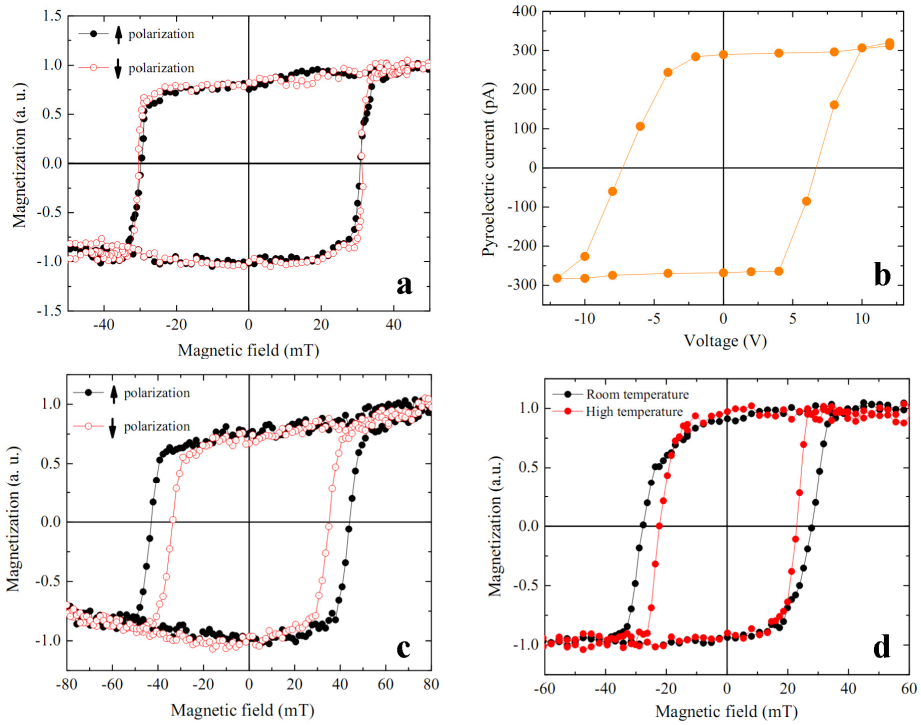

Figure 5.8: (a) At 119.4 °C, well above the ferroelectric-paraelectric phase transition temperature there is no change in coercivity. (b) and (c) are room temperature measurements of the b, ferroelectric loop and c, magnetization loop indicating that the sample is stable. (d) The lower coercivity at high temperature is an expected feature. A Pd/Co sample without the FE layer shows a similar temperature dependence of the coercivity.

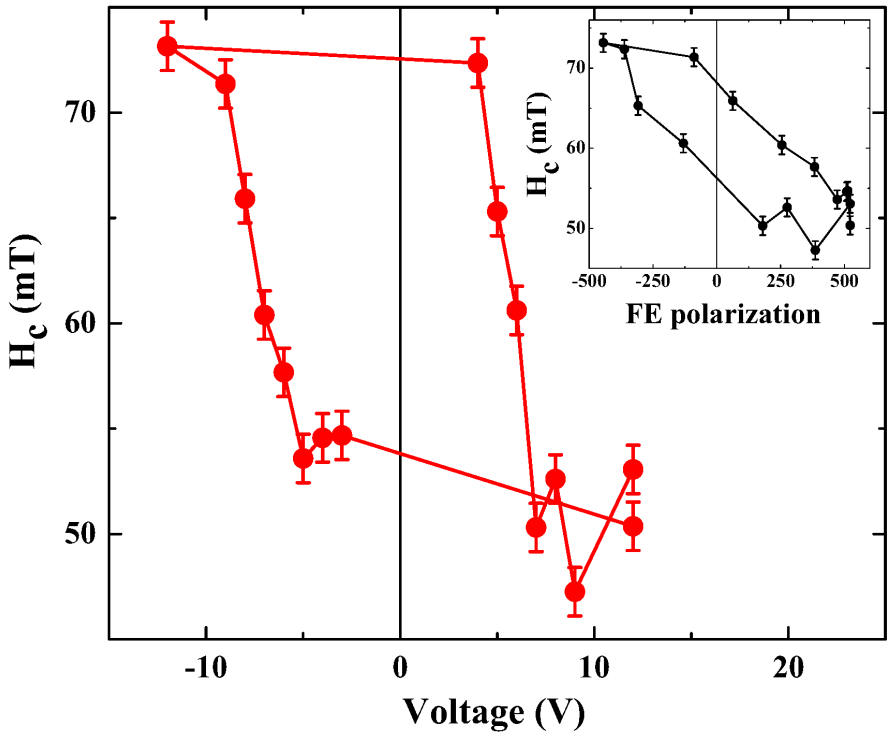

Figure 5.9: Out-of-plane magnetic coercivity, as a function of applied voltage, (and net ferroelectric polarization) measured at a Co thickness of 11.2 Å at zero applied voltage, after the requisite voltage has been applied to change polarization. Coercivity measurements as a function of applied voltage show a shape similar to the ferroelectric polarization. Inset: out-of-plane coercivity as a function of ferroelectric polarization (as measured by the pyroelectric current). The polarization values corresponding to applied voltage were taken from a polarization hysteresis loop similar to that shown in Figure 5.3.

Investigations of the magnetic coercivity at intermediate polarization states demonstrated that the magnetic coercive field is proportional to the net ferroelectric polarization, as shown in figure 5.9, in which the magnetic coercive fields for out-of-plane hysteresis loops are plotted as a function of the *applied* electric field, clearly displaying the hysteretic behavior corresponding to the ferroelectric polarization state. The inset of figure 5.9 shows the magnetic coercive field plotted as a function of the ferroelectric film polarization (with the relative polarization values obtained empirically

from the pyroelectric hysteresis loop), revealing the proportionality between the two, apart from a small remaining hysteresis, which we attribute to incomplete ferroelectric domain switching. The ferromagnetic domains are a few microns in size,[29] and about two orders of magnitude larger than the ferroelectric domains in P(VDF-TrFE), which are 30 nm to 50 nm in size.[30] Hence, each ferromagnetic domain experiences an electric field that results from the *average* macroscopic polarization.

The results of these experiments show that the changes in magnetic behavior cannot be attributed to volume effects. Symmetry considerations dictate that there should be no change in the in-plane strain in the ferroelectric film on polarization reversal, and therefore no strain effects in the Co. (Any out-of-plane strain in the ferroelectric film would not have induced stress in the films, because the sample thickness was unconstrained.) Further, any residual strains in the polymer ferroelectric film are unlikely to perturb the Co, because of the much lower stiffness coefficient of the polymer. MOKE measurements in a heterostructure containing both ferroelectric and ferromagnetic components, will contain an electro-optic signal from the ferroelectric that will contribute to the measured MOKE intensity. This will change the Kerr intensity (height of the MOKE loop) but essentially will have no effect on the resultant coercivity change. Thermomagnetic effects will also have no effect on the observed coercivity change with ferroelectric polarizations. (See chapter 4)

The high electrical polarization charge, 0.1 C/m^2, at the polymer surface contributes an appreciable electric field. If we assume a 15 Å naturally occurring overlayer of CoO,[31] the electric field penetrating the Co surface is calculated to be 8.7 x 10^8 V/m. This electric field will extend into the metallic Co layer over a distance of ~ 1.5

Å, altering the spin polarization over this depth because of unequal spin-up and spin-down screening charge densities.[2,5] This large electric field value is larger than the expected breakdown voltage for a transition metal oxide such as CoO. Breakdown fields for CoO have not been measured, but the band gap of 2.4 eV implies a breakdown field of the order of 3 x 10^8 V/m, [32] about a factor of three smaller than the electric field we expect using the full polarization of the ferroelectric. There are several uncertainties that exists because (i) the interface between the metallic Co and the polymer ferroelectric is not well known, and hence the interface may contain other materials, (ii) the polarization at the interface may in fact not be the full polarization of the ferroelectric, leading to lower values of the surface charge density and (iii) the interface between the Co and polymer layers is not smooth and the chemistry of the interface changes after polymer deposition and annealing of the sample as shown and described in figure 5.6. Reactions between Co and polymers form carboxylates, metallic Co and hydroxides[23] and the rates of formation are dependent on temperature and time, making the exact interface structure subject to some uncertainty. Our results and interpretation are similar to those in $Fe_{80}Co_{20}$/MgO and Co40Fe40B20/MgO heterostructures, in which the presumed electric field at the surface of the MgO is comparable or larger than the experimentally observed breakdown voltage in thin MgO films.[33] Comparison of our results with other theoretical and experimental values (see table 5.1) indicates that our values of the ME coupling are of the same order of magnitude. Our data indicate a change in the anisotropy due to the induced electric field of $\Delta K_{eff}/\Delta E$ = 2.47 x 10^{-5} J/m^{2}V. This may be compared to the experimentally obtained values of 8.8 x 10^{-5} J/m^{2}V found in a Fe/MgO heterostructure[10] with an applied electric field of 10^8 V/m. Theoretical and experimental values of electric

field control of surface anisotropy changes [1] of ~ 10^{-14} J/Vm are comparable to our experimentally observed value $\Delta K_s/\Delta E$ ~ 2.34 x 10^{-14} J/Vm. In $Fe_{80}Co_{20}$/MgO structures[34] very large values of $\Delta K_s/\Delta E$=83 x 10^{-14} J/Vm have been reported, much larger than theoretically predicted values.[35] The table 5.1 below shows a detailed comparison of anisotropy changes with electric field.

Materials		Surface anisotropy change (ΔK_s) ($\mu J/m^2$)	Electric field (V/m)	$\frac{\Delta K_s}{\Delta E}(J/Vm)$
Fe (0.48nm)/MgO Nature Nanotech. 4, 406 (2009)	Experiment	8.4	10^8	4.2 x 10^{-14}
$Fe_{80}Co_{20}$ (0.5nm)/MgO APL 96, 022506 (2010)	Experiment	15	4 x 10^8	3.75 x 10^{-14}
Fe (15 ML) /vacuum	Theory	400	10^{10}	2 x 10^{-14}
Pt/Fe/Pt PRL 102, 247203 (2009)	Theory	--	10^{10}	7.2 x 10^{-14}
$Fe_{80}Co_{20}$ (0.55nm)/MgO APL 96, 142512 (2010)	Experiment	833	10^9	83 x 10^{-14}
$Co_{40}Fe_{40}B_{20}$ (1.33nm) / MgO APL 96, 212503 (2010)	Experiment	33	10^9	3.3 x 10^{-14}
Pd/Co(9.4 Å)/PVDF Our value	Experiment	40	8.7 x 10^8	2.3 x 10^{-14}

Table 5.1: Different experimental and theoretical values of surface anisotropy change with electric field.

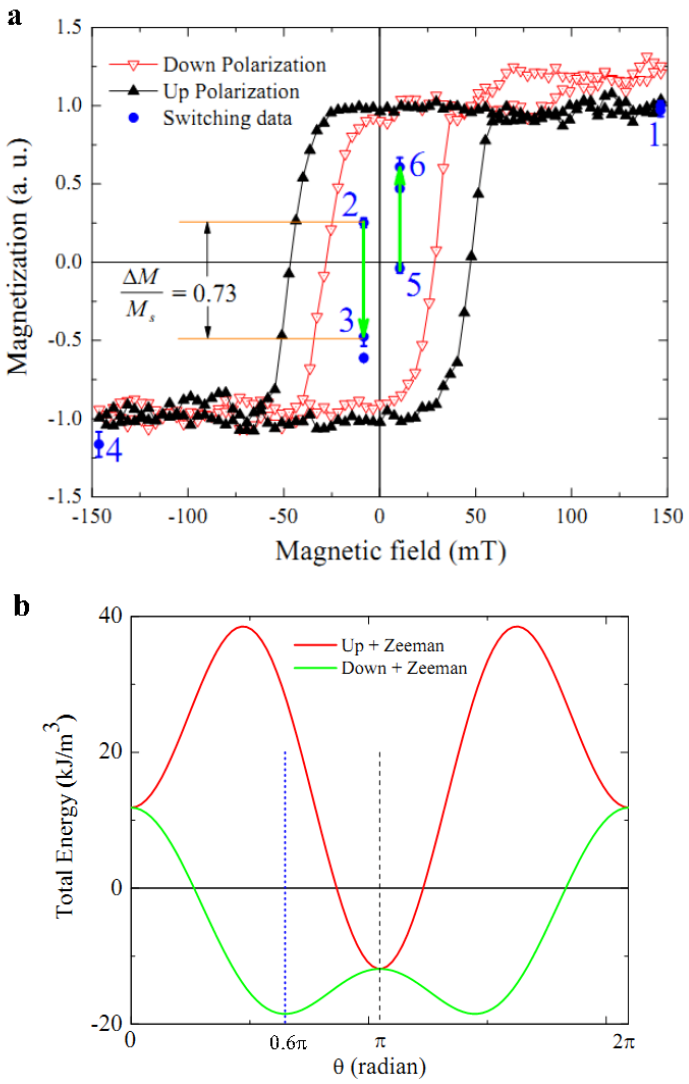

Figure 5.10: The red (open triangles) and black (closed triangles) magnetic hysteresis loops for Co thickness of 8.8 Å correspond to polarization pointing down and up respectively. (a) Starting from positive magnetic saturation, with polarization pointing up, we reverse the magnetic field to -8.3mT resulting in a lowering of the magnetization to point 2. Switching the FE polarization to down results in a switching of the magnetization to point 3, due to the lowering of the energy barrier with the change in polarization. Point 3 is stable and switching back to up polarization does not switch the magnetization back to point 2. Similarly after negative magnetic saturation and polarization up, we increase the field to 5, switch the FE polarization to down resulting in a change of the magnetization to point 6. Switching back to up polarization does not alter state 6, which like 3 is stable to changes in the ferroelectric polarization. (b) Calculations of the magnetic free energy consisting of the magnetic anisotropy (which is altered by the direction of ferroelectric polarization) and Zeeman energies for the two polarization states. Note the lowering of the energy barrier when the polarization is switched from up to down and the minima of energy occurring at $\theta = 0.6\pi$.

The effect of the ferroelectric polarization on the magnetic anisotropy energy is also apparent in an investigation of the magnetic switching behavior, as illustrated by figure 5.10 (a). The two out-of-plane magnetization hysteresis loops, one for polarization up and the other for polarization down, are shown for the Pt/Co film at a Co thickness of 8.8 Å. The ferroelectric film was polarized up, and the magnetic film was saturated, resulting in the magnetization denoted as point 1 in figure 5.10 (a). On reversing the applied magnetic field to –8.34 mT, the magnetization value dropped rapidly (a consequence of magnetic relaxation effects) to the state denoted by point 2, where it was stable for an extended period of time. Switching the ferroelectric film to the opposite (*down*) polarization state resulted in an abrupt reverse of the magnetization to point 3 in the hysteresis loop. Reversing the polarization to *up* had no effect on the magnetization. A similar sequence with polarization up, negative magnetic saturation, reversal of the magnetic field to +10.43 mT and switching of the polarization results in the magnetization switching from points 5 to 6. Points 2 to 3 and points 5 to 6 are irreversible with electric field, requiring the presence of a magnetic field to reverse the magnetization state.

The irreversibility of the polarization-induced switching results from the free-energy landscape of the magnetic state and its dependence on the polarization direction. The magnetic free energy in a uniaxial system with no magnetocrystalline anisotropy may be written as $U = K_{eff} \sin^2 \theta - \vec{M} \bullet \vec{H}$, where K_{eff} is the effective anisotropy, which in our sample is dependent on the electric field, θ is the angle the magnetization makes with the normal to the film and M and H are the saturation magnetization and applied magnetic field, respectively. Because we could not measure the in-plane magnetization

for the 8.8 Å film, we use the K_{eff} values for the 13.5 Å film, 37.6 kJ/m^3 and –16.3 kJ/m^3 for up and down polarization states, respectively, to calculate the free energy curves shown in figure 5.10 (b). For up polarization, at an applied field of –8.3 mT, the free energy barrier to magnetization reversal prevents rotation of the magnetization into the field direction, and the magnetization is stable at $\theta = 0$ corresponding to point 2 in Figure 5.10 (a). Switching to down polarization lowers the energy barrier with the minimum of energy occurring at $\theta = 0.6\pi$, *i.e.,* the magnetization lies close to the in-plane direction at point 3 in Figure 5.10 (a). Because PMOKE measures only the perpendicular component of the magnetization, we expect to measure a value of $-0.36M_s$, close to the actual value of $-0.5M_s$, which was measured at point 3. The irreversibility of this transition is due to the large energy barrier encountered in going from point 3 to point 2 (or from point 6 to point 5).

The results described here occur in all samples of this structure. Data for a variety of samples grown in different runs are shown in figure 5.11. In all cases, the out-of plane magnetic coercivity is larger for up polarization, while the reverse is true for the in-plane magnetic coercivity. The Pd/Co sample and the Pt/Co sample-1 are described earlier in figure 5.5. The Pt/Co samples 2 and 3 are samples with a uniform thickness of Co, with all other parameters being the same.

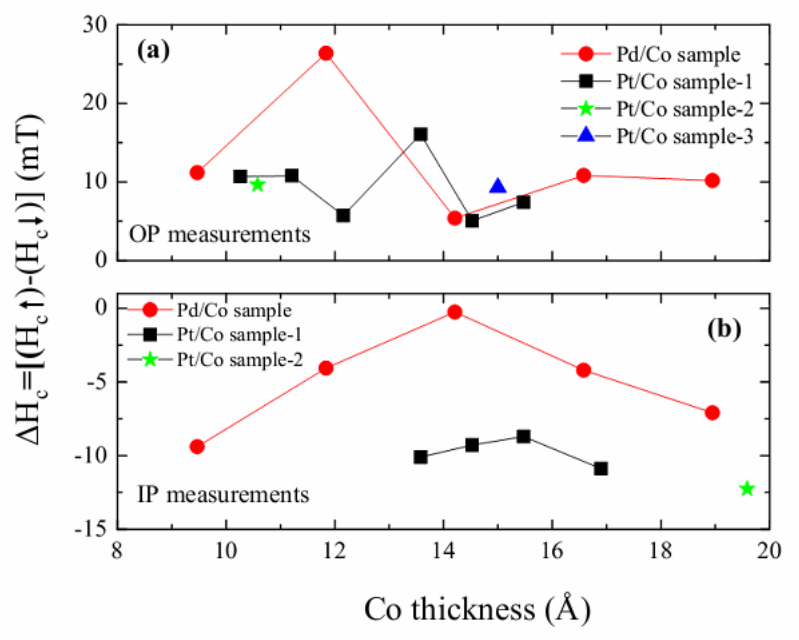

Figure 5.11: Change in coercivity with ferroelectric polarization in a variety of Co/P(VDF-TrFE) samples. (a) Out-of-plane coercivity measurements on four different samples indicate that the coercivity for up polarization is always larger than for down polarization. (b) In-plane coercivity measurements on three different samples indicating that the magnetic coercivity is always larger for down polarization.

5.4 Conclusions

In conclusion, we have shown that the electric polarization state of a polymer ferroelectric thin film substantially alters the magnetic anisotropy of a thin film transition metal ferromagnet, changing the magnetization easy axis from out-of-plane to in-plane for sufficiently thin ferromagnetic films. This magnetization switching from out-of-plane to in-plane is achieved using an applied voltage of only 12 V, is stable at remanence, and is irreversible with electric field. The change in magnetic anisotropy is proportional to the electrical polarization of the polymer ferroelectric and the effect is absent in the

paraelectric phase above the ferroelectric-paraelectric transition temperature. Moreover, this behavior is achieved in a device with relaxed constraints on the ferroelectric/ferromagnetic interface as exemplified by the ex-situ growth of the ferroelectric in a water sub-phase and the naturally occurring oxide layer on the ferromagnet. Both of these features confer distinct benefits in the realization of non-volatile memory devices and are in stark contrast to the demanding fabrication requirements of oxide ferroelectric films. The changes in the surface anisotropy induced by the direction of FE polarization, 30-70 $\mu J/m^2$, are comparable to previous experiments [10] as is the magnetoelectric anisotropy coupling coefficient, $\Delta K_{eff}/\Delta E$.

The substantial mismatch between the stiffness coefficients of the ferromagnet and the ferroelectric precludes strain effects and the weak interfacial coupling rules out atomic rearrangements at the interface. Hence we infer that this is purely an electric field effect, arising from the large surface charge density at the ferroelectric/feromagnet interface that results in a large electric field that will penetrate the metallic Co over a distance equal to the screening length. This alters the anisotropy energy barrier for magnetic switching allowing for electric control of magnetic switching at very low applied voltages of ±12V, with the magnetic state remaining stable in the absence of applied voltage.

5.5 Acknowledgements

This work is supported by the National Science Foundation through the Materials Research Science and Engineering Center program under Grant No. DMR-0820521.

5.6 References

[1] Duan, C. G. *et al.,* Surface magnetoelectric effect in ferromagnetic metal films. *Phys. Rev. Lett.* **101,** 137201 (2008).

[2] Zhang, S. Spin-Dependent Surface Screening in Ferromagnets and Magnetic Tunnel Junctions. *Physical Review Letters* **83,** 640 (1999).

[3] Duan, C. G. *et al.,* Tailoring magnetic anisotropy at the ferromagnetic/ferroelectric interface. *Appl. Phys. Lett.* **92,** 122905 (2008).

[4] Nakamura, K. *et al.,* Origin of electric-field-induced modification of magnetocrystalline anisotropy at Fe(100) surfaces: Mechanism of dipole formation from first principle. *Phys. Rev. B* **80,** 172402 (2009).

[5] Cai, T. *et al.,* Magnetoelectric coupling and electric control of magnetization in ferromagnet/ferroelectric/normal-metal superlattices. *Phys. Rev. B* **80,** 140415(R) (2009).

[6] Rondinelli, J. M. Stengel, M. & Spaldin, N. A. Carrier-mediated magnetoelectricity in complex oxide heterostructures. *Nature Nanotechnology* **3,** 46 (2008).

[7] Chiba, D. Yamanouchi, M. Matsukura, F. & Ohno, H. Electrical manipulation of magnetization reversal in a ferromagnetic semiconductor *Science* **301,** 943 (2003).

[8] Ohno, H. *et. al.,* Electric-field control of ferromagnetism. *Nature* **408,** 944 (2000).

[9] Weisheit, M. *et al.,* Electric Field-Induced Modification of Magnetism in Thin-Film Ferromagnets. *Science* **315,** 349 (2007).

[10] Maruyama, T. *et al.,* Large voltage-induced magnetic anisotropy change in a few atomic layers of iron. *Nature Nanotech.* **4,** 158 (2009).

[11] Shiota, Y. *et al.,* Voltage-assisted magnetization switching in ultrathin $Fe_{80}Co_{20}$ alloy layers, *Applied Physics Express* **2,** 063001 (2009).

[12] Endo, M. Kanai, S. Ikeda, S. Matsukura, F. & Ohno H. Electric-field effects on thickness dependent magnetic anisotropy of sputtered $MgO/Co_{40}Fe_{40}B_{20}/Ta$ structures. *Appl. Phys. Lett.* **96,** 212503 (2010).

[13] Sahoo, S. *et al.,* Ferroelectric control of magnetism in $BaTiO_3$/Fe heterostructures via interface strain coupling. *Phys. Rev. B* **76,** 092108 (2007).

[14] Spaldin, N. A. & Ramesh, R. Electric-field control of magnetism in complex oxide thin films. *MRS Bulletin* **33,** 1047 (2008).

[15] Duan, C. G. Jaswal, S. S. & Tsymbal, E. Y. Predicted Magnetoelectric effect in Fe/$BaTiO_3$ Multilayers: Ferroelectric Control of Magnetism. *Phys. Rev. Lett.* **97,** 047201 (2006).

[16] Ducharme, S. Palto, S. P. & Fridkin, V. M. Ferroelectric and Dielectric Thin Films. **3,** 545-591 (edited by H. S. Nalwa, Academic Press, San Diego, 2002).

[17] Palto, S. *et al.,* Ferroelectric Langmuir-Blodgett films. *Ferroelectrics Lett.* **19,** 65 (1995).

[18] Carcia, P. F. Perpendicular magnetic anisotropy in Pd/Co and Pt/Co thin-film layered structures. *J. Appl. Phys.* **63,** 5066 (1988).

[19] Lee, J. W. Jeong, J. R. Shin, S. C. Kim, J. & Kim, S. K. Spin -reorientation transitions in ultrathin Co films on Pt(111) and Pd(111) single-crystal substrates. *Phys. Rev. B* **66,** 172409 (2002).

[20] Sorokin, A. V. Fridkin, V. M. & Ducharme, S. Pyroelectric study of polarization switching in Langmuir-Blodgett films of poly(vinylidene fluoride trifluoroethylene). *Journal of Applied Physics* **98,** 044107 (2005).

[21] Lopez, J. M. Sun, Y. Burton, J. D. Tsymbal, E. Y. & Velev, J. P. Organic multiferroic tunnel junctions with ferroelectric poly(vinylidene difluoride) barriers. *Nano Lett.* **11,** 599 (2011).

[22] Blinov, L. M. Fridkin, V. M. Palto, S. P. Sorokin, A. V. and Yudin, S. G. Thickness Dependence of Switching for Ferroelectric Langmuir Films. Thin Solid Films, **284-85,** 474 (1996).

[23] Leidheiser, H. & Deck, P. D. Chemistry of the Metal-Polymer Interfacial Region. *Science* **241,** 1176 (1988).

[24] Tompkins, H.G. & Augis, J.A. The oxidation of cobalt in air from room temperature to 467°C. *Oxidation of metals,* 16, 355 (1981).

[25] Bai, M. Poulsen, M. & Ducharme, S. Effects of annealing conditions on ferroelectric nanomesa self-assembly. *J. Phys.: Condens. Matter* **18,** 7383 (2006).

[26] Sorokin, A. V. Ducharme, S. & Fridkin, V. M. Pyroelectric study of a polarization switching in Langmuir-Blodgett films of poly(vinylidene fluoride - trifluoroethylene). *J. Appl. Phys.* **98,** 044107 (2005).

[27] Johnson, M. T. Bloemen, P. J. H. den Broeder, F. J. A. & de Vries J. J. Magnetic anisotropy in metallic multilayers. *Rep. Prog. Phys.* **59,** 1409 (1996).

[28] Poulsen, M. Sorokin, A. V. Adenwalla, S. Ducharme, S. & Fridkin, V. M., Effects of an external electric field on the ferroelectric-paraelectric phase transition in polyvinylidene fluoride-trifluoroethylene copolymer Langmuir–Blodgett films. *J. Appl. Phys.* **103,** 034116 (2008).

[29] Allenspach, R. Stampanoni, M. & Bischof, A. Magnetic domains in thin epitaxial Co/Au(111) films. *Phys. Rev. Lett.* **65,** 3344 (1990).

[30] Rodriguez, B. J. Jesse, S. Kalinin, S. V. Kim, J. & Ducharme, S. Nanoscale polarization manipulation and imaging of ferroelectric Langmuir-Blodgett polymer films. *Appl. Phys. Lett.* **90,** 122904 (2007).

[31] Maat, S. Takano, K. Parkin, S. S. P. & Fullerton, E. E. Perpendicular Exchange Bias of *Co/Pt* Multilayers. *Phys. Rev. Lett.* **87,** 087202 (2001).

[32]Li-Mo Wang, PROC. 25th INTERNATIONAL CONFERENCE ON MICROELECTRONICS, Relationship between Intrinsic Breakdown Field and Bandgap of Materials (2006).

[33] D. V. Dimitrov et al., Appl. Phys. Lett. 94, 123110 (2009).

[34] Seung-Seok Ha et al., Appl. Phys. Lett. 96, 142512 (2010).

[35] M. Tsujikawa and T. Oda, J. Phys.: Condens. Matter 21, 064213 (2009).

Chapter 6

The sweep rate dependence of the electrical control of magnetic coercivity

A. Mardana, Stephen Ducharme and S. Adenwalla

This chapter has been accepted in Journal of Applied Physics for publications. Minor changes from the original journal article have been made for this dissertation

6.1 Introduction

In recent years, research on the electrical control of magnetic properties in composite materials via magnetoelectric coupling has accelerated, leading to the realization of exciting fundamental physics phenomena, in addition to potential spintronics applications. Electric fields in magnetic thin films have been shown to control the magnetic anisotropy,[1,2,3,4,5] the magnetization, the Curie temperature[6,7,8] and the spin polarization.[9] Ferroelectric/ferromagnetic heterostructures provide an easy route for the application of large electric field but in the majority of previous studies the strain-mediated coupling[10,11] between the components overwhelms electric-field induced effects.[12,13] We have previously measured large polarization induced changes in the magnetic coercivity and anisotropy of thin Co films in a Co / P(VDF-TrFE) bilayer.[14] P(VDF-TrFE) is a ferroelectric copolymer with a large polarization and a stiffness coefficient that is approximately two orders of magnitude below that of Co. This combination produces a large electric field of 8.8 x 10^8 V/m at the surface of the Co but

very little, if any, strain in the Co layer, thereby enabling the investigation of purely electric field effects.

Our previous results[14] (see Chapter 5) can be summarized as follows. The polarization of the polymer ferroelectric has a significant effect on the coercivity and magnetic anisotropy of the thinnest Co films. The out-of-plane coercivity is significantly larger for up polarization (i.e. for the polarization pointing away from the Co layer), whereas the opposite is true for the in-plane coercivity. The magnetic anisotropy energy can be altered by as much as 50% by switching the ferroelectric polarization from up to down as calculated from in-plane and out-of-plane hysteresis loops. For the thinnest films, the easy magnetization axis switches from out-of-plane to in-plane as the ferroelectric polarization is switched. The change in coercivity is proportional to the ferroelectric polarization, as confirmed by taking magnetization loops at intermediate polarization values. The magnetization can be rotated through a large angle using only electric fields and this rotation is electrically irreversible, because the electric field changes the free energy of the thin ferromagnetic film. Experiments in the paraelectric phase above the ferroelectric-paraelectric transition temperature of the P(VDF-TrFE), at which no changes in the coercivity are seen, confirm that these large changes in the anisotropy arise from the large electric field at the surface of the Co layer, created by the presence of the ferroelectric polarization.

The ability to change the magnetic coercive field using an electric field has tremendous potential applications in magnetic recording media, because it enables electric field writing of the magnetic state. This chapter's research is motivated by the well-known dependence of the magnetic coercivity on the magnetic field sweep rate,

prompting us to investigate how the polarization-induced changes in coercivity, ΔH_c, behave as a function of magnetic field sweep rate. To our knowledge, few if any studies of this dependence exist and, as we shall show below, the results are quite striking, even at fairly slow sweep rates and over a small range.

The sweep rate dependence of the magnetic coercivity, H_c is well known and is most apparent in magnetic thin films.[15,16,17,18,19] The magnetic coercivity decreases with the field sweep rate, approaching the intrinsic coercivity for very slow sweep rates. Because magnetization reversal occurs by thermally activated processes, magnetization switching times depend on the energy barrier to be overcome, an energy barrier that depends (among other things) on the externally applied field. Hence, the coercive field, defined as the field at which half the sample volume has switched,[15] is highly dependent on sweep rate. Because the exact dependence of H_c on sweep rate varies with extrinsic film properties (grain size, roughness), our ferromagnetic/ferroelectric heterostructured sample consists of a single wedge shaped Co layer, in order to minimize these effects. In addition, we measured the sweep rate dependence of identically grown bare Co thin films to check for coercive field effects due to the P(VDF-TrFE) overlayer.

6.2 Experimental Procedures

The samples consisted of [A] a set of bare Co films of varying thicknesses (3 nm, 5 nm and 10 nm) on a 50 nm Pt seed layer and [B] one wedge sample with a ferroelectric overlayer consisting of Glass / Pt (50 nm) / Co (2.5 Å - 21.5 Å) / [P(VDF-TrFE) 70:30] 100 ML / Al (26 nm) as shown in figure 6.1. The wedge angle of the Co layer in this latter sample [B] is 2.7×10^{-6} degree. All samples were grown on glass substrates. The

Co and Pt layers were deposited by sputtering through shadow masks that were 1 mm wide and 15 mm long (for set [A]) and 0.5 mm wide and 40 mm long for the wedge shaped Co layer for set [B]. The deposition rates of Co and Pt were 0.2 Å/s at 2 x 10^{-3} Torr argon pressure.

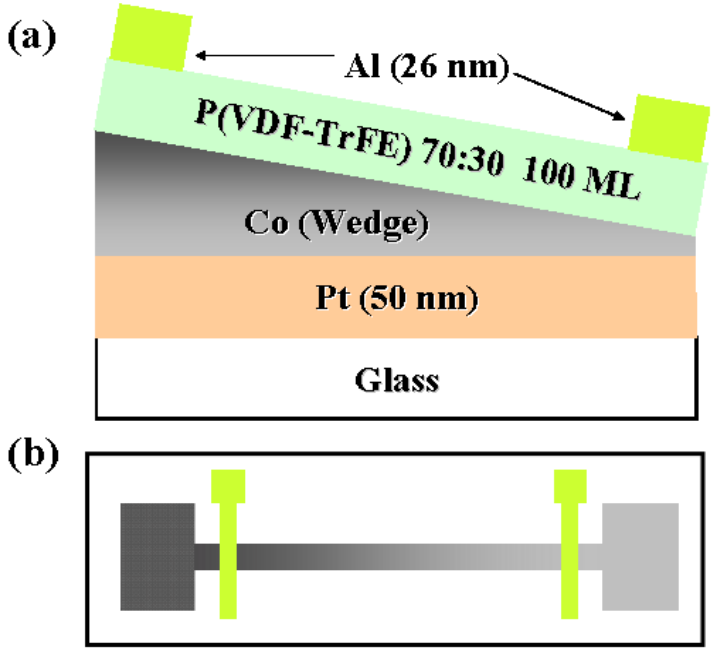

Figure 6.1: Sample schematic diagram. (a) Cross sectional view of sample [B]: Glass / Pt (50 nm) / Co (2.5 Å – 21.5 Å) / [P(VDF-TrFE) 70:30] 100 ML / Al (26 nm). The Co wedge angle was 2.7 x 10^{-6} degree. (b) Top view of the sample [B]. LMOKE and PMOKE were done on the thick and thin edge respectively as shown in the diagram.

The 180 nm thick ferroelectric polymer layer on the wedge-shaped Co was grown ex-situ by the Langmuir-Blodgett (LB) technique (details of the deposition are given in chapter 2). The sample was annealed at 135 °C for one hour, resulted in a crystalline

ferroelectric film. Upper electrodes of Al (26 nm thick) were deposited by thermal evaporation through shadow masks of width 0.2 mm at discrete regions along the Co wedge. Copper wires were attached to the top and bottom electrodes with silver paint to enable the measurement and switching of the ferroelectric polarization. The ferroelectric layer has been characterized using the Chynoweth method with a laser power of 1 mW and in reference to an optical chopper frequency of 2 kHz. The pyroelectric current is measured using a lock-in amplifier with 1 s time constant. The pyroelectric loop of sample [B] is shown in figure 6.2. The magneto-optical Kerr Effect (MOKE) was used to characterize the in-plane and out of plane magnetic behavior of all samples in longitudinal and polar configurations respectively.

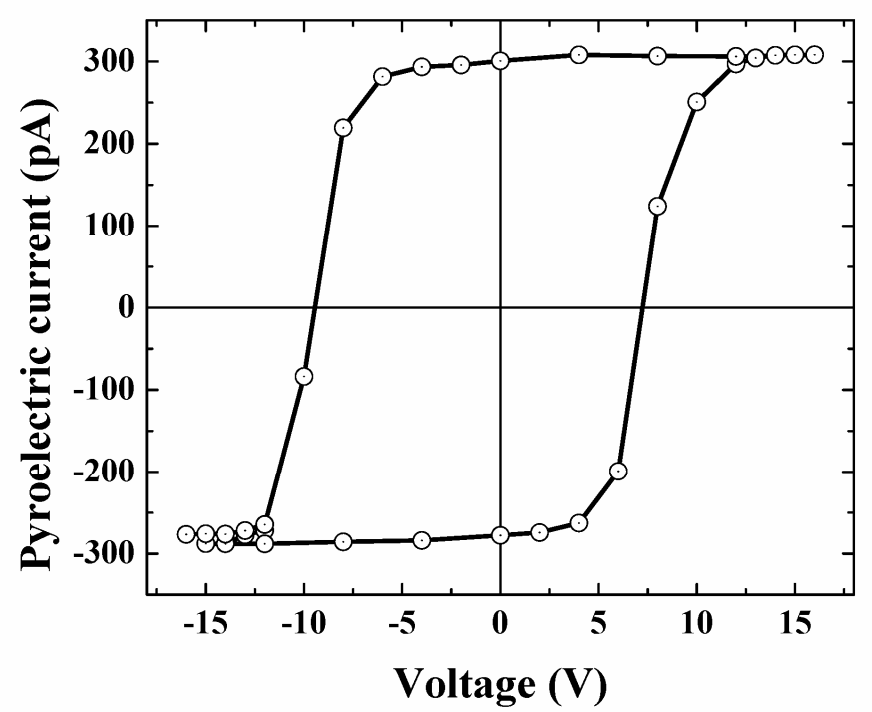

Figure 6.2: Ferroelectric polarization hysteresis loop as measured by the pyroelectric current vs applied voltage in one of the spots for sample [B].

6.3 Results and Discussions

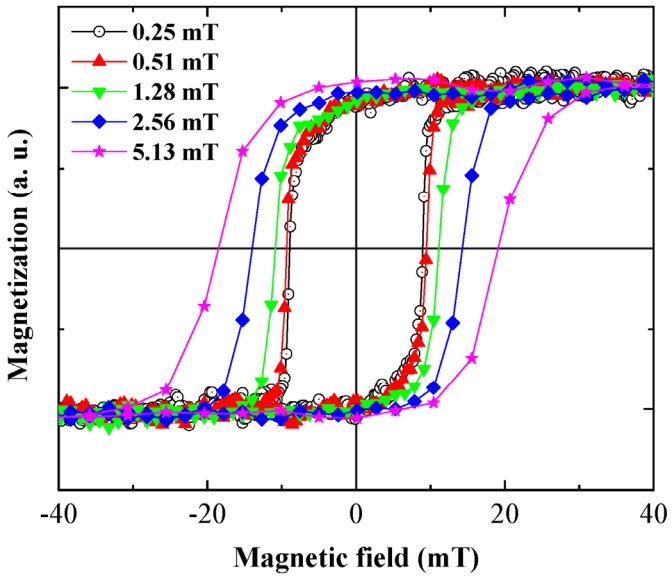

Figure 6.3: Step size dependence of magnetic coercivity in the Pt(50 nm)/Co(5 nm) sample. The coercivity increases with increasing step size.

The magnetic coercivity increases with increasing step size as shown in figure 6.3 for the sample consisting of Pt(50 nm)/Co(5 nm). The dependence of the magnetic coercivity on magnetic field step size as a function of film thickness is shown in figure 6.4. Since the delay between each step is identical for all measurements (300 ms), the step size may be taken as a proxy for the sweep rate. Both step size and effective sweep rate are indicated on the horizontal axis, with the sweep rate ranging from 0.85 mT/s to 20.25 mT/s. Measurements were made on the three bare Pt/Co samples as well as on two ends of the Co/P(VDF-TrFE) sample at positions along the Co wedge that correspond to thicknesses of 10.5 Å and 19.5 Å. The out-of-plane (PMOKE) measurements were done at a Co thickness of 10.5 Å and the in-plane (LMOKE) measurements were done at a Co

thickness of 19.5 Å corresponding to out-of plane and in-plane magnetization easy axes at the respective thicknesses. Over this rather restricted range of sweep rates, the thinnest sample of set [A] 3 nm sample shows the maximum change in coercivity of 41.6 mT whereas the 5 nm and 10 nm sample show changes of 16 mT and 14 mT respectively, confirming the sweep rate dependence as well as the thickness dependence that has previously been observed. [15-19] The coercivity of the ferromagnetic/ferroelectric sample is shown in figure 6.4(b), for both directions of polarization, with red and black data points indicating down and up polarization respectively. The solid data points are for LMOKE measurements at a Co thickness of 19.5 Å and the open data points are for PMOKE measurements for a Co thickness of 10.5 Å. The coercive field and its dependence on sweep rate are quite different from the expected dependence. With these thinner films, we expect a larger coercive field and much stronger sweep rate dependence than was obtained for the 3 nm bare Co film. We attribute this to chemical changes at the interface arising from the presence of the P(VDF-TrFE). Our earlier work has shown a substantial shift of the spin reorientation transition when the P(VDF-TrFE) layer is annealed and we expect that a similar phenomena is responsible for the coercive field data. As expected from our earlier measurements, the in-plane coercivity for up (pointing away from the Co surface) polarization is always smaller whereas for out-of-plane coercivity the reverse is true. Polarization switching was accomplished with an applied voltage of ± 20 V and all data are taken at zero applied voltage.

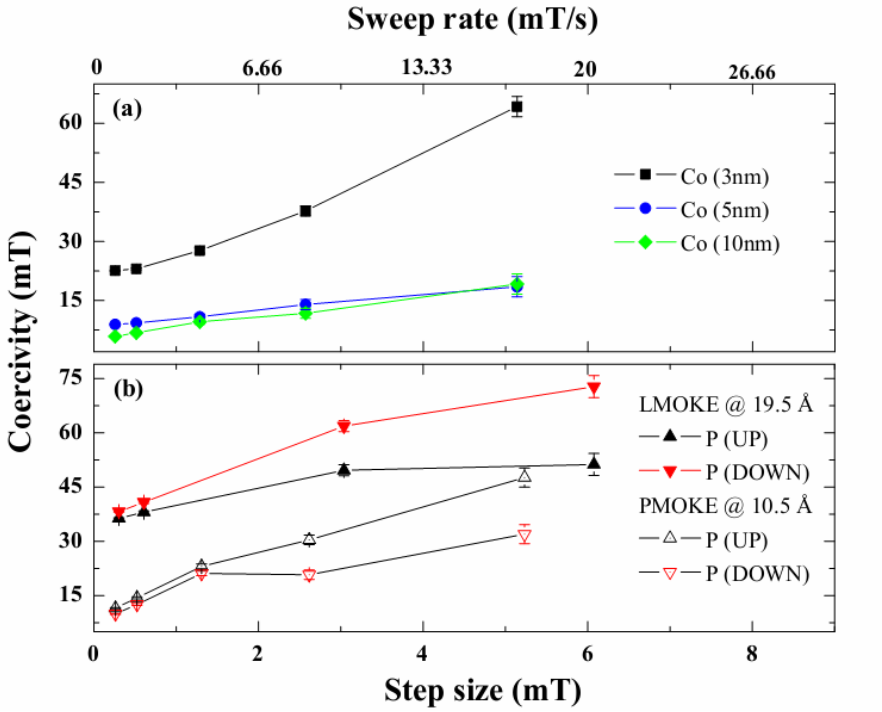

Figure 6.4: Magnetic coercivity as a function of sweep rate. (a) LMOKE measurements of sample set [A] consisting of bare Co on a Pt (50 nm) seed layer. (b) LMOKE and PMOKE measurements of sample [B] The solid red and black data are for LMOKE measurements at a Co thickness of 19.5 Å with the symbol direction depicting the FE polarization direction. The open red and black data are for PMOKE measurements at a Co thickness of 10.5 Å. The lines are guides to the eye.

We are interested in how this difference in coercivity $\Delta H_c = H_c(\uparrow) - H_c(\downarrow)$, depends on the field sweep rate. This dependence is indicated in figure 6.5 in which the normalized difference $\Delta H_c / H_c(\uparrow)$ is plotted as a function of step size and sweep rate for both the in-plane data at a thickness of 19.5 Å and the out-of-plane data at a thickness of 10.5 Å. The blue lines indicate the sweep rate of our previous experiments, albeit on different samples. There is a remarkably strong dependence of this change in coercivity

on the sweep rate, all the more striking because the range of sweep rates used is quite modest. This dependence on the sweep rate implies that the electric field from the polymer must influence the magnetic domain structure, but the mechanism behind this remains unclear. Domain motion with the application of electric fields has been previously observed in $Fe_{0.7}Ga_{0.3}$ / $BaTiO_3$ [20] and CoFe / $BaTiO_3$ layered samples, [21] but in those samples, strain coupling between the two materials is shown to be the driver behind the domain wall motion. This is unlikely to be the case in our samples.

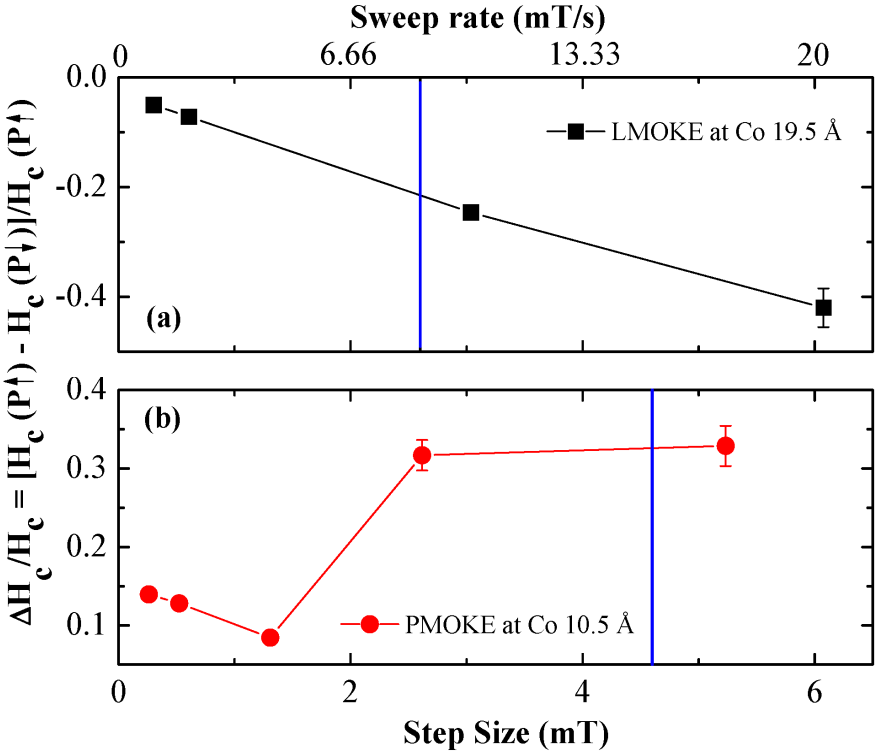

Figure 6.5: The normalized electric field induced difference in coercivity, $\Delta H_c/H_c$ as a function of magnetic field sweep rate, showing a substantial dependence. (a) In-plane LMOKE measurements for a Co thickness of 19.5 Å and (b) Out-of-plane PMOKE measurements for a Co thickness of 10.5 Å. The blue line is the sweep rate for our earlier reported measurements.[14]

6.4 Conclusions

In conclusion, we have investigated the effect of sweep rate on the electric field driven changes in magnetic coercivity in a polymer ferroelectric/ferromagnetic bilayer. Because of the large mismatch in stiffness coefficients, the magnetic changes with ferroelectric polarization that are observed are solely due to the presence of the electric field, and not to strain. In this magnetoelectric heterostructure, there is a substantial sweep rate dependence of the electric-field driven changes in magnetic behavior, even over the small range of fairly slow sweep rates investigated. Because most studies of the electric control of magnetism have been reported in very thin magnetic films and because the dynamic effect in these thin films can be very large, the field sweep rate is an important parameter in any measure of magnetoelectric coupling in heterostructured thin films.

6.5 Acknowledgements

This research is supported by the National Science Foundation through the MRSEC program under Grant No. DMR-0820521 and ECCS Grant No. 1101256.

6.6 References

[1] C. G. Duan, *et al., Appl. Phys. Lett.* **92,** 122905 (2008).

[2] K. Nakamura *et al., Phys. Rev. B* **80,** 172402 (2009).

[3] J. M. Rondinelli et al., *Nature Nanotechnology* **3,** 46 (2008).

[4] Duan, C. G. *et al., Phys. Rev. Lett.* **101,** 137201 (2008).

[5] Maruyama, T. *et al., Nature Nanotech.* **4,** 158 (2009).

[6] H. Ohno et al., Nature **408,** 944 (2000).

[7] T. Diet et al., *Science* **287,** 1019 (2000).

[8] D. Chiba et al, Science **301,** 943 (2003).

[9] V. Garcia et al., Science **327,** 1106 (2010).

[10] S. Sahoo *et al., Phys. Rev. B* **76,** 092108 (2007).

[11] N. A. Spaldin et al., *MRS Bulletin* **33,** 1047 (2008).

[12] Cai, T. *et al., Phys. Rev. B* **80,** 140415(R) (2009).

[13] Zhang, S. *Physical Review Letters* **83,** 640 (1999).

[14] A. Mardana *et al., Nano Letters* **11,** 3862 (2011).

[15] M. P. Sharrock, *J. Appl. Phys.* **76,** 10 (1994).

[16] P. Bruno *et al., J. Appl. Phys.* **68,** 11 (1990).

[17] W. Kleemann, *Annu. Rev. Mater. Res.* **37,** 415 (2007).

[18] M. P. Sharrock *et al., IEEE Trans. Magn. MAG* **17,** 3020 (1981).

[19] R. W. Chantrell *et al., J. Phys. D: Appl. Phys.* **21,** 1469 (1988).

[20] T. Brintlinger *et al., Nano Lett.* **10,** 1219 (2010).

[21] Lahtinen *et al.,* http://arxiv.org/abs/1109.5514.

Chapter 7

Summary & Future

This thesis presents experimental results on the magnetoelectric (ME) interactions between a transition metal ferromagnet, cobalt, and a ferroelectric copolymer P(VDF-TrFE) in thin film heterostructures. The results describe both the magnetic control of ferroelectric polarization as well as the ferroelectric control of magnetic anisotropy. Our choice of materials results in a considerable mismatch in the stiffness. Metallic cobalt is 100 times stiffer than the polymer ferroelectric and this mismatch has consequences for the interpretation of our data.

For magnetic control of ferroelectric polarization the samples consist of a metallic cobalt layer deposited on the polymer film. The ferromagnetic layer is not constrained by the substrate as it floats on the soft polymer layer so any strain in the Co layer due to magnetostriction will be transferred to the polymer layer. A large change in polarization is observed with the applied magnetic field perpendicular to the sample (which is also perpendicular to the easy magnetization axis). This polarization change is reversible and possesses odd symmetry with respect to the positive and negative magnetic field direction. After magnetic saturation the effect vanishes and careful demagnetization restores the effect albeit at a smaller magnitude. This implies that the presence of multiple magnetic domains in the ferromagnetic layer is necessary for this effect.

A possible origin of this magnetoelectric coupling is the flexoelectric effect, the change in polarization due to a strain gradient in the ferroelectric film. In order to quantify and explore this effect, future experiments include the measurement of the

flexoelectric coefficient of the Langmuir-Blodgett deposited P(VDF-TrFE) thin films. Because the magnetic domain structure plays an essential role and because the changes in polarization will occur chiefly at magnetic domain walls, both the magnetic domain orientation and the ferroelectric domain behavior must be observed. This can be conveniently done using magnetic force microscopy (MFM) and piezoelectric force microscopy (PFM) in applied magnetic fields to visualize the changes in ferroelectric domain polarization with changes in the magnetic domain structure. This will allow us to map out this ME effect in a single domain wall and to investigate how it depends on the domain wall widths, magnetostriction and the angle between the adjacent domains. The domain wall width and the domain structure depend on the film thickness as well as on the deposition parameters; we have the freedom to control both the magnitude and the sign of the effect. Magnetostriction can be controlled by the choice of magnetic material, such as with high magnetostriction Terfenol-D or with small magnetostriction permalloy.

An experimental study of the ferroelectric control of magnetic anisotropy in a wedge shaped Co layer overlaid with P(VDF-TrFE) is also presented. This detailed study has shown a shift in the spin-reorientation transition region to thicker Co after deposition and annealing of the P(VDF-TrFE), an effect attributed to chemical changes at the interface in ambient conditions. Changes in the ferroelectric polarization from up (pointing away from the Co layer) to down resulted in smaller out-of-plane magnetic coercivity and larger in-plane coercivity. The magnetic anisotropy, calculated using the area method, is shown to change by as much as 50% as the ferroelectric polarization switches from up to down. With a sufficiently thin Co film, the magnetic easy axis can be switched from out-of-plane to in-plane, by changing only the direction of the ferroelectric

polarization. This effect of this polarization change on magnetic coercivity vanishes in the paraelectric phase of the ferroelectric layer as there is no polarization charge present. The change in magnetic coercivity is also proportional to the ferroelectric polarization as confirmed by taking magnetization loops at intermediate polarization values. Rotation of the magnetization through a large angle by polarization switching is shown. These large changes in magnetic anisotropy arise from the polarization charges at the Co interface. The screening charges in the ferromagnetic layer are spin dependent and depending on the polarization direction there is a spin imbalance in the ferromagnetic layer, leading to an change in magnetic anisotropy.

To maximize this effect, future studies using a half-metallic ferromagnet will be performed. Since the screening lengths depends on the spin up and spin down electrons, the maximum change in magnetic anisotropy should be observed with a half-metal, in which one spin sub-band is filled and the other is empty. Another possibility is to use other transition metal ferromagnets such as Fe to see this change in magnetic anisotropy. In the present study, the interface between the Co and the polymer layers is contaminated because the polymer layer is grown ex-situ. In order to see this effect at a clean interface experiments that allow for the in-situ deposition (via evaporation) of a ferroelectric VDF oligomer on the Co wedge are planned. The effect of the screening charges can be enhanced by the deposition of a high-K dielectric material and the choice of a variety of dielectric materials deposited in-situ on the Co wedge will measure theoretical predictions of linear proportionality between screening charges and the dielectric constant.

In conclusion, the ME effects presented here have been studied from the perspective of basic research, rather than for engineering applications. Further studies will improve the understanding of the effect and the ability to optimize it using different materials and measurements. Future results may enable a more realistic model of multifunctional devices. Potential applications in ME sensors or transducers with lower cost and higher performance are possible. Electric field control of magnetic data storage devices are attractive because of the possibilities for lower power consumption and less heating. One possible application of the ferroelectric control of magnetic anisotropy is to use it in Magnetoresistive Random-Access Memory (MRAM) technology. Polarization reversal can be used to store the data by switching the magnetic layer using only electric fields. Further studies of the fundamental physics of a variety of ME effects will provide understanding as well as vision for future devices and technology.